

UNIVERSIDADE DE SÃO PAULO – USP

Faculdade de Ciências Farmacêuticas

Programa de Pós Graduação em Tecnologia Bioquímico-Farmacêutica

Caracterização biofísica de cubossomos, designados para entrega de fármacos, e sua interação com uma droga modelo: o caso da Miltefosina.

Bárbara Malheiros

Orientador: Prof. Dr. Leandro Ramos Souza Barbosa

Dissertação submetida à Faculdade de Ciências Farmacêuticas para a obtenção do grau de Mestrado em Ciências, área de concentração Tecnologia Bioquímico Farmacêutica.

São Paulo

Novembro 2018

VERSÃO CORRIGIDA

Ficha Catalográfica elaborada eletronicamente pelo autor, utilizando o programa desenvolvido pela Seção Técnica de Informática do ICMC/USP e adaptado para a Divisão de Biblioteca e Documentação do Conjunto das Químicas da USP

Bibliotecária responsável pela orientação de catalogação da publicação:
Marlene Aparecida Vieira - CRB - 8/5562

M249c MALHEIROS, BÁRBARA
Caracterização biofísica de cubossomos, designados para entrega de fármacos, e sua interação com uma droga modelo: o caso da Miltefosina / BÁRBARA MALHEIROS. - São Paulo, 2018.
136 p.

Dissertação (mestrado) - Faculdade de Ciências Farmacêuticas da Universidade de São Paulo.
Departamento de Tecnologia Bioquímico-Farmacêutica.
Orientador: Barbosa, Leandro Ramos Souza

1. Nanopartículas. 2. Drug Delivery. 3. Cubossomos. 4. Lipídios. 5. Auto agregação (Self-assembly). I. T. II. Barbosa, Leandro Ramos Souza, orientador.

Bárbara Malheiros

Caracterização biofísica de cubossomos, designados para entrega de fármacos, e sua interação com uma droga modelo: o caso da Miltefosina.

Comissão Julgadora da Dissertação para obtenção do Título de Mestre

Prof. Dr.

Orientador/Presidente

Prof. Leandro Ramos Souza Barbosa – FCF/USP e IF/USP

Denise Freitas Siqueira Petri – IQ/USP

1º. Examinador

Carlota de Oliveira Rangel Yagui – FCF/USP

2º. Examinador

Eneida de Paula - Unicamp

3º. Examinador

São Paulo, 5 de Novembro de 2018

University of São Paulo – USP
Pharmaceutical Sciences Faculty
Graduation Program in Pharmaceutical and Biochemical Technologies

**Biophysical Characterization of cubosomal nanoparticles
intended for drug delivery applications and its interaction with a
model drug: the miltefosine case.**

Bárbara Malheiros

Advisor: Prof. Dr. Leandro Ramos Souza Barbosa

Dissertation submitted to the School of
Pharmaceutical Sciences in fulfilment of the
requirements for the degree of the Master in
Sciences, concentration area Biochemical-
Pharmaceutical Technology.

São Paulo

November 2018

Resumo

MALHEIROS, B. **Caracterização biofísica de cubossomos, designadas para entrega de fármacos, e sua interação com uma droga modelo: o caso da Miltefosina.** 2018. Dissertação de Mestrado - Faculdade de Ciências Farmacêuticas, Universidade de São Paulo, São Paulo, 2018.

Nanomedicina é o campo de estudo mais promissor dentro da nanotecnologia atualmente. O uso de nanopartículas visa melhorar a eficiência de fármacos que possuem baixa solubilidade em meios aquosos (moléculas muito hidrofóbicas) ou que possuem muitos efeitos colaterais indesejados. Neste contexto, as nanopartículas oferecem proteção e veículo para tais moléculas. Para isso, cubossomos são nanopartículas capazes de encapsular tanto as moléculas hidrofóbicas como as hidrofílicas em sua estrutura. Cubossomos também apresentam aproximadamente 50% de áreas hidrofílica e hidrofóbica, sendo capaz de encapsular grandes quantidades de moléculas teóricamente. Particularmente, cubossomos são nanopartículas de fácil produção devido à sua matéria prima serem lipídios (por exemplo, monoleína (GMO) ou fitantriol (PHY)) que se auto associam em meio aquoso. Neste projeto, os dois lipídios citados foram escolhidos para a produção dos cubossomos empregando-se protocolos bem estabelecidos da literatura. Uma fármaco modelo, miltefosina (MILT), foi escolhida para o estudo da interação com as nanopartículas.

Cubossomos de monoleína (GMO) revelaram simetria cristalográfica $Im3m$ e parâmetro de rede de 15.3(7) nm, as nanopartículas apresentaram tamanhos em torno de 300(8) nm e PDI 0.160(20). MET revelou partículas quadradas com tamanhos ~350 nm e a crio microscopia mostrou partículas com estrutura interna bem definida e tamanhos variados (200 a 500 nm), os parâmetros de rede calculados se mostraram da ordem de ~10 nm, compatíveis com as medidas de SAXS. O encapsulamento da MILT nos cubossomos foi possível até 4% w/w sem perda de morfologia. Para 5% w/w MILT as nanopartículas já apresentavam perda de cristalinidade na sua estrutura, evidenciado por crio microscopia. Análise por MET revelou que quanto mais MILT era encapsulada nos cubossomos, maiores ficaram as nanopartículas. Com a amostra de 1.5% w/w foi feita a crio microscopia, que revelou cubossomos com estrutura interna bem definida e um envelope (possivelmente formado pelo polímero) na sua superfície. Os parâmetros de rede calculados foram da ordem de ~10 nm também.

O myverol (Myv) é uma mistura comercial que contém aproximadamente 60% de GMO, e neste projeto foi proposto um protocolo *bottom up* para cubossomos feitos de Myv. A produção dessas nanopartículas também revelou, por SAXS, estrutura cristalográfica Im3m e um parâmetro de rede de 12.30(12) nm. DLS apresentou partículas de tamanho 280(5) nm e polidispersão moderada 0.115(52). MET mostrou partículas quadradas e cúbicas com tamanhos de ~500 nm. O encapsulamento da MILT revelou que o fármaco interage com os cubossomos aumentando seu parâmetro de rede, até uma concentração de 4% w/w. Curiosamente, para algumas concentrações de MILT havia presença de outras estruturas evidenciadas por SAXS. MET revelou nanopartículas com muita polidispersão, com tamanhos variando entre 200 nm e 2 µm.

Cubossomos de PHY foram reproduzidos com sucesso a partir do protocolo escolhido, em meios aquoso, tampão PBS e 2.25% glicerol. SAXS revelou nanopartículas com simetria cristalográfica Pn3m e parâmetro de rede 6.74(04) nm. Por DLS, o tamanho das partículas foi de ~450 nm e polidispersão moderada 0.161(10). Medidas de NTA foram consistentes com DLS, mostrando uma larga distribuição de tamanhos e concentração de partículas $\sim 10^{16}$ partículas/mL. MET revelou cubossomos quadrados e mais arredondados de tamanhos variados. Criomicroscopia apresentou partículas com estrutura interna bem definida, tamanhos variados (confirmando a polidispersão) e parâmetro de rede calculado em ~6.5 nm, compatível com medidas de SAXS. Essas amostras também foram submetidas a liofilização e descobriu-se que mesmo depois da re-hidratação, as partículas ainda mantiveram as mesmas características da amostra original. A extrusão também foi feita com o objetivo de melhorar a polidispersão e controlar o tamanho das partículas, novamente, os cubossomos demonstraram manter sua estrutura interna depois desse processo, diminuindo seus tamanhos e diminuindo a polidispersão dos sistema. MILT foi encapsulada de duas formas: passiva (co-solubilização) e ativa (adição depois que as nanopartículas foram formadas). Com até 5% w/w de MILT incorporada, os cubossomos mantiveram sua estrutura cristalográfica, porém em concentrações de 10%, 15% e 20% w/w, o fármaco provocou transição de fase para simetria Im3m. Em baixas concentrações, MILT aumentou os parâmetros de rede dos cubossomos e a hipótese levantada foi que a droga se insere na bicamada lipídica das nanopartículas. DLS revelou que MILT não altera o tamanho das partículas nem sua polidispersão. MET revelou partículas quadradas e arredondadas com tamanhos maiores que os medidos por DLS. Para a amostra 4% w/w, a crio microscopia foi realizada e as partículas encontradas apresentaram estrutura interna e parâmetro de rede calculado ~7 nm, compatível com medidas de SAXS.

Co-solubilização e adição depois do preparo se mostraram equivalentes para o encapsulamento da MILT. Todas as amostras também foram submetidas a um estudo de temperaturas para investigar transições de fase, baseando-se nos diagramas de fase dos lipídios. Foi descoberto que os cubossomos, sem a droga, a 65 °C sofrem transição para a fase isotrópica L_2 e quando MILT está incorporada essa transição não acontece. DLS também revelou que as partículas não têm seus tamanhos alterados com o aumento de temperatura.

Por fim, cubossomos mostraram ser excepcionais conseguindo manter suas características físico-químicas mesmo quando submetidos a ambientes extremos, como a liofilização, a extrusão e a altas temperaturas.

Palavras chave: *drug delivery*, cubossomos, monoleína, fitantriol, miltefosina, nanopartículas de cristal líquido, SAXS, parâmetro de rede, Cryo-EM, estrutura cúbica

Abstract

MALHEIROS, B. **Biophysical Characterization of cubosomal nanoparticles intended for drug delivery applications and its interaction with a model drug: the miltefosine case.** 2018. Master thesis – Pharmaceutical Sciences Faculty, University of de São Paulo, São Paulo, 2018.

Nanomedicine is one of the most promising fields in nanotechnology nowadays. The use of nanoparticles as carriers aims to improve efficiency of drugs that possess low solubility in aqueous environment (very hydrophobic molecules) or that have a lot of undesired side effects. In this way, nanoparticles offer both a protection for the molecules and a carrying vehicle. On this ground, cubosomes are nanoparticles capable of storing both hydrophilic and hydrophobic molecules within its structure, in addition, cubosomes have approximately 50% hydrophilic and hydrophobic areas. Therefore, they can carry much more molecules than liposomes for instance. In particular, cubosomes are quite easy to produce due to its base product, lipids (like monoolein (GMO) or phytantriol (PHY)) that self-assembly in water media. In this project, both lipids were chosen to produce the cubosomes from well-established protocols in literature. A model drug, miltefosine (MILT), was chosen to study the interaction of such nanosystem with a guest molecule.

GMO cubosomes revealed to have $Im\bar{3}m$ crystallographic symmetry and lattice parameter 15.3(7) nm, particles presented sizes 300(8) nm and moderate polydispersion 0.160(20). TEM revealed squared particles with sizes \sim 350 nm, cryo-EM presented particles with internal structure and varied size (from 200 to $>$ 500 nm). From FFT analysis, the calculated lattice parameter remained in the order of \sim 10 nm compatible with SAXS measurements. MILT loading into cubosomes was possible up to 4% w/w without loss of cubosomes structure. For 5% w/w MILT, the nanoparticles were already losing their crystalline structure, as evidenced by cryo-EM. TEM analysis reveals that as more MILT is loaded into the cubosomes, their sizes increased. For sample 1.5% w/w MILT cryo-EM presents nanoparticles with organized internal structure and an envelope (hypothesized to be a polymer coating) in its surface. Calculated lattice parameters are in the order of \sim 10 nm.

Myverol (Myv) is a commercial mixture that contains \sim 60% GMO, in this project it was proposed a bottom up protocol for Myv-based cubosomes. The production of these

nanoparticles also revealed, by SAXS, $Im\bar{3}m$ symmetry and lattice parameter 12.30(12) nm. DLS revealed particle size 280(5) nm and moderate polydispersion 0.115(52). TEM shows square and cubic nanoparticles with sizes \sim 500 nm. MILT loading into Myv-cubosomes revealed that the drug interacts with the nanoparticle by enlarging their lattice parameter as more MILT is loaded (up to 4% w/w). Curiously, for some MILT concentrations the presence of other unknown cubic structures was evidenced by SAXS. TEM revealed nanoparticles with huge polydispersion, with sizes ranging from 200 nm to 2 μ m.

PHY based cubosomes were successfully reproduced by the chosen protocol, in both water, PBS buffer and 2.25% glycerol medium. SAXS revealed crystallographic structure $Pn\bar{3}m$ and lattice parameter 6.74(04) nm. DLS measured sizes \sim 450 nm and moderate polydispersion 0.161(10). NTA measurements were consistent with DLS, revealing a broad size distribution and total particle concentration of $\sim 10^{16}$ particles/mL for each sample. TEM revealed square and rounder particles in varied size. Cryo-EM micrographs presented particles with internal structure and varied size confirming moderate polydispersion. The FFT analysis revealed calculated lattice parameters \sim 6.5 nm, compatible with SAXS data. Samples were submitted to lyophilization and found that after re-hydration they still hold the same characteristics (morphology, size) as the original sample. Extrusion was also performed in order to improve polydispersion and control particle size, again cubosomes held their internal structure after the process, diminishing their sizes and improving monodispersity. MILT was loaded into cubosomes via co-solubilization and addition after the nanoparticles were formed. Up to 5% w/w the cubosomes incorporated MILT without loss of crystallographic structure, but at 10%, 15% and 20% w/w, the drug provoked phase change for $Im\bar{3}m$ symmetry. At the lower concentrations, MILT enlarged the lattice parameter of cubosomes and it was hypothesized that MILT inserted itself into the bilayer of the nanoparticles. DLS reveals that the drug does not change particle size or polydispersion. TEM revealed square and rounder particles in sizes slightly bigger than DLS. For sample 4% w/w, Cryo-EM presented particles with internal structure and calculated lattice parameter \sim 7 nm compatible with SAXS measurements for this sample. Co-solubilization and addition after nanoparticle preparation proved out to have the same effect on cubosomes loaded with MILT. All samples were submitted to higher temperatures to investigate phase change, based on phase diagram of the lipid. It was found that for the blank samples at 65 °C the cubosomes suffer phase change for isotropic phase L_2 , when MILT is loaded into the nanoparticles this phase change does not

happen. DLS revealed also that at higher temperatures, particle size does not change, neither polydispersion.

Finally, cubosomes proved to be remarkable nanoparticles that hold their physico-chemical characteristics even when submitted to extreme environments (lyophilization, extrusion and higher temperatures.)

Key-words: drug delivery, cubosomes, monoolein, phytantriol, miltefosine, liquid crystalline nanoparticles, SAXS, lattice parameter, Cryo-EM, cubic structure

“The scientist does not study nature because it is useful; he studies it because he delights in it, and he delights in it because it is beautiful”

Henri Poincaré

Acknowledgments

First of all, I would like to thank my family, my father Ricardo and my mother Lúcia, because without them it would never be possible for me to pursue my passion for science and physics. They always supported me both emotionally and with money, providing the perfect environment for me to develop myself professionally. I also would like to thank my sister Amanda for her friendship and companionship, when in moments of stress she always had a joke or a say that made me feel better.

Secondly, I would like to express my deepest gratitude for my supervisor Leandro Barbosa for trusting me this master project and the microscopies for the group. Without him pushing me and encouraging every day in the lab I would not have gained this much knowledge and astuteness I have now. I must thank for the encouragement in learning deeply about cryo electron microscopy and all detailed physical phenomena behind experiments. I thank a lot for all conversations, results discussions, experiments, lunches, general help and patients throughout this project. His advices and orientations were essential for guiding me to this academic life. His friendship I will take for all my professional and personal lives.

Third, I would like to thank my friend Laura Garcia Araujo, she is my dear friend since we were five years old. Without her friendship I would have been much less happy and less excited about everything in my life. I thank for all time spend with me and for all companionship. Even when we stayed weeks without seen each other, I would always receive a nice message from her. I wish this friendship lasts for as long as we live =)

I would also like to offer my special thanks my project friend Raphael Dias de Castro, for all companionship, discussions and python routines he borrowed me throughout these two years. I learned a lot of programming skills with him and also I laughed a lot about daily things. I also wish to carry his friendship forever.

I must also express my great appreciation for all Biophysics/Biosystems group: Juliana, Natalia, Frederico, Luiz, Giovana, Bruna, Mayra, Marcelo. Always making jokes and cheering for each other every day.

In addition, I thank prof. Dr. Rosangela Itri and her group for all discussion, group gatherings, laughs and support throughout these two years. Their friendship was a very

important part of my master. Prof Rosangela's advices and suggestions were fundamental for my professional growing.

I also thank prof. Dr. Carlota Rangel and her group for all help with pharmaceutical terms and experiment understanding, and for all group gatherings that taught me a lot about nanoparticles in pharmaceutical assays. With them I could learn a bit about the pharmaceutical point of view about my project. Their teachings enhanced my transdisciplinary vision of applied sciences.

I thank prof. Dr. Catherine Rigollet and Dr. Ali Najafi, from University of Groningen, for their nice friendship and support during my master.

I express my great appreciation to Dr. Alexandre Cassago for the cryo microscopy training at LNNano and for all good humor jokes and funny stories during the Cryo-EM sessions.

I thank Roberto Cabado for all TEM measurements at ICB-USP.

I thank Dr. Evandro Duarte for all help with DLS measurements.

I thank Ludmilla David and prof. Dr. Eneida de Paula for the NTA measurements.

I thank LNLS and LNNano for the usage of their facilities.

Last but not least, my gratitude for all financial support from Brazilian National Council for Scientific and Technological Development (CNPq) for my scholarship (process:133375/2017-0) and by the financial support from Coordenação de Aperfeiçoamento de Pessoal de Nível Superior (CAPES) – finance code 001. I also thank São Paulo Research Foundation (FAPESP) for financing a great part of the project (#2015/15822-1).

Summary

List of figures	3
List of tables	8
List of Abbreviations.....	9
1. Introduction	10
1.1 Nanotechnology and Nanomedicine	10
1.2 Cubosomes as drugs carriers	13
1.3 Miltefosine	21
2. Objectives.....	22
3. Materials and Methods	23
3.1 Materials.....	23
3.2 Equipments.....	23
3.3 Methods.....	24
3.3.1 Monoolein (GMO) based Cubosomes.....	25
3.3.2 Myverol (MYV) based Cubosomes	26
3.3.3 Phytantriol (PHY) based cubosomes.....	27
4. Experimental Techniques	29
4.1 Small angle X-rays scattering (SAXS).....	29
4.2 Dynamic light scattering (DLS)	35
4.3 Nanoparticle Tracking Analysis (NTA).....	38
4.4 Transmission electron microscopy and cryo-EM (TEM).....	40
5. Results and discussion.....	46
5.1 Monoolein based cubosomes	46
5.1.1 Effect of temperature on cubosomal structure.....	50
5.1.2 Miltefosine interaction	51
5.2 Myverol based cubosomes	58
5.2.1 Myverol based interaction with miltefosine	64
5.3 Phytantriol based cubosomes	69
5.3.1 PHY - cubosomes in the absence of MILT	70
5.3.2 Temperature influence – blank cubosomes	85
5.3.3 Miltefosine interaction with Phy-cubs	87
5.3.3.1 Co-solubilization method	87

5.3.3.2 Temperature influence for loaded cubosomes	98
5.3.3.3 Addition of MILT after cubosomal dispersion was prepared.....	101
5.3.3.4 Temperature effect on cubosomes for MILT added after preparation.....	110
6. Conclusions	113
7. Future Perspectives.....	114
8. Bibliography	115

List of figures

Figure 1. The variety of nanoparticles studied in the last 40 years of research, in terms of shape, materials used and potential additions to the nanoparticles surfaces. From (SUN et al., 2014).	11
Figure 2. Schematic of a multi stimuli nanoparticle, where it can be loaded with a drug and coated by a ligand to target a specific cell. Or nanoparticle that will be sensitive to stimuli such as pH, temperature. From (TORCHILIN, 2014).	12
Figure 3. Statistical data from Web of Science® platform for the researched topic "cubosomes", up to 2017. Accessed in 27/07/2018.	14
Figure 4. Chemical structures of a) monoolein (GMO) and b) phytantriol (PHY) lipid molecules. From: Pubchem.	15
Figure 5. Monoolein phase diagram. This molecule can self-assembly in various structures, from lamellar to cubic (Pn3m and Ia3d) and hexagonal depending on the hydration percentage and temperature. Curiously, at room temperature, for hydrations higher than 30% wt/wt only cubic structures are formed. Adapted from (CAFFREY, 2009).	16
Figure 6. PHY phase diagram in water. The molecule also shows great polymorphism in which approximately 30% of its phase diagram holds cubic structure. Adapted from (AKBAR et al., 2017)	17
Figure 7. Chemical structure of Pluronic® copolymer family. For F127: $x=100$ and $y=65$. From (CHONG et al., 2011)	18
Figure 8. Schematic structures of water channel disposition (green) and lipidic moiety of cubic self-assembly represented by the theoretical surfaces in blue. Adapted from (AZMI; MOGHIMI; YAGHMUR, 2015).	19
Figure 9. Interaction of the stabilizer polymer F127 with both PHY and GMO cubosomes, showing that Phy-cubs the polymer stays adsorbed in the surface of the nanoparticle and in the GMO-cubs the polymer interacts with the lipid bilayer inside the nanostructure. From (DONG et al., 2012).	20
Figure 10. Chemical structure of MILT. From Pubchem.	21
Figure 11. Flow chart for cubosomal production. In the TD approach, both lipid and polymer are melted forming a bulk phase when water is added. Then, a high energy input breaks the bulk phase into nanoparticles. For the BU approach, the lipid is solubilized into a hydrotome and this solution is dropwised to a polymer aqueous solution, making very small nanoparticles. A low energy input helps smaller particle to aggregate into bigger ones, forming the cubosomes.	25
Figure 12. SAXS scheme setup with an example of multi lamellar esicles sample. A X-rays source produces the primary beam and magnetic lenses define the volume of the beam. A sample holder is located in the beam path, so when X-rays pass through they are scattered by the sample in all directions. The detector, located in a distance of the sample read the incoming photons in a maximum angle of 2θ . The integrated image from the detector reveals a curve that gives information about the sample. From: http://www.mrl.ucsb.edu/~safinyaweb/XRD.htm	30
Figure 13. Example of some Bragg's planes. Adapted from https://sites.ifi.unicamp.br/lfmoderna/conteudos/difracao-de-raio-x/	31
Figure 14. Schematic of X-ray interaction with the crystal lattice. Incoming waves, all in phase, interact with different lattice planes, distanced by d . When interacting with the first surface plane, the wave scatter with an angle θ . When interacting with the second plane, the incoming wave needs to travel an additional length $d\sin\theta$. In order to the scattered waves to be again in phase, a condition needs to be obeyed. This condition is Bragg's Law. Adapted from: http://www.didaktik.physik.uni-muenchen.de/elektronenbahnen/en/elektronenbeugung/einfuehrung/bragg-bedingung.php .	31
Figure 15. SAXS data for PHY cubic bulk phase at 25 °C showing Pn3m symmetry. From (BARAUSKAS; LANDH, 2003).	33
Figure 16. DLS apparatus scheme. A laser is used to enlighten the sample followed by the detection at 90° by a photon detector. This data is then analyzed by a correlator that returns a function which gives information about	

<i>the size of the particles in the studied system. From https://lsinstruments.ch/en/technology/dynamic-light-scattering-dls.</i>	35
<i>Figure 17. DLS measured correlation functions and relation to particle size populations. From the fluctuation of the scattering light, the software calculates a correlation function that discriminates bigger from smaller particles by the shape of the curve. Subsequently, a distribution size is calculated. From: http://www.otsukael.com/product/detail/productid/23/category1id/2/category2id/2/category3id/32.</i>	36
<i>Figure 18. Detailed information about the correlation function of smaller particles (blue curve) and bigger particles (red curve). Note that for smaller particles in the sample, the correlation function decays to zero more rapidly than for bigger particles. Adapted from: https://www.news-medical.net/whitepaper/20141221/Using-DLS-Deconvolution-Algorithms-to-Acquire-Intensity-Weighted-Particle-Size-Distribution-from-Measured-Correlogram.aspx</i>	37
<i>Figure 19. Scheme of the NTA measurement apparatus. The sample is loaded into a glass chamber where a laser beam passes through the dispersion, particles scatter the light that is detected on an optical microscope. Particles can be inside and outside the objective focus. Then, from the recorded movie, single particles are followed and their mean displacement is measured, given the basis for size calculations. Adapted from (JARZEBSKI et al., 2017).</i>	38
<i>Figure 20. Screen shot of a recorded movie from NTA measurement software. Each white dot in the screen represents a particle in suspension, note that blurred dots are not in the focal plane of the objective, but they are still measured.</i>	39
<i>Figure 21. TEM schematics of the experimental apparatus. An electron gun generates the beam that hits the specimen. Through magnetic lenses, the transmitted beam is conducted to a fluorescent screen or directly to a camera in order to record data. Adapted from https://s10.lite.msu.edu/res/msu/botonl/b_online/e03/03e.htm.</i>	41
<i>Figure 22. Example of nanoparticles TEM micrograph, showing the square shape of the cubosomes,</i>	42
<i>Figure 23. Cryo-EM example of cubosomes micrograph. The structure inside each particle reveals details about the internal organization of each particle.</i>	43
<i>Figure 24. A cryo electron tomography gives information about the sample in different axis by rotating the sample holder. In this case, Sagalowicz et al. simulated reflections calculated for cubosomes diffraction as viewed by different axis. This was used as basis of the FFT analysis for the cryo-EM micrographs. Adapted from (SAGALOWICZ et al., 2007).</i>	44
<i>Figure 25. Schematics of the FFT analysis performed for each found particle in cryo-EM micrographs. First, a region inside the particle was chosen, then a FFT of that region was made. After indexing all planes based on Figure 24, a mask containing only one specific pair of planes was made. Subsequently, an inverse FFT was done with the mask and a plot profile reveals the interplanar distance between planes.</i>	45
<i>Figure 26. SAXS data for GMO-cubs with indexed diffraction peaks. This plot is typical from nanoparticles with internal structure, peaks indicating the reflections planes and the numbers attributed to them are the Müller indices (MAZZONI et al., 2016).</i>	46
<i>Figure 27. TEM Micrographs at left and a histogram (right) for obtained particle sizes from the TEM experiment. All found particles in the micrographs had sizes ~350 nm, compatible with DLS measurements.</i>	48
<i>Figure 28. Cryo-EM data for GMO-cubs sample. Micrographs show the internal structure the nanoparticles revealed by the entangled lines seen inside the cubosomes. Green arrows and the orange star point the presence of vesicles and a bigger vesicle which seems to be around the cubosome.</i>	49
<i>Figure 29. Calculated FFT for some particles in Figure 28. From these, a lattice parameter can be calculated.</i>	50
<i>Figure 30. SAXS data for GMO-cub sample in different temperatures. The blue curve shows cubosomes at 37 °C, in which peaks have shifted slightly, indicating that lattice parameter changed and the nanoparticles expelled from its structure as a response to temperature increase.</i>	51
<i>Figure 31. TEM micrographs for cubosomes loaded with MILT at different quantities. It is notable that up to 4% w/w cubosomes in square shapes still exist, only at 5% w/w the nanoparticles lose their shapes, being mostly spherical.</i>	53
<i>Figure 32. GMO-cubs size distribution histogram from obtained micrographs 0.5% w/w and 1% w/w MILT.</i>	54
<i>Figure 33. GMO-cubs size distribution histogram from obtained micrographs 1.5% w/w and 2% w/w MILT.</i>	54

Figure 34. GMO-cubs size distribution histogram from obtained micrographs 3% w/w and 4% w/w MILT. ____	54
Figure 35. Size distribution from histograms from the TEM micrographs (Figure 31) for the loaded GMO cubosomes. One can say that for concentrations higher than 3% w/w, MILT increases the size of the cubosomes. _____	55
Figure 36. Cryo-EM micrographs for 5% w/w MILT sample. Green arrows display vesicles present in the sample and the black arrow point to the detailed structure of a found particle, which presents some internal structure. _____	56
Figure 37. Cryo-EM micrographs for sample 1.5% w/w MILT. Arrows indicate vesicle particles coexisting with the cubosomes. In addition, an envelope is clearly seen around the particles, this is thought to be the F127 polymer acting on the surface of the cubosomes. _____	57
Figure 38. FFT's from some particles in the micrographs of Figure 37. Not all particle could give a clear FFT, therefore, only particles with the given shapes were taken into account for the lattice parameter calculation. _	57
Figure 39. SAXS data for myverol cubosomes a increasing F127 concentration relatively to the lipid weight. It can be seen that for low percentages, 5% to 8%, there is coexistence of phases Pn3m and Im3m in the sample. At higher F127 concentrations, only Im3m phase exists. _____	59
Figure 40. SAXS data for Myv-cubs in both water and glycerol media. Indexed peaks rise in the overall curve, revealing cubic structure for these cubosomes in both media. _____	60
Figure 41. TEM micrographs for MYV-cubs produced by bottom up (BU) method in water medium. Particles have a mean size around ~500 nm and they display leaked shapes, the assumption is that vacuum may have interfered in the overall shape of particles. Although their motifs continue to be square. _____	61
Figure 42. TEM micrographs for MYV-cubs in 2.25% w/v glycerol. Differently from water, in this sample besides cubosomes (pink circles), other particles appear in the sample (green arrows), they present varied shapes and some leakage. These other particles are thought to be formed by the other molecules in myverol. _	62
Figure 43. Myverol blank cubosomes SAXS data over temperatures. It is clear that over the influence of higher temperatures, the cubosomes go under phase transition from cubic phase (blue arrows) to hexagonal phase (green arrows). This feature is probable to happen due to the other molecules present in the myverol mixture. 63	
Figure 44. SAXS results for loaded Myv-cubs in water medium. The addition of MILT to the cubosomes does not destroy the crystallographic Im3m symmetry of the nanoparticles but alters its lattice parameter, given by the shifts in the peaks positions. _____	65
Figure 45. SAXS results for loaded Myv-cubs in 2.25% glycerol medium. The addition of MILT to the cubosomes does not affect particle crystallographic symmetry but at 0.5%, 1% and 2% there are other unknown particle structures in the sample, given by the peaks at low q values. Overall, for Im3m cubosomes, MILT only affects the lattice parameter inflicted by the first peaks shift for lower q values. _____	66
Figure 46. Calculated lattice parameters for Myv-cubs loaded with MILT in both water and glycerol aqueous media. Comparing values through statistical methods, MILT only significantly alters the lattice parameter of the cubosomes when in 4% w/w. _____	67
Figure 47. TEM micrographs for Myv-cubs loaded with 2%w/w MILT. Most particles presented square shapes with irregular surface. Significant size polydispersion is revealed since particles present varied sizes from ~400 nm to 2 μ m. _____	68
Figure 48. TEM micrographs for Myv-cubs loaded with 3%w/w MILT. Particles revealed square shapes and similarly to sample 2% w/w, polydispersion is also very present in these samples, where sizes fluctuate between ~400 nm to 1 μ m. _____	68
Figure 49. SAXS curve for cubosomes in water media with indexed crystallographic peaks. Each number refers to a crystallographic index, the Muller indices, which indicates the reflection planes in the diffraction peaks. ____	70
Figure 50. SAXS curves for cubosomes in different media (PBS, glycerol and water). It is clear that the change in aqueous media does not affect the cubosomes inner structure, once all curves were analogous. The difference in intensity only refers to a slight variation in the concentration of the samples (~25 mg/mL). _____	71
Figure 51. Lyophilized A) and extruded B) cubosomes in water medium. In both procedures the sample loses concentration, but when lyophilized this feature is far more evident. Although there is no change in the inner structure of the cubosomes after both processes. _____	73

Figure 52. Lyophilized A) and extruded B) cubosomes in PBS medium. Four peaks clearly rise in the lyophilized sample, showing that PBS seems to be a favorable environment for cubosomes formation after re-hydration. In the extruded sample, cubosomes also lose some concentration but all diffraction peaks are still visible. _____	74
Figure 53. Extruded samples in water media. A) Raw data from DLS, as can be seen, when extruded over the filters the particles have their correlation functions changed, moving toward smaller sized. B) Compilation of size stability over time: overall, the samples in all four weeks have shown to be very stable with no major fluctuations in the mean diameter. _____	75
Figure 54. NTA data for Phy-cubs in water medium. Cubosomes presented a wide size distribution before extrusion in a 0.05 μm pore filter (blue curve), with mean value $\sim 353(9)$ nm, after extrusion (red curve) the particles revealed mean size $\sim 200(3)$ nm. Interestingly, concentration of particles also increased when extruded, indicating that bigger particles were broken into smaller ones. _____	77
Figure 55. NTA data for Phy-cubs in PBS medium. The original sample (blue) also presented a broad size distribution with mean size $\sim 330(2)$ nm, the extruded sample (red) revealed particles with mean size $\sim 217(4)$ nm but no significant changes in particle concentration in the sample. The lyophilized sample (black) presented mean size $\sim 303(7)$ nm with great loss in particles concentration. _____	78
Figure 56. TEM micrographs of blank cubosomes in water. All found particles had sizes bigger than 500 nm. The micrographs with the orange star marking shows peculiar cubic structure in the sample, these structures are thought to be cubosomes, as seen by different planes in the electron microscope. _____	79
Figure 57. TEM data from literature. 1) Results from (NASR; GHORAB; ABDELAZEM, 2015) where the circle represents a GMO cubosome. 2) Results from (LUO et al., 2015) Both blank and with the studied drug, respectively. Both papers report sizes in TEM bigger than DLS. _____	80
Figure 58. TEM micrographs for Phy-cubs in PBS media. Comparing these particles with the ones in Figure 56, there is no difference in the shape of cubosomes, although, all found nanoparticles in PBS presented smaller size than those prepared in water. _____	80
Figure 59. Extruded cubosome in a 0.05 μm pore filter. Micrographs present nanoparticles in varied size, most of them particles reveal sizes ~ 300 nm, compatible with DLS measurements. _____	81
Figure 60. Lyophilized cubosomes in PBS media. Cubosomes present sizes similar to the original sample (see Figure 58). These data reinforces that cubosomes still hold cubic structure after lyophilization and rehydration. _____	82
Figure 61. Cryo-EM data for PHY cubosomes in water medium. Many particles were found with diverse sizes, indicating considerable polydispersion. Most particles present internal order given by the structure in their morphologies. Green arrows also display unilamellar vesicles and orange arrows display multilamellar vesicles _____	83
Figure 62. Cryo-EM micrograph of Phy-cubs showing the presence of vesicles in the sample coexisting with cubosomes. Green arrows display unilamellar vesicles and orange arrows display multilamellar vesicles. _____	83
Figure 63. Some calculated FFT's from particles in Figure 61. Some particles presented clearer FFT patterns than others, given by the easiness to recognize a pattern in the FFT. _____	84
Figure 64. SAXS data for Phy-cubs in water medium over temperature. Up to 50 $^{\circ}\text{C}$ cubosomes hold their internal structure, only expelling water, given by the peak shifting for higher q values. At 65 $^{\circ}\text{C}$ the system entered an isotropic phase. _____	86
Figure 65. SAXS data for Phy-cubs in PBS medium over different temperatures. Similarly to water, up to 50 $^{\circ}\text{C}$ cubosomes hold their internal structure Pn3m, the peak shifting for higher q values indicates that cubosomes expel water as the temperature rises. At 65 $^{\circ}\text{C}$ the system also became isotropic. _____	86
Figure 66. SAXS data for MILT loaded Phy-cubs at room temperature. From the curves, it is clear that MILT does not destroy the cubosomes internal structure, but it changes the diameter of the water channels, given by the peak shifting to lower q values. MILT enlarged the lattice parameter. _____	87
Figure 67. SAXS results for MILT loaded Phy-cubs in PBS (left) and glycerol (right) media. Similarly to water, MILT did not destroyed cubosomal internal structure but it shifted the peaks, indicating that an enlargement in the lattice parameters. _____	88
Figure 68. Calculated SAXS lattice parameters Phy-cubs in water, glycerol and PBS media. For all aqueous media, MILT increased the lattice parameter of the cubosomes. Taking for instance blank cubosomes vs 4% w/w	

MILT, a significant difference of ~1.0 nm was shown. Another interesting feature is that up to 1% w/w MILT has the same effect on lattice parameter for all three aqueous media, but for 2% w/w beyond, slight changes could be seen from water to PBS and glycerol.	89
Figure 69. DLS results for samples in water medium over a period of four weeks. MILT does not seem to influence particle size (left) neither polydispersion (right). Samples presented great stability over a month measured.	91
Figure 70. DLS results for Phy-cubs samples in PBS medium, followed over three weeks. Similarly to water, MILT does not seem to influence particle size (left), although, for 3% w/w and 4% w/w there is a significant reduction in particle size. Except from sample 2% w/w, polydispersion (right) was compatible between all samples.	91
Figure 71. TEM micrographs for Phy-cubs sample with loaded 3% w/w MILT in water medium. The found particles revealed sizes smaller than those detected by DLS.	92
Figure 72. TEM micrographs for Phy-cubs samples loaded with 3% w/w MILT in PBS medium. Curiously, the found particles presented sizes similar to DLS measurements. In this samples, cubosomes presented square and hexagonal shapes, indicating that nanoparticles were seen in different axis regarding the electron beam.	93
Figure 73. SAXS results for Phy-cubs loaded with higher amounts of MILT, through co-solubilization method, in water medium. MILT does not affect the cubosomal structure up to 10% w/w, but in this concentration, there is an indicative of a new phase forming (green arrow). For 15% and 20% w/w cubosomes assume the Im3m symmetry.	94
Figure 74. SAXS results for sample in PBS medium. Differently from water medium, in PBS the phase transition of cubosomes begins at 10% w/w with coexistence of phases. For both 15% and 20% w/w only Im3m cubosomes are seen in the colloidal dispersion.	95
Figure 75. Calculated lattice parameters for Phy-cubs in both Pn3n and Im3m phases. The green circle displays the calculated lattices for the Pn3m nanoparticles showing an increase as more MILT is encapsulated into cubosomes. The purple circle displays the calculated lattices for the Im3m phases, showing a great difference with the blank sample (0% w/w).	96
Figure 76. DLS measurements for samples with higher MILT quantities loaded in water medium. Sizes (left graph) do not seem to be altered by the higher quantities of loaded MILT, note that for 15% and 20% w/w, the mean diameters reflect sizes for the Im3m populations included. For PDI (right graph), the 15% and 20% w/w increases the polydispersion of the colloidal system due to the coexistence of different populations, Im3m and Pn3m.	97
Figure 77. DLS measurements for higher quantities loaded MILT cubosomes in PBS medium. Curiously, when loaded with the highest concentration of MILT, sizes (left) are much bigger than other samples and also PDI (right) is higher, note that this measurements reflect only the Im3m cubosomes in the sample. For all other loaded amounts (5%, 10% and 15% w/w) neither particle size or PDI values were altered by the presence of the drug.	98
Figure 78. SAXS data for sample 1% w/w MILT at different temperatures. In this concentration, MILT does not prevent cubosomes from undergoing phase transition at 65 °C.	99
Figure 79. SAXS data for sample 3% w/w MILT. Curiously, at this concentration cubosomes still exist at 65 °C. It can be inferred that MILT holds the structure together because it is inserted into the lipid moiety.	100
Figure 80. DLS measurements for size (left graph) and PDI (right graph) over temperatures. Curiously, temperature did not influence particle size or polydispersion. For samples 0% and 1% w/w MILT, sizes and PDI at 65°C reflect the measurements for the isotropic phase L2 (see PHY phase diagram, Figure 6).	101
Figure 81. SAXS results for cubosomes loaded with MILT from a stick solution after the dispersion was prepared. Interestingly, even for higher amounts of MILT (5% to 15%), the molecule did not changed the structure of the cubosomes as in the co-solubilization case (see Figure 73).	102
Figure 82. SAXS results for samples in PBS (left graph) and glycerol (right graph) media. Similarly to water, for low concentrations of added MILT, the molecules also inserts itself into the lipid moiety of the cubosomes. Interestingly, for higher quantities (10% and 15% w/w), the first peak from the Im3m structure also appears.	103

Figure 83. Calculated lattice parameters for cubosomes loaded with MILT after preparation. Up to 5% w/w loading, the lattice parameter was shifted by ~1 nm, but for higher concentrations (10% and 15%), an increase of almost ~3.5 nm was revealed.	104
Figure 84. Lattice parameter comparison for both co-solubilization and addition to already prepared cubosomes MILT loading methods. For water medium, both methods were proven to exert the same effect on the cubosomes.	105
Figure 85. Lattice parameter comparison for MILT loading methods in PBS and glycerol media. As can be seen, in PBS (left graph) the calculated lattices are higher when adding MILT after the nanoparticles preparation. For glycerol medium (right graph) this deviation is lower but still happens.	106
Figure 86. DLS measurements of size (upper graph) and PDI (down graph) for cubosomes loaded with MILT after preparation. Interestingly, MILT also does not seem to influence neither particle size or polydispersion.	107
Figure 87. Cryo-EM micrographs for sample 4% w/w MILT in water medium. In all micrographs, the internal structure of the cubosomes is well defined, the particles surface showed no features differently from the blank samples (Figure 61). Cubosomes in this sample have both rounder and square shapes and varied size, confirming the DLS measured polydispersion. The orange arrow points out a curious particle structure, in which the cubosome seems to be linked to a big vesicle, in addition, inside this structure other smaller vesicles and cubosomal particles can be found.	108
Figure 88. FFT of some particles from Figure 87. Notice that almost all FFT's have a hexagonal motif, while only one (blue star) displays a square motif, indicating that this particle alone was frozen in a tilted angle.	109
Figure 89. SAXS measurements for samples with loaded MILT after cubosomal preparation, in water medium. A) 1% w/w MILT, up to 50 °C the colloidal system is still cubic with all six peaks well defined, at 65°C there is coexistence of hexagonal (red arrows) and cubic phases. B) 3% w/w MILT and C) 5% w/w MILT present only cubic phase Pn3m throughout all temperatures. D) At 10% w/w MILT, as temperature rises, the first peaks of Im3m cubic phase (blue arrows) becomes more evident in the curve.	111
Figure 90. SAXS measurements for samples with loaded MILT after cubosomal preparation, in PBS medium. A) 1% w/w MILT, up to 50 °C the colloidal system is still cubic with all six peaks well defined, at 65°C there is complete phase transition for hexagonal phase (red arrows). B) At 3% w/w MILT there is coexistence of hexagonal (red arrows) and cubic phases at 65 °C. C) 5% w/w MILT and D) 10% w/w MILT only cubic Pn3m phase exists in the samples	112

List of tables

Table 1. Space groups symmetry for cubic structures possible for cubosomes.	34
Table 2. Peak positions and the calculated lattice parameter for GMO-cub.	47
Table 3. Interpretation of SAXS data for determination of cubic space group symmetry.	48
Table 4. Calculated quantities of MILT loaded into the cubosomes, both in mass, mg/mL and mol concentrations.	52
Table 5. Calculated masses and concentrations of incorporated MILT for Myv-cubs.	64
Table 6. Calculated chosen percentages of MILT incorporated into the cubosomes.	69
Table 7. Calculated Lattice parameters of cubosomes in different aqueous media. There is no change in the water channels of the nanoparticles prepared in water, PBS or glycerol.	71
Table 8. Peak positions and ratios for cubosomes samples in different aqueous media. Showing that Phy-cubs have Pn3m crystallographic symmetry.	72

List of Abbreviations

BU – Bottom up

Cryo-EM – Cryogenic transmission electron microscopy

DLS – Dynamic light scattering

FDA – Food and Drug Administration

FFT – Fast Fourier transform

F127 – Poloxamer 407 / Pluronic® F127

GMO – Monoolein

GMO-cubs – Monoolein based cubosomes

LNLS – Laboratório Nacional de Luz Síncrotron

LNNano – Laboratório Nacional de Nanotecnologia

MILT – Miltefosine

MYV – Myverol

Myv-cubs – Myverol based cubosomes

NTA – Nanoparticle tracking analysis

PBS – Phosphate buffered saline

PDI – Polydispersion

PHY – Phytantriol

PHY-cubs – Phytantriol based cubosomes

SAXS – Small angle X-rays scattering

TD – Top down

TEM – Transmission electron microscopy

1. Introduction

1.1 Nanotechnology and Nanomedicine

Nanotechnology is the field of study that addresses particles with dimensions no bigger than 1000 nm, where the first studies were conducted in 1958 (NIKALJE, 2015). Since then, nanotechnology has revolutionized many areas of knowledge and technology. This multidisciplinary area has been growing both in research and industry. For the past 40 years or so, the investments made in this very are considerably growing (CHENG et al., 2016). Nanotechnology encompasses many study fields, such as, materials, energy, agriculture, food, electronics, optics, medicine, biotechnology. Opportunities appear every day with the discovery of new features. To illustrate it, in electronics, a lot of storage devices like USB's and external HD's are only possible because the semiconductors now have higher efficiency due to nanotechnology achievements (LI; LIU, 2017). In food and agriculture areas, the advent of nanofertilizers, water retenders, nutrient monitors, nanosized food additives and nanocoating to preserve food along with food processing and packing are examples (SINGH et al., 2017). Finally, in materials, a variety of applications have grown, for example, industrial applications for recycling, nanomedicine, biotechnology, among others (KLEANDROVA et al., 2015).

Particularly in medicine, nanotechnology has brought great revolution (RIZVI; SALEH, 2018). The first generation of nanosystems for medicine were developed between 1950 and 1970, where the delivery mechanisms were not well understood yet and liposomes were the first nanoparticles used for drug delivery (MUDSHINGE et al., 2011). Most formulations were designed only for oral or transdermal administration and vaccines were the very first application (LEE; YUN; PARK, 2015). The second generation happened between 80's and 2010 where clinical trials took place (PARK, 2013). A lot of discoveries were made in this period. In the turn of the 21st century, it was found that nanosystems may behave differently and so research to better understand their characteristics began. In 1995 the first liposomal drug formulation (Doxil) was approved by the Food and Drug Administration (FDA) for the release of doxorubicin (ZHANG et al., 2008). From then, new ways of administrations have been available for nanosystems, for instance, as intravenous route.

The advantages of nanostructured systems for drug delivery can be named as follows: to improve pharmacokinetics, to obtain better targeting sites (improve specificity), to reduce side effects, to provide sustained and controlled release, to improve circulation time and bioavailability, among others (CAI et al., 2017). Biochemical reaction times are shorter, so these systems are much more sensitive (JURJ et al., 2017)(NIKALJE, 2015). On the other hands, drawbacks still need to be improved. Costs of production are the biggest disadvantage, along with their unique physico-chemical features that may induce differentiated body distribution and toxicity (MENG et al., 2018)(JENA et al., 2013).

Nowadays, we stand on the 3rd generation of nanotechnology in drug delivery and some new formulations are already marketed in Europe and the USA (GAN et al., 2013), others are in final clinical trials and regulatory approval steps (KAURAV et al., 2016)(MURA; NICOLAS; COUVREUR, 2013). With the better understanding of the structural characteristics of the nanosystems, a variety of different shapes and formats for nanoparticle design has been developed in the last years, Figure 1 shows the most common and studied nanoparticles (NALLA, 2017)(SUN et al., 2014).

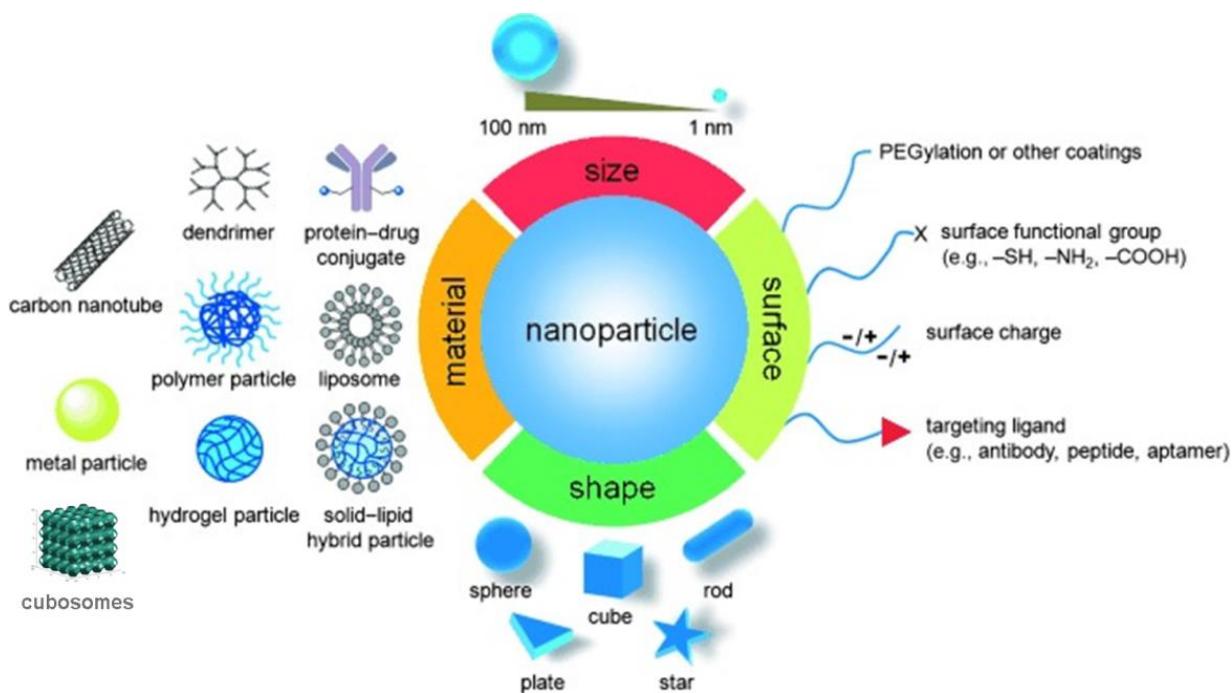


Figure 1. The variety of nanoparticles studied in the last 40 years of research, in terms of shape, materials used and potential additions to the nanoparticles surfaces. From (SUN et al., 2014).

Nanoparticles can be made of a variety of materials, from metals (Au or Ag) to lipids, polymers and carbon. All the prime-matter materials must be biodegradable and biocompatible (JURJ et al., 2017). Their shapes define the physicochemical properties and how each nanoparticle will release the load. Many structures are being studied, for instance, micelles, liposomes, dendrimers, hydrogels, vesicles, cubosomes, polymersomes, among others (AKHTER et al., 2018). In addition, shape is also variable, going from regular spherical arrangement to rod like, to amorphous and even cubic arrangement. Each shape is thought to better fit a designed application (WAKASKAR, 2018)(ANSELMO; MITRAGOTRI, 2017). Therefore, nanoparticles properties such as shape, surface charge and lipophilicity, size, geometry, density, etc. are important features that determine the nanoparticle lifetime and possible application. Most nanosystems can be pictured as macromolecular matrices in which drugs are dispersed on their bulk or external surface (BLANCO; SHEN; FERRARI, 2015)(CABAN et al., 2014).

With the better understanding of physico-chemical properties of the nanoparticles, the arising theranostic field of study promises to develop nanoparticles with multi stimuli, helping on both imaging and treatment at the same time (TEBALDI et al., 2018)(NASERI et al., 2018)(BAO; MITRAGOTRI; TONG, 2013). These nanosystems must be able to encapsulate and hold targeting agents in their structures, as shown in Figure 2. These nanoparticles will be the future of medicine and diagnosis (LIU et al., 2016). Liposomes are the most used nanoparticles for theranostic purposes, but other structures are also being quoted, due to their higher encapsulation potential, this is the case of cubosomes (BOLLA et al., 2018)(TORCHILIN, 2014).

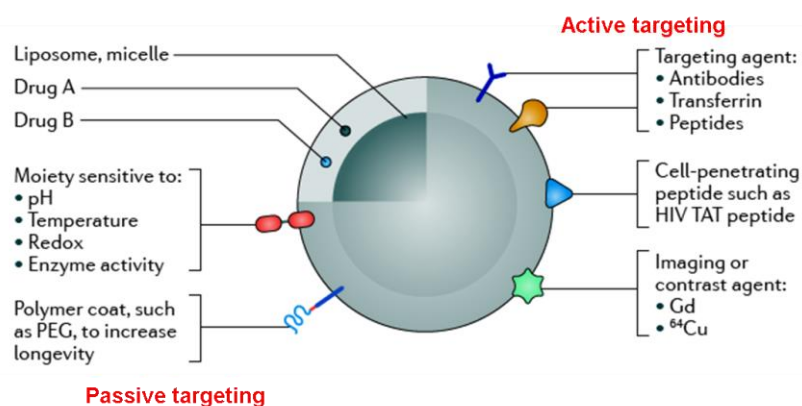


Figure 2. Schematic of a multi stimuli nanoparticle, where it can be loaded with a drug and coated by a ligand to target a specific cell. Or nanoparticle that will be sensitive to stimuli such as pH, temperature. From (TORCHILIN, 2014).

Finally, in terms of targeting, for cancer cases for instance, there are two main approaches, “passive” or “active”. For passive targeting the nanoparticles accumulate on the desired area through the enhanced permeability and retention effect (EPR), due to their reduced sizes and since tumors present high vascular blood vessels around them, nanoparticles have a great probability of be attached there (JURJ et al., 2017)(CABAN et al., 2014). Active targeting stands for nanoparticles that carry ligands within its structure, they can be remotely applied and targeted the desired tissue/organ. Usually, the number of nanosystems that reach the targeted area is the same for both targeting approaches, but *in vitro* studies show that nanoparticles with ligands show superior cellular uptake (LEE; YUN; PARK, 2015).

Regardless of the administration route, nanoparticles interact with cells predominantly via phagocytosis, pinocytosis, mediated internalization or fusion with cellular membrane, after that they undergo cellular internalization in which drug release happens (MUNTIMADUGU; KOMMINENI; KHAN, 2017)(DESHPANDE; SINGH, 2017). Depending if the drugs are located into the hydrophobic or hydrophilic moieties, release mechanisms can be varied. Sustained delivery can be achieved by diffusion of the drug throughout the matrix of the nanoparticle. There is also burst delivery, when nanoparticles are degraded or suffer erosion and then release the drugs into cellular media (AKHTER et al., 2018)(MO; MILLERET; NAGARAJ, 2017). The shape of the nanosystem will rule the release processes (BLANCO; SHEN; FERRARI, 2015).

1.2 Cubosomes as drugs carriers

Cubosomes are new nanoparticles that began to be get attention in 1995, as can be seen in Figure 3, with the first publications explaining cubosomes morphology (STEN ANDERSSON, M. JACOB LIDIN, 1995). In previous years, the discussion about bicontinuous liquid crystal phases was already happening, and authors could already see the applications for drug delivery (MARIANI; LUZZATI; DELACROIX, 1988)(LUZZATI et al., 1968)(LUZZATI; HUSSON, 1962). The bulk phase of these liquid crystals was well known along with their modeled morphological surfaces (ANDERSSON et al., 1999). A number of lipids (mainly monoglycerides, glycolipids, urea amphiphilies, phytantriol...) were found to

show polymorphism in which the cubic phases would also be formed (MO; MILLERET; NAGARAJ, 2017)(AZMI; MOGHIMI; YAGHMUR, 2015).

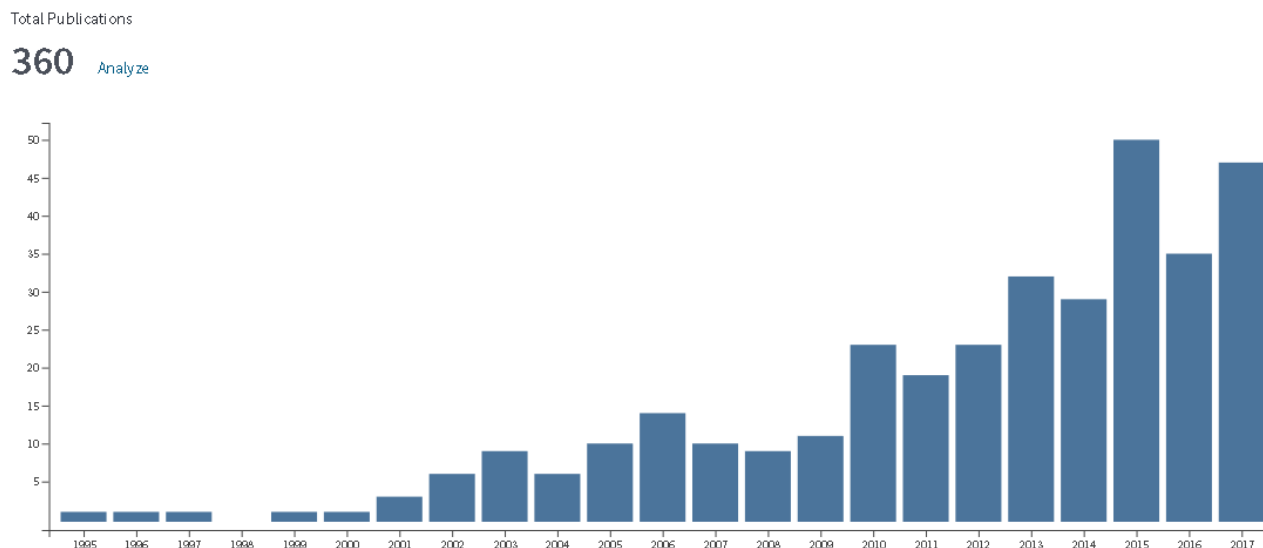


Figure 3. Statistical data from Web of Science® platform for the researched topic "cubosomes", up to 2017.

Accessed in 27/07/2018.

Not all lipids can self-assemble into cubic structures due to their shapes and critical packing parameter, in general, amphiphilic molecules and surfactants have this capacity. Mainly, the hydrophobic effect along with van der Waals interactions rule the ordering of the molecules (KULKARNI, 2012) and there are ordered and amorphous kinds of self-assembly. A phase diagram of a molecule displays its polymorphism at given degrees of hydration, revealing the all possible assembly structures (AZMI; MOGHIMI; YAGHMUR, 2015). The packing parameter is a theoretical measurement that can predict which phases may preferentially be formed to a given lipid, once the lengths and volume of the hydrophobic chain are known, as well as the surface area of the polar head group (RIZWAN; BOYD, 2015).

Cubosomes are soft tridimensional nanostructures composed by non-connected water channels that are formed by lipid bilayers, in which three possible cubic structures can be formed (LANCELOT; SIERRA; SERRANO, 2014) they will be presented as follows. This cubic phase is regarded as the most complex in liquid crystalline systems and the size of water channels, thus the capacity to be loaded, differs from one phase to another (LAKSHMI et al,

2014). Furthermore, these nanoparticles come from the breaking of bulk cubic phases, resulting in a colloidal suspension (KARAMI; HAMIDI, 2016)(PAN et al., 2013).

A few amphiphilic molecules can self-assemble into cubic structure, but the most studied ones are glyceryl monooleate/monoolein (GMO) and phytantriol (PHY), Figure 4 shows their chemical structures.

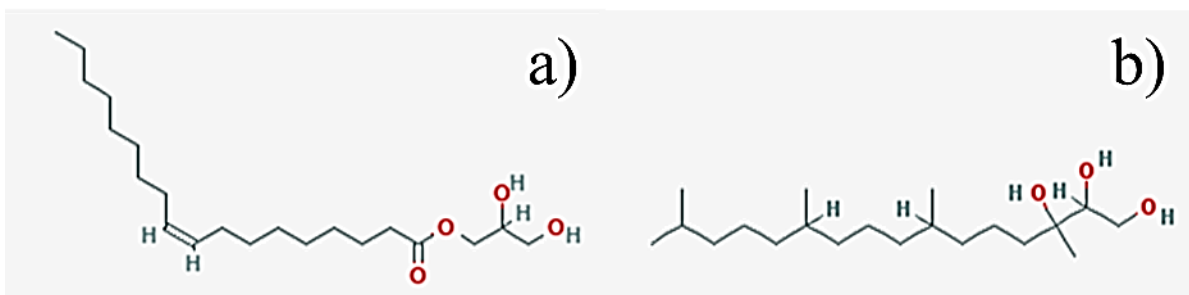


Figure 4. Chemical structures of a) monoolein (GMO) and b) phytantriol (PHY) lipid molecules.

From: Pubchem.

GMO is an interesting molecule for nanocarrier production, once it is non-toxic, biodegradable and biocompatible, being used in food industry as an emulsifier (SERIEYE et al., 2017). GMO is considered generally recognized as safe (GRAS) and approved by the Food and Drug Administration (FDA) for usage in food additives. This molecule also presents hemostatic effects and antibacterial properties (ERICSSON et al., 2009). Figure 5 shows monoolein phase diagram, where it can visit cubic structures (Pn3m and Ia3d) as well as lamellar and hexagonal phases. Its geometry favors the formations of cubic structure, once approximately 50% of the phase diagram is composed by this structures (PAN et al., 2013). Interestingly, GMO is able to self-assemble into cubic structure in excess of water (> 50% w/w) as Figure 5 shows.

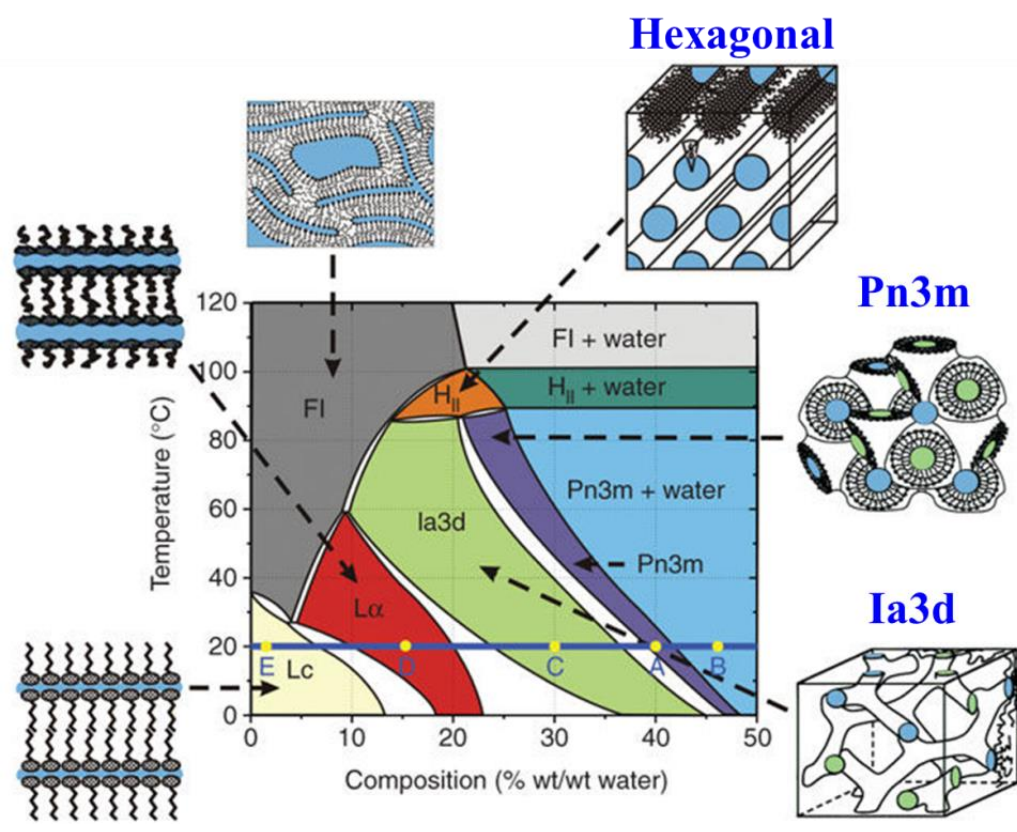


Figure 5. Monoolein phase diagram. This molecule can self-assemble in various structures, from lamellar to cubic (Pn3m and Ia3d) and hexagonal depending on the hydration percentage and temperature. Curiously, at room temperature, for hydrations higher than 30% wt/wt only cubic structures are formed. Adapted from (CAFFREY, 2009).

The other studied molecule, phytantriol (PHY), has been explored for cubosomes production since the 2000's. It is also biocompatible, has cosmetic applications and displays cubic self-assembled structure in excess of water (BARAUSKAS; LANDH, 2003). Its phase diagram is quite similar to that of GMO, as shown in Figure 6, where Pn3m and Ia3d are the cubic phases. PHY became an interesting molecule to nanocarrier production because it does not have a saturation in the alkyl chain, as GMO has, along with the absence of an ester bond in the polar head group, making PHY less susceptible to degradation by the gastrointestinal track, compared to GMO (KARAMI; HAMIDI, 2016). Nguyen et al. (NGUYEN et al., 2011) have simulated a digestion with HCl and pancreatic enzymes, finding that PHY cubosomes did not change their cubic phases when exposed to acidic environment or enzymes for several hours. In contrast, GMO cubosomes changed for hexagonal phase during the same process. It was hypothesized that the molecule suffered cleavage and acid-catalyzed

degradation (NGUYEN et al., 2011). This makes PHY a more suitable lipid for cubosomal production aiming oral administration due to its higher chemical stability.

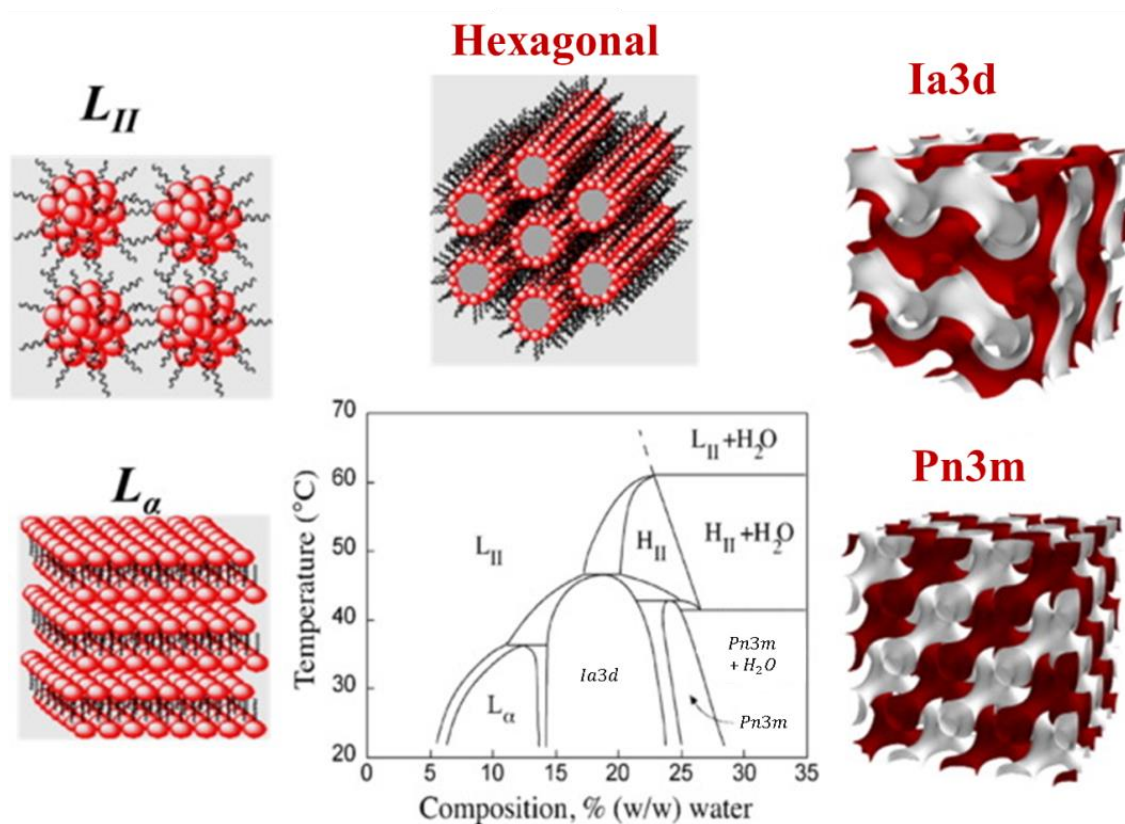


Figure 6. PHY phase diagram in water. The molecule also shows great polymorphism in which approximately 30% of its phase diagram holds cubic structure. Adapted from (AKBAR et al., 2017).

Cubosomes show high surface area ($\sim 400 \text{ m}^2/\text{g}$) and can incorporate both hydrophobic, hydrophilic and amphiphilic molecules (LAKSHMI, et al. 2014). Approximately 50% of the nanoparticle volume is hydrophobic, making the cubosomes suitable for high drug load (ESPOSITO, MARIANI, DRECHSLER, 2016). These nanoparticles also have two main conformations, an “open” one, where the water channels communicate with the external medium, and a “closed” one, in which only one channel communicates with the external environment. It is thought that the “closed” conformation gives more stable cubosomes, but both conformations are present in a colloidal dispersion (KIM et al., 2015). Rizwan et al (RIZWAN et al., 2007) studied GMO and PHY cubosomes with cryo field emission scanning electron microscopy and found that nanoparticles displayed tortuous structure with both spherical and cubic morphologies. (RIZWAN et al., 2007). This features

influence drug release, that in cubosomes case is mostly sustained through diffusion. In addition, when a drug is incorporated into the nanoparticle, it becomes part of its matrix and molecules can be loaded into the cubosomes via both cosolubilization or added after the nanoparticles were formed. External disturbances of temperature, pH, pressure, osmotic imbalance can also influence drug upload and release (MO; MILLERET; NAGARAJ, 2017).

When the bulk phase is broken into nanoparticles, in order to prevent aggregation, a stabilizer (usually a polymer) is added to the colloidal system. In the literature, the most employed stabilizer is a triblock copolymer Poloxamer 407 (commercially known as Pluronic F127®)(F127), see Figure 7, which restrain coalescence by steric repulsion (KARAMI; HAMIDI, 2016). Other molecules have also been reported to perform the same role as F127, such as tween 80, oleic acid and vitamin E (SERIEYE et al., 2017)(YOUNUS et al., 2018)(FRASER et al., 2013)(CHONG et al., 2011). F127 is a biocompatible molecule, nontoxic and approved by the FDA for pharmaceutical usage (KHATTAK; BHATIA; ROBERTS, 2005)(DUMORTIER et al., 2006).

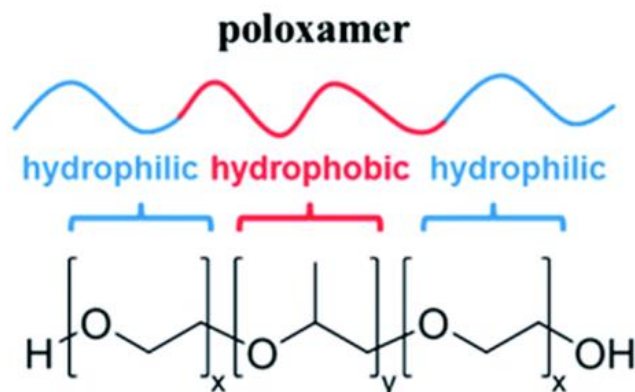


Figure 7. Chemical structure of Pluronic® copolymer family. For F127: $x=100$ and $y=65$. From (CHONG et al., 2011)

In cubosomes nanoparticle formulations, GMO presents another crystallographic structure (Im3m) due to the addition of F127 (LANCELOT; SIERRA; SERRANO, 2014), in this new structure, the disposition of the water channels change, as can be seen in Figure 8.

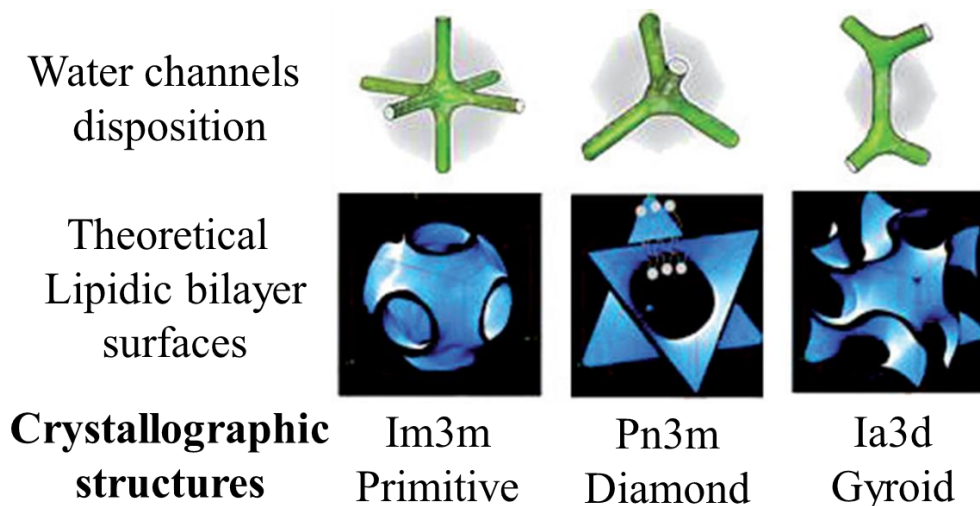


Figure 8. Schematic structures of water channel disposition (green) and lipidic moiety of cubic self-assembly represented by the theoretical surfaces in blue. Adapted from (AZMI; MOGHIMI; YAGHMUR, 2015).

F127 molecules interact with lipid monolayers by inserting itself into hydrophobic spaces, therefore tightening lipidic molecules (PATEL et al., 2009). The polymer also has amphiphilic properties, therefore, in PHY cubosomes, it is thought to be on the external surface, once the structural crystallographic parameters of colloidal system from PHY and PHY+F127 do not change. On the other hand, for GMO cubosomes, F127 has been shown to interact with the bilayer of the nanoparticle, once the crystallographic parameter as well as the inner structure change in the presence of a polymer (DONG et al., 2012), as shown in Figure 9.

Finally, other polymers from the Pluronic® family can be used as stabilizer, making cubosomes with the same crystallographic structure as F127, or diverse. In a study by Chong et al. (CHONG et al., 2011) various types of poloxamer/pluronics were studied and it was shown that P123, P104 and P84 makes PHY cubosomes with different crystallographic structures (CHONG et al., 2011).

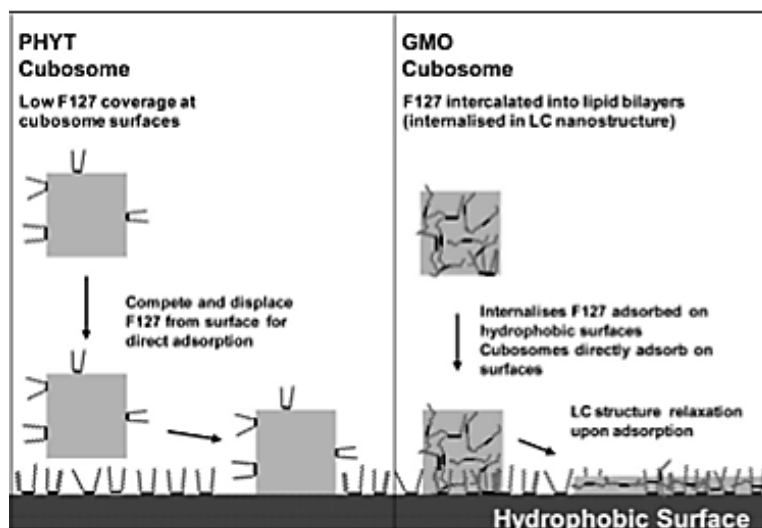


Figure 9. Interaction of the stabilizer polymer F127 with both PHY and GMO cubosomes, showing that Phy-cubs the polymer stays adsorbed in the surface of the nanoparticle and in the GMO-cubs the polymer interacts with the lipid bilayer inside the nanostructure. From (DONG et al., 2012).

The main advantages of using cubosomes are that this nanosystem can carry more than one drug or two different molecules (for instance a peptide and a drug, or a ligand and a drug) and the higher hydrophobic volume enables cubosomes to support large drug loads in its matrix (KARAMI; HAMIDI, 2016). When prepared in a sterile environment, the colloidal suspension is said to be stable for months without changes on its internal structure (RIZWAN; BOYD, 2015). Finally, cubosomes are nanoparticles resistant to pH variations, a few studies were conducted in the past showing that the nanoparticles retain cubic structure even in acidic media. Most papers report the activity of GMO cubosomes only, showing that PHY has not been well explored in this subject yet. Muller et al showed that GMO cubosomes exist in pH 6 and 10 with coexistence of Im3m and Pn3m phases (MULLER; SALONEN; GLATTER, 2010). Nazaruk et al also have studied both GMO and PHY cubosomes in 5.5, 5.8 and 7.5 pH showing the nanoparticles do not alter their internal structure (NAZARUK; MAJKOWSKA-PILIP; BILEWICZ, 2017)(NAZARUK et al., 2014).

1.3 Miltefosine

Miltefosine, hexadecylphosphocholine (MILT), belongs to the class of synthetic alkylphospholipids that was first synthesized in 1985 (PACHIONI et al., 2013). Its structure is shown in Figure 10.

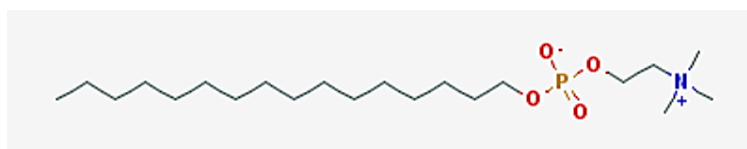


Figure 10. Chemical structure of MILT. From Pubchem.

MILT is efficient for treatment of fungal, bacterial infections. It also presents a strong antineoplastic effect (MUNOZ et al., 2013) and potency against leishmanial activity (RÍOS-MARCO et al., 2017). Since its approval, by the FDA in 1992, MILT has been used for oral treatment of visceral and cutaneous leishmaniasis in a maximum single dose of 20 mg/kg (EISSA et al., 2015) in the following countries: India, Germany, Colombia and United States (BARIONI et al., 2015). For cancer treatment, it has only been approved for topical treatment in breast skin cancer metastases cancer and cutaneous lymphoma (ALONSO; ALONSO, 2016).

The mechanisms of action of MILT are related with disturbing the cell membrane and interfering with phospholipid metabolism (PACHIONI et al., 2013). In more detail, recently a simulation study was performed by Malta de Sá et al. in which results show that MILT has a preference to interact with membranes containing cholesterol, therefore interacting with the cell lipid rafts signaling (DE SÁ et al., 2015).

MILT while a very interesting molecule for medicine, it presents high gastrointestinal toxicity and high hemolytic potential, limiting its applications and administered dose (DA GAMA BITENCOURT et al., 2016). MILT is also a very hydrophobic molecule, its critical micellar concentration (CMC) is approximately $\sim 50\mu\text{M}$ (BARIONI et al., 2015) and LogP 6.7 (from Pubchem). Hence, it is important to study this molecule interaction with nanoparticles in order to make its use more efficient, preventing side effects while enhancing the drug efficiency.

2. Objectives

The main goal of this project was to produce and characterize the cubosomal dispersion in the presence and absence of miltefosine (MILT).

For that purpose, first we were dedicated to find in literature a suitable protocol for cubosomes production, both for GMO and PHY lipids. The cubosomes dispersions were characterized by a number of biophysical techniques, like small angle X-rays scattering, dynamic light scattering, nanoparticle tracking analysis and electron microscopy.

After that, we studied the interaction of MILT with both GMO and PHY cubosomes in a wide range of MILT loading. In this period, the goal was to define the MILT amount that altered the structure of the cubosomes.

Once reaching a reproducible system, techniques such as extrusion and lyophilization were performed in order to study possible ways of conserving the cubosomal dispersion and to have a better control of size and polydispersion of the nanoparticles.

Results are divided in three main parts: GMO/Myverol cubosomes and PHY cubosomes. Each part presents the results obtained with each studied system separated into blank samples (0% MILT), temperature influence and interaction with MILT.

3. Materials and Methods

3.1 Materials

Materials used in the project:

- 1-Oleoyl-rac-glycerol $\geq 99\%$ - Monoolein/ Glycerol Monooleate – (356.6 g/mol and 0.969 g/cm³)
- Hexadecyl phosphocholine $\geq 98\%$ - Miltefosine (407.6g/mol and 1.020 g/cm³)
- Pluronic® F-127 – Poloxamer 407 – purified (102.1 g/mol and 1.095 g/cm³)
- Phosphotungstic acid hydrate - $H_3[P(w_3O_{10})_4] \cdot H_2O$

All purchased products from Sigma-Aldrich®/Merk® were used as received.

- (2S,3S)-3,7,11,15-tetramethylhexadecane-1,2,3-triol $>99\%$ - Phytantriol (330.5 g/mol and 0.932 g/cm³)

Purchased from Avanti Polar Lipids Inc.

- Ethyl Alcohol (Ethanol) 99.5% - Dinâmica Química Contemporânea Ltda.
- Methyl Alcohol 99.8% - CAQ – Casa da Química Ind. e Comp. Ltda.
- Ultrapure water from Milli-Q® water – Merck Millipore - Integral Water Purification System for Ultrapure Water
- Myverol 18-99k was a gift from Kerry® Bio-Science Inc. (Campinas - Brazil) and it was used as received.

3.2 Equipments

- Precision Balance – BEL Engineering model M124A
- Ultrasonic bath Emasonic E30H - Elma Schmidbauer GmbH - Potency 240 W
- Heat Bath – Novatécnica Equipamentos para Laboratório – NL1225
- Digital Termo-Hygrometer model 7666-02-0-00 - Incoterm
- Rotary evaporator – Fisatom model 804 70-130 W 60 Hz

- Magnetic Stirrer – LGI Scientific – 0-2500 rpm 500 W
- Solution stirrer AP56 – Phoenix Lufanco – 3800 rpm
- Pipette series – LabmatePro – HTL Lab Solutions
- Mini Extruder – Avanti Polar Lipids Inc.
- Polycarbonate membranes for extrusion (0.4 μm , 0.2 μm , 0.1 μm . 0.05 μm and 0.03 μm pore size) – Avanti Polar Lipids Inc.
- Liotop® L101 Lyophilizer

3.3 Methods

Cubosomes can be produced by two main methods, a top down and a bottom up approaches (KARAMI; HAMIDI, 2016). A flow chart explains and points out the differences between methods, see Figure 11.

In the top down method (TD), both lipid and stabilizer polymer are melted together and the addition of water to the mixture forms a bulk phase. The nanoparticles are formed by the breaking of the bulk phase with the addition of a high energy input, such as sonication or homogenization (SPICER et al., 2001)(MURGIA et al., 2010)(ESPOSITO et al., 2015). This method often produces cubosomes with varied size and considerable polydispersion (NAZARUK; MAJKOWSKA-PILIP; BILEWICZ, 2017).

In the bottom up (BU) approach, the lipid is solubilized into a hydrotope (often an alcohol) and dropwised into a polymer aqueous solution. Small particle particles are formed in this process, then a low energy input (magnetic stirring or vortexing) is applied in order to aggregate the smaller particles into bigger ones (SPICER et al., 2002)(RIZWAN et al., 2011)(AZHARI et al., 2016). This method is known as crystallization from precursors and it is known to produce cubosomes with similar sizes and lower polydispersion comparing to TD approach (KIM et al., 2018).

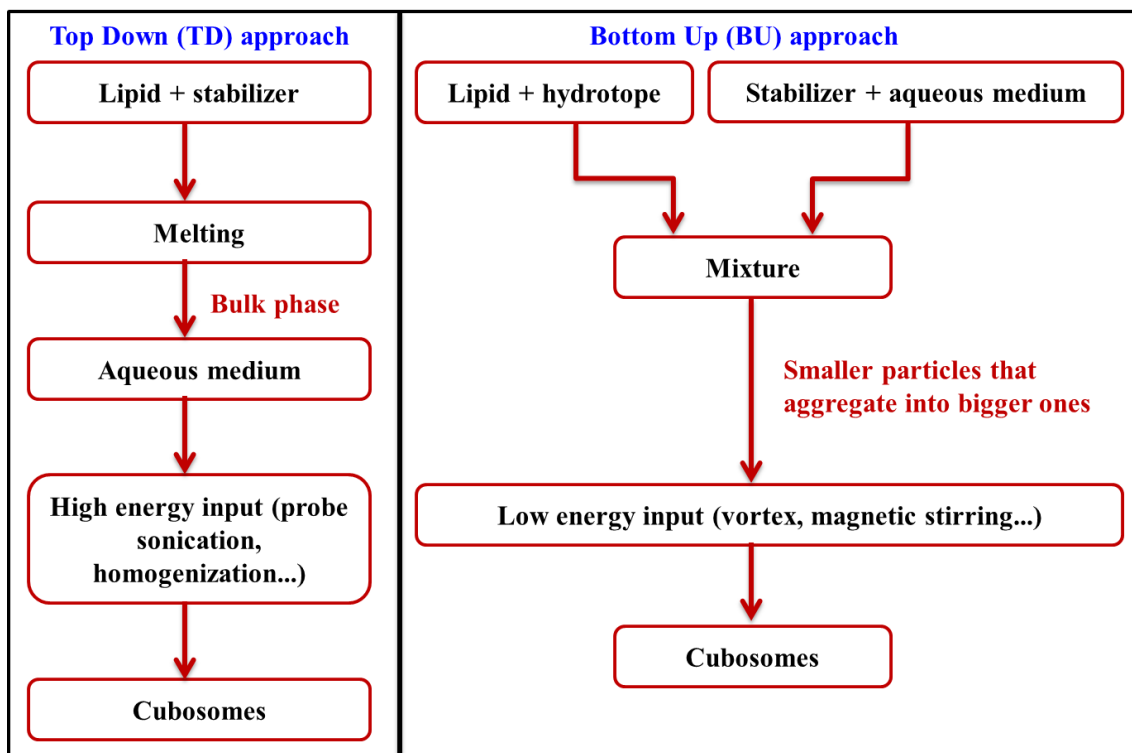


Figure 11. Flow chart for cubosomal production. In the TD approach, both lipid and polymer are melted forming a bulk phase when water is added. Then, a high energy input breaks the bulk phase into nanoparticles. For the BU approach, the lipid is solubilized into a hydrotope and this solution is dropwised to a polymer aqueous solution, making very small nanoparticles. A low energy input helps smaller particle to aggregate into bigger ones, forming the cubosomes.

3.3.1 Monoolein (GMO) based Cubosomes

In the beginning of the project, the protocol developed by Spicer et al. was chosen to produce the monoolein (GMO) based cubosomes in the top down (TD) approach (SPICER et al., 2001). The following production steps were taken.

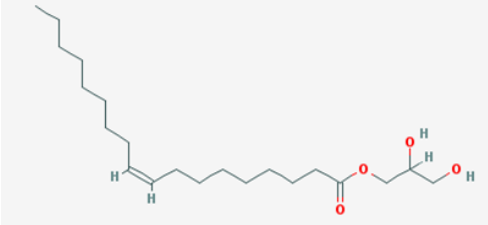
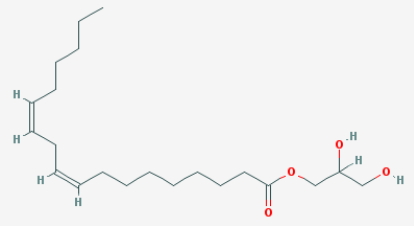
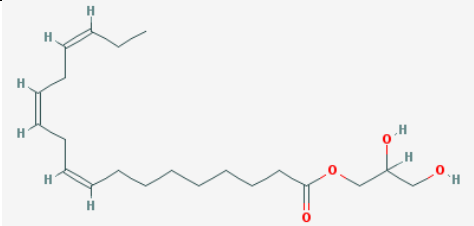
Monoolein (GMO) and Poloxamer-407/Pluronic-F127 (F127) were weighted in mass proportions (92:8). The final solution had the following proportions in mass: 98% water, 1.8% GMO and 0.2% F127. Briefly, 46 mg of GMO and 4 mg of F127 were weighted together and melted, after that, 3mL of ultrapure water was added to the melted mixture. The final suspension was brought to a bath sonicator at 60 °C for an hour. At the end of the process, a milky solution was formed. Samples were kept stored at room temperature until experiments were performed.

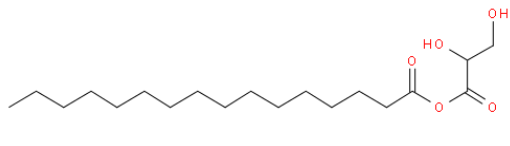
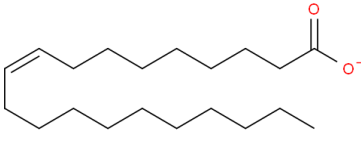
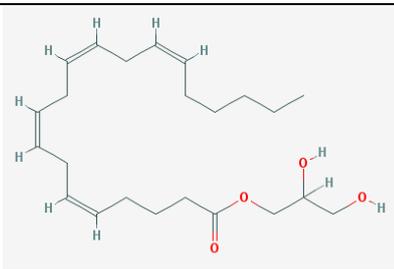
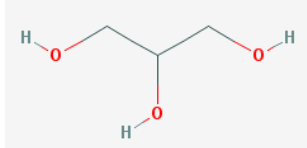
For the loaded cubosomes, MILT was first put into a stock solution of 10 mg/mL (4.9 mM) in methanol. Then, chosen percentages of MILT were added to the melted solution before the addition of water.

3.3.2 Myverol (MYV) based Cubosomes

After receiving myverol (MYV) 18-99k from Kerry®, a protocol was proposed by us, in an attempt to find a bottom up (BU) approach for GMO based cubosomes.

MYV is known to be a mixture of lipids (monoglycerides) which contains at least 60% of glyceryl monooleate (GMO) (CLOGSTON et al., 2000)(DONG et al., 2010)(HEDEGAARD et al., 2013)(PHAM et al., 2015)(VAN 'T HAG et al., 2017). The following table discriminates each found molecule in the MYV mixture along with their chemical structures.

Chemical composition of Myverol 18-99K - (DONG et al., 2010)		
Percentages (%)	Molecule	Chemical Structure (From Pubchem)
58.3	glyceryl monooleate	
12.2	glyceryl monolinoleate	
5.1	glyceryl monolinolenate	

3.9	glyceryl monopalmitate	
1.7	glyceryl monostearate	
0.96	glyceryl monogadoleate	
0.2	glyceryl arachidonate	
0.1	free fatty acids	--
0.04	glycerol	

The following protocol was proposed to produce GMO based cubosomes. First, 100 mg of GMO (approximately 154 mg of MYV) was weighted and solubilized into 5 mL of ethanol. Then, 50 mg of F127 was solubilized into 22.5 mL of ultrapure water. Both solutions were kept at 60 °C. Subsequently, the MYV suspension was dropwised into the F127 solution. The final mixture was kept under magnetic stirring at 60 °C for 15 minutes. Finally, the solution (~30 mL) was brought to a rotary evaporator for approximately 10 minutes until the final volume was lower than 4 mL. Then the resulting concentrated solution was completed to a final volume of 4 mL.

For the loaded cubosomes, MILT was first put into a stock solution of 10 mg/mL (4.9 mM) in methanol. Then, chosen percentages of MILT were added to the GMO/ethanol solution.

3.3.3 Phytantriol (PHY) based cubosomes

The chosen protocol was a bottom up (BU) approach based on the detailed study by Akhlagui et al. (AKHLAGHI et al., 2016). Briefly, 100 mg of PHY was weighted and solubilized into 10 mL of ethanol (~30 mM). Then 25 mg of F127 was solubilized in 22.5 mL (~2 mM) of ultrapure water, or 2.25 w/v glycerol or PBS buffer, and both solutions were kept at 45 °C in a thermal bath. Subsequently, the PHY solution was dropwised into the F127 solution,. The final mixture was kept under magnetic stirring for 10 minutes at 45 °C. Finally, the final solution (~33 mL) was brought to a rotary evaporator until the final volume was visibly under 5 mL. Then, the resulting concentrated solution was completed for a final volume of 5 mL. Samples were stored into glass vials at room temperature. Final sample concentrations were ~75 mM PHY and ~0.4 mM F127.

After cubosomal preparation, for extrusion, the final dispersion was diluted two times and extruded through the filters available in the laboratory. For lyophilization, samples were plunged into liquid nitrogen (-70 °C) overnight and the evaporation process was performed at -53 °C for 22h in low pressure (0.120 mBar).

For the loaded cubosomes, two procedures were tested, cosolubilization and addition after cubosomal dispersion was produced. For the cosolubilization, MILT was first put into a stock solution of 10 mg/mL (4.9 mM) in methanol. Then, chosen percentages of MILT were added to the PHY solution in the beginning of the process. For the addition method, MILT was also put into a stock solution of 10 mg/ml (4.9 mM) in water or 2.25% w/v glycerol or PBS buffer, to be added into the cubosomal dispersion. It is believed that the MILT suspension was filled with micelles since this stock solution was over the MILT CMC of ~50 μ M.

4. Experimental Techniques

4.1 Small angle X-rays scattering (SAXS)

This technique has the purpose of analyzing scattering patterns of samples (ANGELOVA et al., 2012), revealing structural features and interactions between nanoparticles or proteins (KHATUN et al., 2016)(PILLON; GUARNÉ, 2017). In case of a cubosomal dispersion, the most important are the results of the X-rays diffraction, in order to verify if there is a periodic structure or not (CHIARI- et al., 2017). The advantage of this technique is that samples can be in liquid or gaseous states, therefore, the nanoparticle can be measured on its natural environment. In addition, SAXS gives a statistical overview of the sample characteristics, instead of a single particle analysis (PILZ; GLATTER; KRATKY, 1979).

SAXS technique is based on wave interference, in which monochromatic X-rays interact with the electrons of the sample. The source of X-rays can be conventional or from a synchrotron accelerator (BARBOSA et al., 2013), Figure 12 shows a schematic representation of the apparatus. When X-rays interact with the sample, two possible interactions occur: elastic or inelastic scattering (HE, 2009). When scattered inelastically, X-rays are absorbed by electrons in the sample and re-emitted as waves of smaller energy. This does not give information about the internal structure of the sample for small angles, so this inelastic scattering is often ignored on data analysis. On the other hand, when the scattering is elastic, the incoming and re-emitted X-rays have the same energy but different phase shifts, leading to the formation of constructive and destructive wave patterns that will be read on a detector (TYLER; LAW; SEDDON, 2015). These detected wave patterns are completely dependent on the organization of the molecules within the sample, in this case, the ordered internal structure of the nanoparticles. To measure SAXS data, detectors stay in a range of 0° to 5° (0.09 radians) related from the primary beam. In Figure 12, one can say that 2θ goes from 0 to 0.09 radians for SAXS measurements.

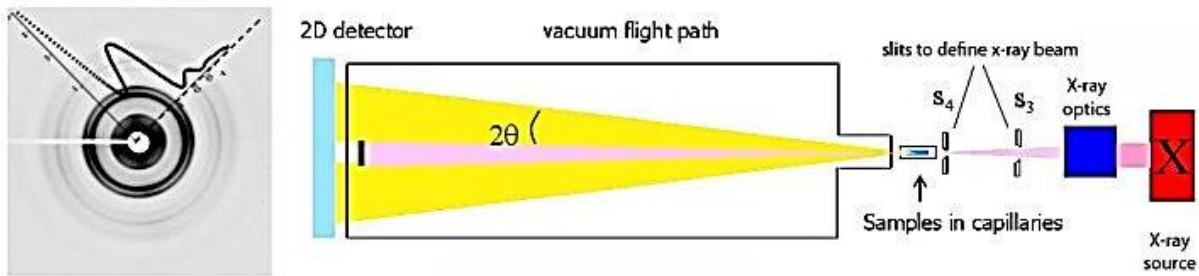


Figure 12. SAXS scheme setup with an example of multi lamellar esicles sample. A X-rays source produces the primary beam and magnetic lenses define the volume of the beam. A sample holder is located in the beam path, so when X-rays pass through they are scattered by the sample in all directions. The detector, located in a distance of the sample read the incoming photons in a maximum angle of 2θ . The integrated image from the detector reveals a curve that gives information about the sample. From: <http://www.mrl.ucsb.edu/~safinyaweb/XRD.htm>

The regular photons/X-rays detector is usually a charge-coupled device (CCD) or a complementary metal oxide semiconductor (CMOS) detector, in which photons generate an electrical current proportional to the number of incoming photons in two directions (two dimensional array) (LESSER, 2014)(FOSSUM; HONDONGWA, 2014)(BRÖNNIMANN; TRÜB, 2016)(LI et al., 2017). At the CCD or CMOS detector, the incoming photons form a collection of circles, like in Figure 12 left, due to the scattering of preferred planes by the ordered structure of the sample. Each circle gives the information of one scattering vector \mathbf{q} when integrated (CULLITY; STOCK, 2014). For the different angles in the circle, an equation can be written:

$$q = \frac{4\pi}{\lambda} \sin \theta \quad (1)$$

Where, q is the scattering vector and λ is the X-rays wavelength.

The periodicity of the system, given by the arrangement of the molecules within the sample, can be related to mathematical planes (Braggs planes), named by their position related to a chosen origin (TYLER; LAW; SEDDON, 2015). Figure 13 shows a few possible planes for a cubic structure that compose the crystal lattice. The given numbers are known as Miller indices, h, k, l respectively.

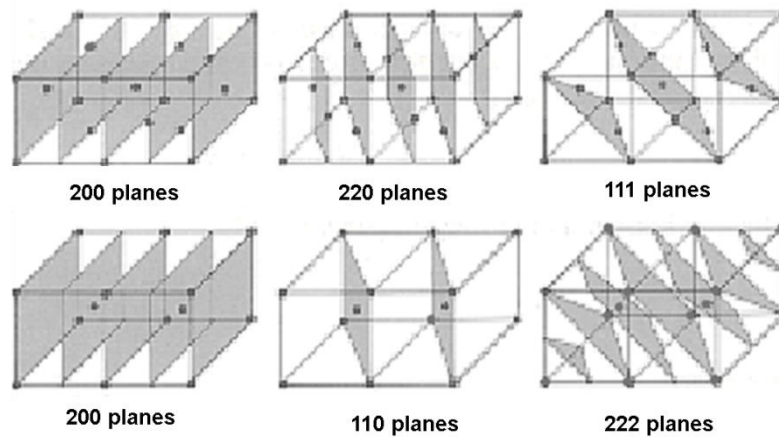


Figure 13. Example of some Bragg's planes. Adapted from <https://sites.ifi.unicamp.br/lfmoderna/conteudos/difracao-de-raio-x/>

The most important information comes from the relationship between scattering vector and the distance between these planes in the crystal lattice (CULLITY; STOCK, 2014). Consider a crystal lattice, as in Figure 14. The incoming X-rays waves come in phase to the lattice. When the wave interacts with the first plane, it scatters subsequently. For the interaction with the second plane, the wave must travel an additional path, given by $d \sin \theta$ in Figure 14.

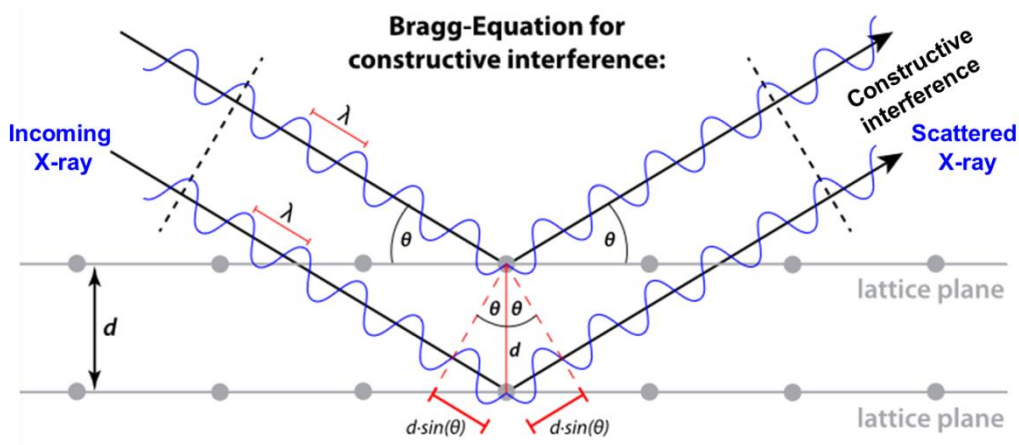


Figure 14. Schematic of X-ray interaction with the crystal lattice. Incoming waves, all in phase, interact with different lattice planes, distanced by d . When interacting with the first surface plane, the wave scatter with an angle θ . When interacting with the second plane, the incoming wave needs to travel an additional length $d \sin \theta$.

In order to the scattered waves to be again in phase, a condition needs to be obeyed.

This condition is Bragg's Law. Adapted from: <http://www.didaktik.physik.uni-muenchen.de/elektronenbahnen/en/elektronenbeugung/einfuehrung/bragg-bedingung.php>.

For the constructive interference of waves to happen in the detector, a condition needs to be obeyed: every additional path must be proportional to the incoming wavelength of the X-rays. This defines Bragg's Law, see equation 2.

$$2d \sin \theta = n\lambda \quad (2)$$

Combining now, equations 1 and 2, it is possible to relate the scattering vector, for the first plane, with the distance between planes:

$$q = \frac{2\pi}{d} \quad (3)$$

Considering now a cubic 3D structure, the distance between planes can be related to each diffraction plane and the distance of repetition of the unit cells in the crystal lattice, the called lattice parameter a . By the symmetry of the problem, one can write:

$$d = \frac{a}{\sqrt{h^2 + k^2 + l^2}} \quad (4)$$

Finally, one can write the relation between measured scattering vector with the lattice parameter of the crystal lattice:

$$q = \frac{2\pi}{a} \sqrt{h^2 + k^2 + l^2} \quad (5)$$

The lattice parameter gives information about the crystal inner structure (ESPOSITO et al. 2016). In the cubosomes case, it can give an indication of the size dimensions of the water channels that form the nanoparticles.

The intensity of the measured scattered X-rays can be described by a theoretical modeling:

$$I \propto N \cdot V^2 \cdot \Delta\rho \cdot P(q) \cdot S(q) \quad (6)$$

Where N is the number of scattering centers (each atom, or particle, or protein), V is the volume of the scattering structure, $\Delta\rho$ is the electronic density of the scattering structure, $P(q)$ is the form factor and $S(q)$ is the structure factor of the scattering structure. In the cubosomes case, $P(q)$ gives information about the lipid bilayers that compose the water channels and $S(q)$ gives information about the crystallographic structure of the nanoparticle

(diffraction peaks). Curiously, $P(q)$, for cubosomes case, is not yet known due to the great difficulty in describing theoretically the electronic density of the bilayer in the nanosystem.

For each peak in the SAXS curve, one can index the diffraction planes for a sample with periodic arrangement. According to the peak positions, one can find the crystallographic symmetry of the sample. For lipids like monoolein and phytantriol, their bulk phase diagrams reveal two possible symmetries: Pn3m and Ia3d (see Figure 5 and Figure 6) (QIU; CAFFREY, 2000)(BARAUSKAS; LANDH, 2003). It is also well known that in the presence of a stabilizing polymer forming the nanoparticle. GMO cubosomes space group Ia3d disappears and Im3m space group appears (FRASER et al., 2013)(CHONG et al., 2012)(DONG et al., 2012).

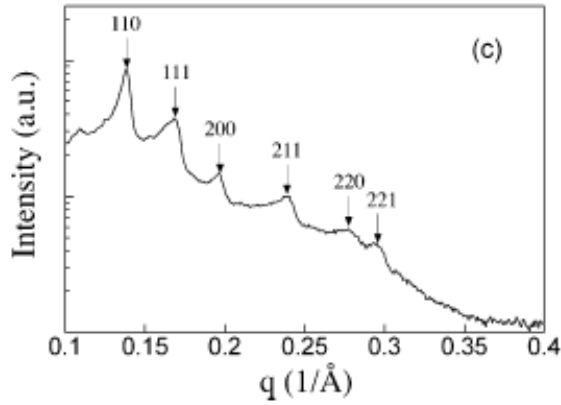


Figure 15. SAXS data for PHY cubic bulk phase at 25 °C showing Pn3m symmetry. From (BARAUSKAS; LANDH, 2003).

For analysis and determination of symmetry space group in each sample, all q_i peaks that appear in SAXS data are evaluated in ratios, as follows:

$$\frac{q_i}{q_1} = \frac{\sqrt{h_i^2 + k_i^2 + l_i^2}}{\sqrt{h_1^2 + k_1^2 + l_1^2}} \quad (7)$$

Then, Table 1 is used to index the plane reflection in the SAXS curve:

Table 1. Space groups symmetry for cubic structures possible for cubosomes.

Space Group	Pn3m	Im3m	Ia3d	Hexagonal
Reflection	$\sqrt{h^2 + k^2 + l^2}$			
100	-	-	-	1
110	$\sqrt{2}$	$\sqrt{2}$	-	-
111	$\sqrt{3}$	-	-	$\sqrt{3}$
200	$\sqrt{4}$	$\sqrt{4}$	-	$\sqrt{4}$
210	-	-	-	$\sqrt{5}$
211	$\sqrt{6}$	$\sqrt{6}$	$\sqrt{6}$	-
220	$\sqrt{8}$	$\sqrt{8}$	$\sqrt{8}$	-
221	$\sqrt{9}$	-	-	-
310	$\sqrt{10}$	$\sqrt{10}$	-	-
311	$\sqrt{11}$	-	-	-
222	$\sqrt{12}$	$\sqrt{12}$	-	$\sqrt{12}$

Note that with SAXS experiment, one can distinguish if a sample has nanoparticles with Im3m or Pn3m symmetry just by the different ratios between in first and second peaks (DONG et al., 2010). In more details, Pn3m peaks have $\frac{q_2}{q_1} = \sqrt{\frac{3}{2}}$ whereas Im3m have $\frac{q_2}{q_1} = \sqrt{2}$. Therefore the ratios between the other peaks are only to confirm the crystallographic structure of the system and to calculate the lattice parameter of the nanoparticles.

Experiments were performed in a Synchrotron accelerator at the National Laboratory of Synchrotron Light (LNLS), Campinas, São Paulo, at the SAXS-1 beamline. Samples were inserted into a mica holder where 300 μ L of each sample were measured for 100 seconds. The used detector was a Pilatus 300k distant by approximately 1 m from the samples. X-rays flux was 10^{10} to $10^{12} \frac{\text{photons}}{\text{second}} / \text{mm}^2$.

For diffraction data analysis, our team colleague Raphael Dias de Castro wrote a python routine that recognizes peaks in the SAXS curve. Knowing the centered positions of each

given peak, the ratios were calculated to investigate the crystallographic space group (Table 1) of the sample, then, a calculation of the lattice parameter (equation 5) was performed for each peak in order to have an average value with a standard deviation. No further analysis, regarding SAXS, was necessary in this project.

4.2 Dynamic light scattering (DLS)

This technique, also called “photon correlation spectroscopy”, measures the diffusion coefficient of a sample and relate it to the size of its components, based on the Brownian motion of the particles and several approximations (BHATTACHARJEE, 2016). It is an experiment considerably used for the study of colloidal systems (HASSAN; RANA; VERMA, 2015).

The apparatus, Figure 16, consists of a laser beam interacting with the sample and being scattered from the particles inside it, to be detected at 90° related to the primary laser beam.

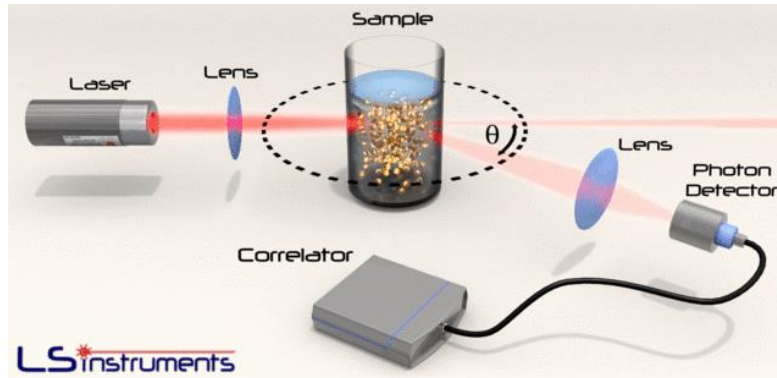


Figure 16. DLS apparatus scheme. A laser is used to enlighten the sample followed by the detection at 90° by a photon detector. This data is then analyzed by a correlator that returns a function which gives information about the size of the particles in the studied system. From <https://lsinstruments.ch/en/technology/dynamic-light-scattering-dls>.

The detected light is an interference pattern, where smaller particles move faster than bigger particles (ZHOU; SU; CAI, 2017). The software interprets the incoming signal as a correlation function, in which calculations by the Stokes-Einstein diffusion theory, equation 8, are done (CHIARI et al., 2017). This theory relates the diffusion coefficient to a

hydrodynamic diameter, D_h , for spherical particles in the sample, depending on viscosity (η) and temperature (T) of the sample.

$$D_h = \frac{k_B T}{3\pi\eta D_d} \quad (8)$$

Where k_B is the Boltzman constant and D_d is the measured diffusion coefficient.

Figure 17 shows a scheme of the detected intensity, the software calculated correlation function and the estimative of particle sizes. Note that for bigger particles the correlation function is displaced to higher correlation times, while for smaller particles the correlation function displays a rapid decay for intermediate correlation times, see Figure 18 for more details.

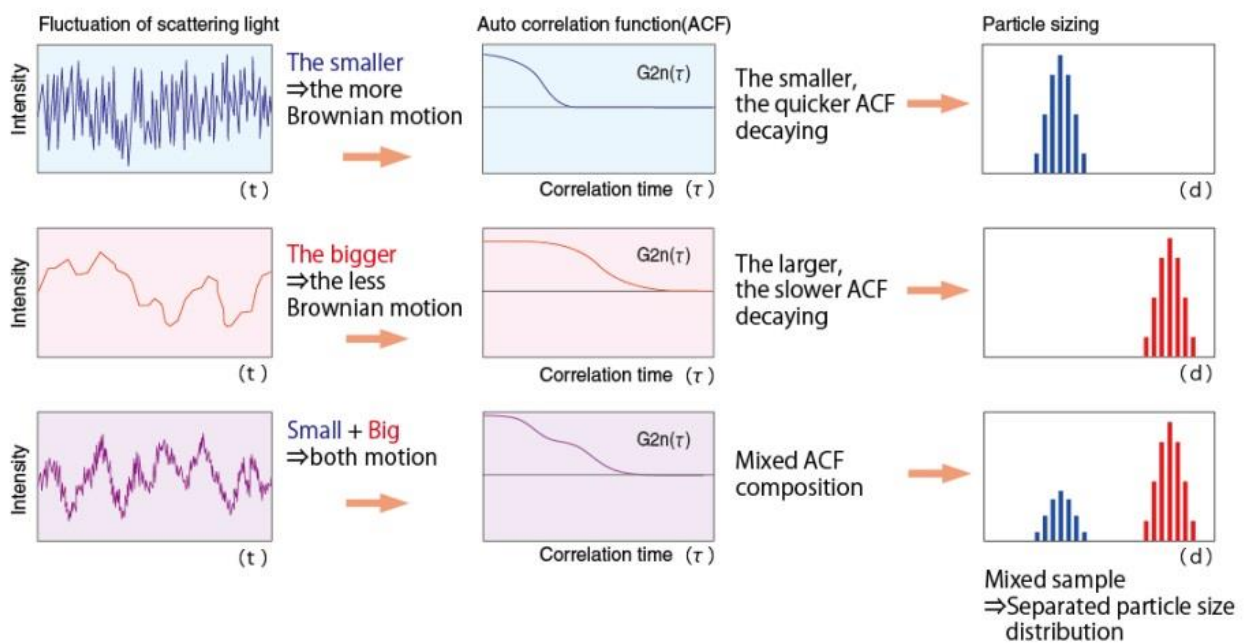


Figure 17. DLS measured correlation functions and relation to particle size populations. From the fluctuation of the scattering light, the software calculates a correlation function that discriminates bigger from smaller particles by the shape of the curve. Subsequently, a distribution size is calculated. From:

<http://www.otsukael.com/product/detail/productid/23/category1id/2/category2id/2/category3id/32>.

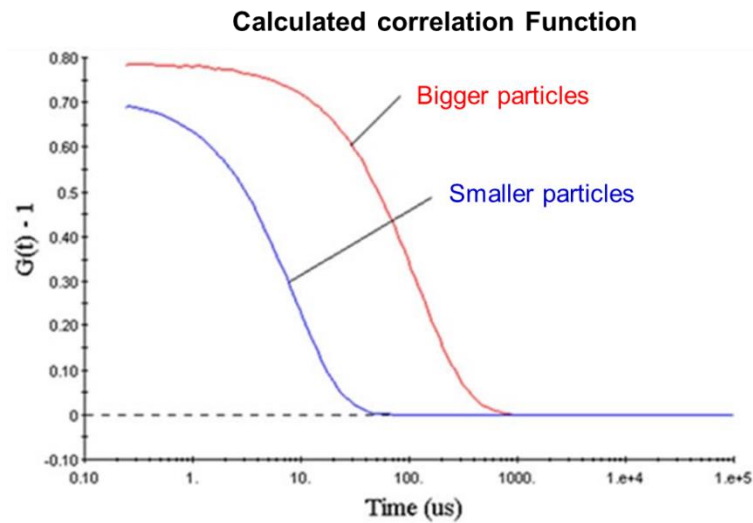


Figure 18. Detailed information about the correlation function of smaller particles (blue curve) and bigger particles (red curve). Note that for smaller particles in the sample, the correlation function decays to zero more rapidly than for bigger particles. Adapted from: <https://www.news-medical.net/whitepaper/20141221/Using-DLS-Deconvolution-Algorithms-to-Acquire-Intensity-Weighted-Particle-Size-Distribution-from-Measured-Correlogram.aspx>

These experiments were performed at Physics Institute (IFUSP) at the Biomembranes Laboratory using a Malvern ZetaSizer ZS90 analyser. Based on a sample dilution curve made by our group, it was found that the higher counting rate for the samples would be acknowledge with a dilution of 20 times. In a disposable cuvette, 100 μL of sample was measured in the apparatus at 22 $^{\circ}\text{C}$, 40 $^{\circ}\text{C}$, 50 $^{\circ}\text{C}$ and 65 $^{\circ}\text{C}$, with a waiting time of 300 seconds for proper sample thermal equilibrium. Samples were measured in quadruplicate. For the correlation function analysis, the Malvern software was used, where the z-average hydrodynamic diameter and polydispersion from the “intensity” data were obtained.

The polydispersity index (PDI) gives information about the overall size distribution of the sample. Therefore, if the sample has particles of similar size ($\text{PDI} \leq 0.2$) or if the sample has many populations of particles in different sizes ($\text{PDI} > 0.2$) (KHATUN et al., 2016). It should be stressed that measurements with $\text{PDI} > 0.5$ are not suitable for DLS measurements.

A major drawback about DLS is that it not a suitable experiment for samples with high polydispersion ($\text{PDI} > 0.2$) and for particles that have varied shape, like cubosomes. Although, since DLS gives a statistical overview of the sample and it is a widely used as characterization technique for cubosomal dispersion (KUMAR; BAPPADITYA; MUHAMMAD, 2017).

Therefore, only the software calculated mean z-average mean diameter and polydispersion from the “intensity” data were taken into account in this project.

4.3 Nanoparticle Tracking Analysis (NTA)

Nanoparticle tracking analysis (NTA) is a complementary technique for particle size distribution in biomaterial samples. It is also based on measuring the Brownian motion of detected particles, but NTA has the advantage of measuring single particles (VARENNE et al., 2016). There is a growing interest in this technique for characterization of nanomaterials, due to its real-time information about the sample (MAGUIRE et al., 2017).

The experimental apparatus is schematized in Figure 19. An aliquot of the sample is loaded into a glass chamber where a laser beam passes through. The particles in suspension scatter light in all directions, where an optical microscope detects all the incoming photons in a CMOS device (JARZĘBSKI et al., 2017). A movie of chosen duration is recorded from particle inside or outside the objective focal plane. The software allows one to set the best conditions regarding camera leveling, screen gain and detection threshold in order to maximize the particles to be analyzed (HOU et al., 2018).

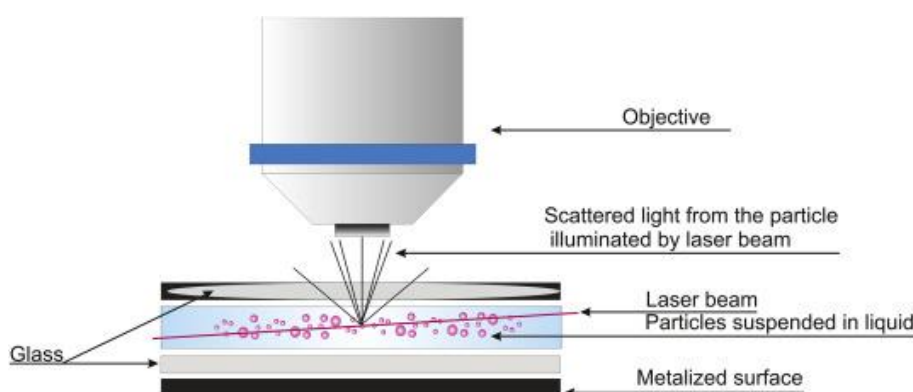


Figure 19. Scheme of the NTA measurement apparatus. The sample is loaded into a glass chamber where a laser beam passes through the dispersion, particles scatter the light that is detected on an optical microscope. Particles can be inside and outside the objective focus. Then, from the recorded movie, single particles are followed and their mean displacement is measured, given the basis for size calculations. Adapted from (JARZĘBSKI et al., 2017).

Then, from the recorded movie (see Figure 20), the software analyzes each particle’s movements and retrieves its mean square displacement in all 3D directions (KESTENS et al.,

2017). In addition, if an optimum measurement of 20 to 60 particles per frame is achieved, knowing the dilution of the system, the software can estimate the nanoparticle concentration at a given sample dilution (GALLEGO-URREA; TUORINIEMI; HASSELLÖV, 2011), from there, one can estimate the total particle concentration in the colloidal dispersion.

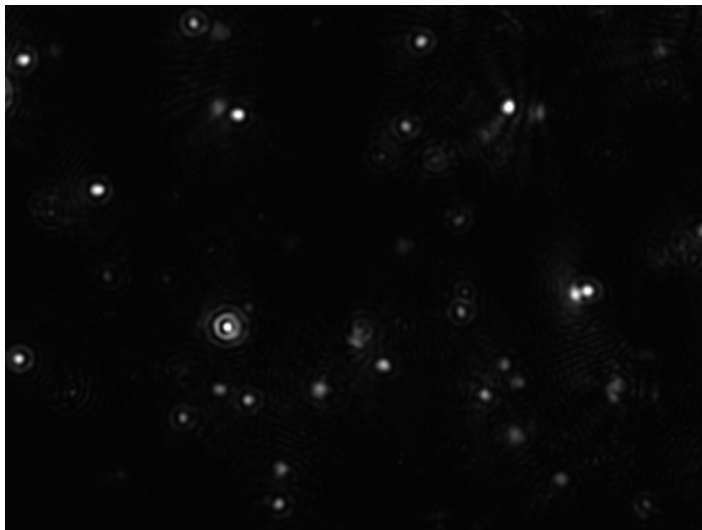


Figure 20. Screen shot of a recorded movie from NTA measurement software. Each white dot in the screen represents a particle in suspension, note that blurred dots are not in the focal plane of the objective, but they are still measured.

For size calculations the software also uses the model of a sphere (RIBEIRO et al., 2018), equation 8, therefore just like in DLS measurements, the software calculated values were taken without any further treatment, although size calculation for this technique is less affected than DLS by the shape of the particles.

Measurements were performed in the Biomembranes Laboratory at UNICAMP – Campinas. A nanoSight NS300 (Malvern Instruments) equipped with a green (532 nm) laser and a sample chamber (manual pumping) was used. Samples were diluted 5000x and measured in triplicate at room temperature (25 °C). The average and standard deviation of these measurements were used to estimate mean size and total particle concentration of the samples.

4.4 Transmission electron microscopy and cryo-EM (TEM)

Transmission Electron Microscopy (TEM) uses an electron beam to study a sample. Differently from SAXS or DLS, TEM is called a single particle technique because it sees only a very small part of colloidal samples, giving information about the particles in a particular vision field (KHATUN et al., 2016)(CHIARI- et al., 2017). Therefore, for this experiment to reflect a statistical point of view about the sample, one must find many particles in various viewing fields (NAGAYAMA, 2011).

Electrons from the beam are accelerated at a given energy (for instance 120 keV or 200 keV) and interact with the sample's electrons by elastic or inelastic scattering (CZARNOCKI-CIECIURA; NOWOTNY, 2016)(FRANKEN; BOEKEMA; STUART, 2017). Figure 21 shows a scheme of the experimental apparatus. Electrons from the beam can be either scattered or absorbed in the sample and the detection of the transmitted electrons is usually made by a CCD or CMOS device, in which the intensity of photons (generated by the interaction of the incoming electrons with a scintillator) is detected in each pixel (TAHERI et al., 2016). Due to the electrons wavelength, it is possible to investigate the structure/organization and morphology of a nanometric sample (DUDKIEWICZ et al., 2011). In the case of cubosomes, the internal morphological structure and size of the nanoparticles can be evaluated (DANINO, 2012).

The experimental apparatus scheme is displayed in Figure 21. The electron gun generates the beam that passes through a series of magnetic lenses (condenser, objective in Figure 21) in order to interact with the specimen/sample. The transmitted electrons then undergo another series of magnetic lenses until they reach the fluorescent screen, where the images are formed and can be seen by the operator. In order to register the micrographs, the fluorescent screen is retracted and the beam is then collected in a CCD or CMOS camera.

TEM experiments were performed at the Biosciences Institute (ICB) at University of São Paulo (USP). In this experiment, the goal was to assess particle size and to investigate possible aggregates on the dispersion, together with an overall vision of the size dispersion within the samples. TEM is not the best technique for cubosomes characterization, due to possible vacuum distortions on particle size. Although, the main goal in trying this characterization technique was to come up with a size analysis method that could complement DLS and NTA measurements.

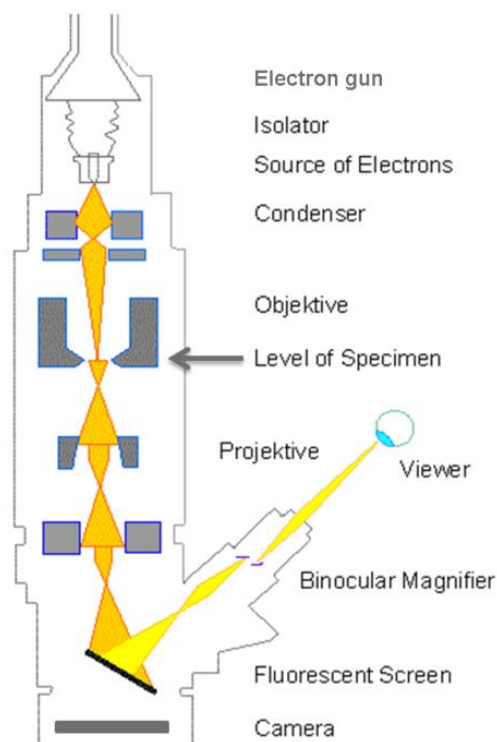


Figure 21. TEM schematics of the experimental apparatus. An electron gun generates the beam that hits the specimen. Through magnetic lenses, the transmitted beam is conducted to a fluorescent screen or directly to a camera in order to record data. Adapted from https://s10.lite.msu.edu/res/msu/botonl/b_online/e03/03e.htm.

Standard procedure (MIELANCZYK et al., 2014) was used for sample preparation. A Formvar/Carbon 200 mesh grid, from Electron Microscopy Sciences®, was used. These grids went through a glow discharging procedure, in which each grid was submitted to a negative plasma (14mA for 20 seconds) before loading the sample, in order to get a hydrophilic surface. The following protocol was used for TEM sample preparation. Briefly, 5 μ L of sample was dropped on the grid for 1min30sec, the excess was dried with absorbent paper. Then, the sample was stained with 5 μ L phosphotungstic acid at 2% w/v for 30 sec, excess was also dried. Finally, the grid was given 2 minutes for total dry in room temperature before being stored in a grid box. Experiments were performed in a FEI Tecnai G² F20 (field-emission gun transmission electron microscope) at 200 kV with a CCD camera Eagle 4k HS.

Cryo-EM was performed at National Laboratory of Nanotechnology (LNNano) at CNPEM in Campinas, São Paulo. These measurements were intended in order to see the internal morphology of the cubosomes along with size and shape distribution (STEWART, 2017).

The automatized standard protocol for cryo-EM sample preparation was performed (MCKENZIE; HOLDER; SOMMERDIJK, 2012). A 300 mesh Holey Lacey Carbon from Ted Pella® was used. Cryo-EM samples are prepared in such a way that amorphous ice is formed in the grid, this feature allows samples to be on their natural aqueous environment without having the vacuum distortions as TEM (BURROWS; PENN, 2013). Briefly, before the automatic procedure, the grids were submitted to a glow discharge procedure (15 mA for 10 seconds) in order to make them more hydrophilic. Then grids were inserted in a Vitrobot® (IANCU et al., 2006)(PASSMORE; RUSSO, 2016) where 3 μ L of sample were added, and left for 20 seconds for sample fixation. Afterwards, an automatic blotting was performed to dry the excess of sample with a negative blotting force (blot force = -5). Subsequently, the grid was rapidly plunged into liquid ethane wrapped into a liquid nitrogen environment. Finally, grids were transposed to a grid box in liquid nitrogen until measurements were made in a JEM-2100 JEOL microscope at 120 kV with a CMOS camera OneView 4K x 4K and software Gatan Digital Micrograph™ 3.01.598.0.

ImageJ® software (NATIONAL INSTITUTES OF HEALTH, 1987) was used to image analysis. At TEM experiment, data acquired from the CCD/CMOS detector was like in Figure 22, in which the contrasted shapes are the particles in the sample. When many particles could be seen in a unique field, sizes were calculated and histograms were made with the information from the software.

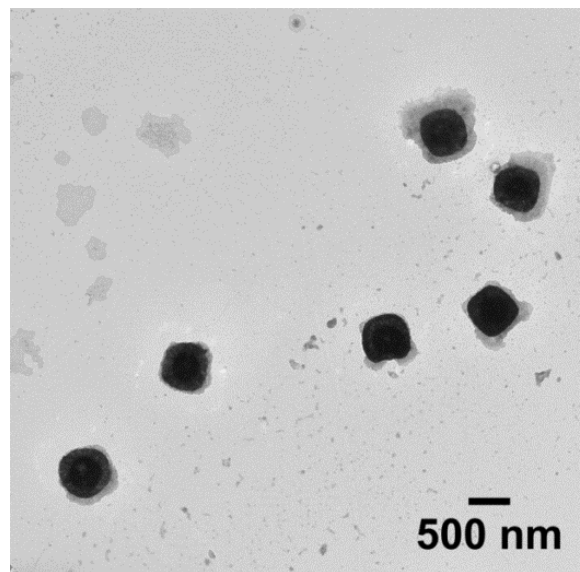


Figure 22. Example of nanoparticles TEM micrograph, showing the square shape of the cubosomes,

From the Cryo-EM micrographs, sizes were also evaluated and the internal structure of the nanoparticles could be assessed and analyzed by the fast Fourier transformation (FFT). Figure 23 shows an example of Cryo-EM micrographs for cubosomes.

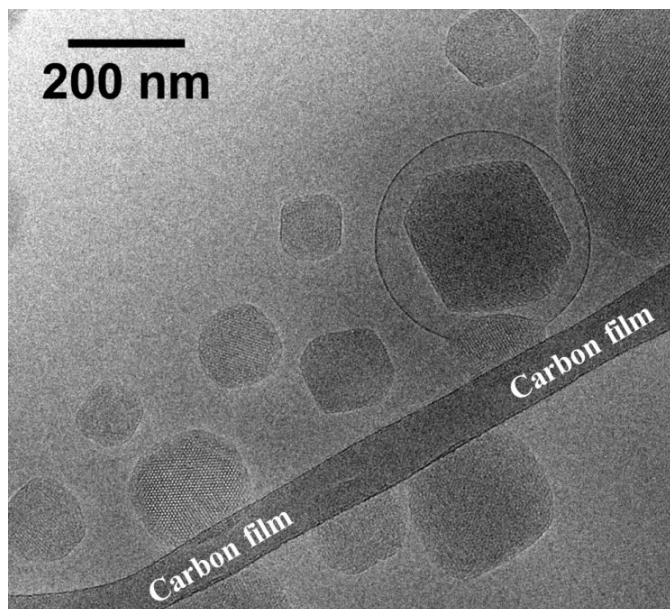


Figure 23. Cryo-EM example of cubosomes micrograph. The structure inside each particle reveals details about the internal organization of each particle.

FFT analysis brings information about the interplanar distances between reflection planes, analogous to SAXS (HELVIG;YAGHMUR,2015). In general, cubosomes are viewed when the electron beam is aligned to the [100] or [111] axis planes. So cubosomes in these conditions have a honeycomb or a square motif in their internal structures. A detailed study by Sagalowicz et al. demonstrated simulated calculations of all possible reflection at a given axis for the cubic $Pn3m$ and $Im3m$ crystallographic structures (SAGALOWICZ et al., 2007). This study was taken as basis for all FFT analysis.

Figure 24 displays the results of a study by Sagalowicz et al. where each line is the simulated reflection planes as seen by a different axis (signaled by the [110], [111], [001]...). Since most part of cubosomes are aligned to the [111] axis, it is difficult to distinguish if a given nanoparticle has $Pn3m$ or $Im3m$ symmetry. For that, a tomography experiments should be made (DEMURTAS et al., 2015). In this project, the SAXS crystallographic found symmetry was taken into account to make the FFT analysis. Therefore, for each sample, the corresponding column was consulted for indexing the points in the FFT.

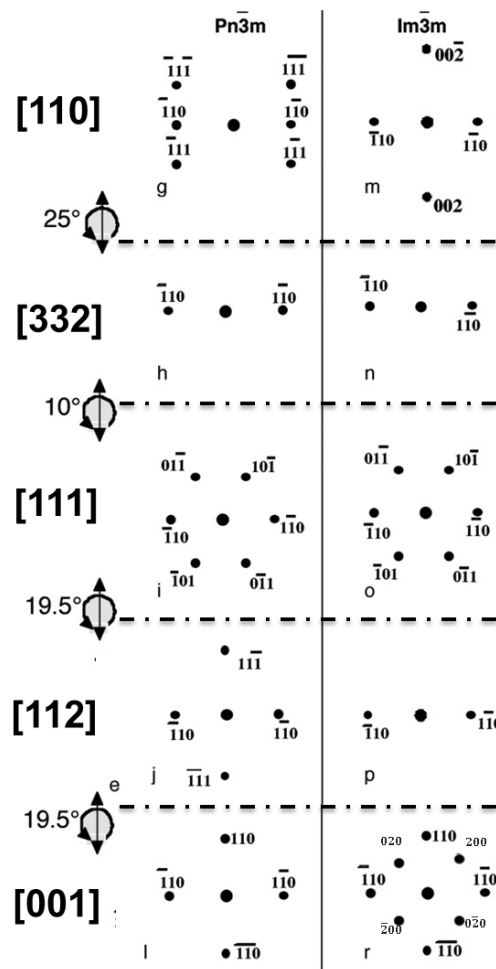


Figure 24. A cryo electron tomography gives information about the sample in different axis by rotating the sample holder. In this case, Sagalowicz et al. simulated reflections calculated for cubosomes diffraction as viewed by different axis. This was used as basis of the FFT analysis for the cryo-EM micrographs. Adapted from (SAGALOWICZ et al., 2007).

Once the points in the FFT were indexed, the following procedures were taken in order to calculate the interplanar distances. Figure 25 displays the schematic flow of the analysis. First a chosen nanoparticle was isolated and a selected area within its structure was delimited (red circle). Then, the FFT provides information of the internal organization in the reciprocal plane, given by dots. The next step would be to index the given reflection planes based on Figure 24. Since no distances calculations can be made in the reciprocal plane, a mask of chosen pair of planes was made in order to provide an inverse FFT. The inverse FFT, back to the real plane, have information about the interplanar distances. Finally, a plot profile was made in order to measure this distances, 10 lines were chosen to compose the plot in order to make an average and standard deviation of the found distances.

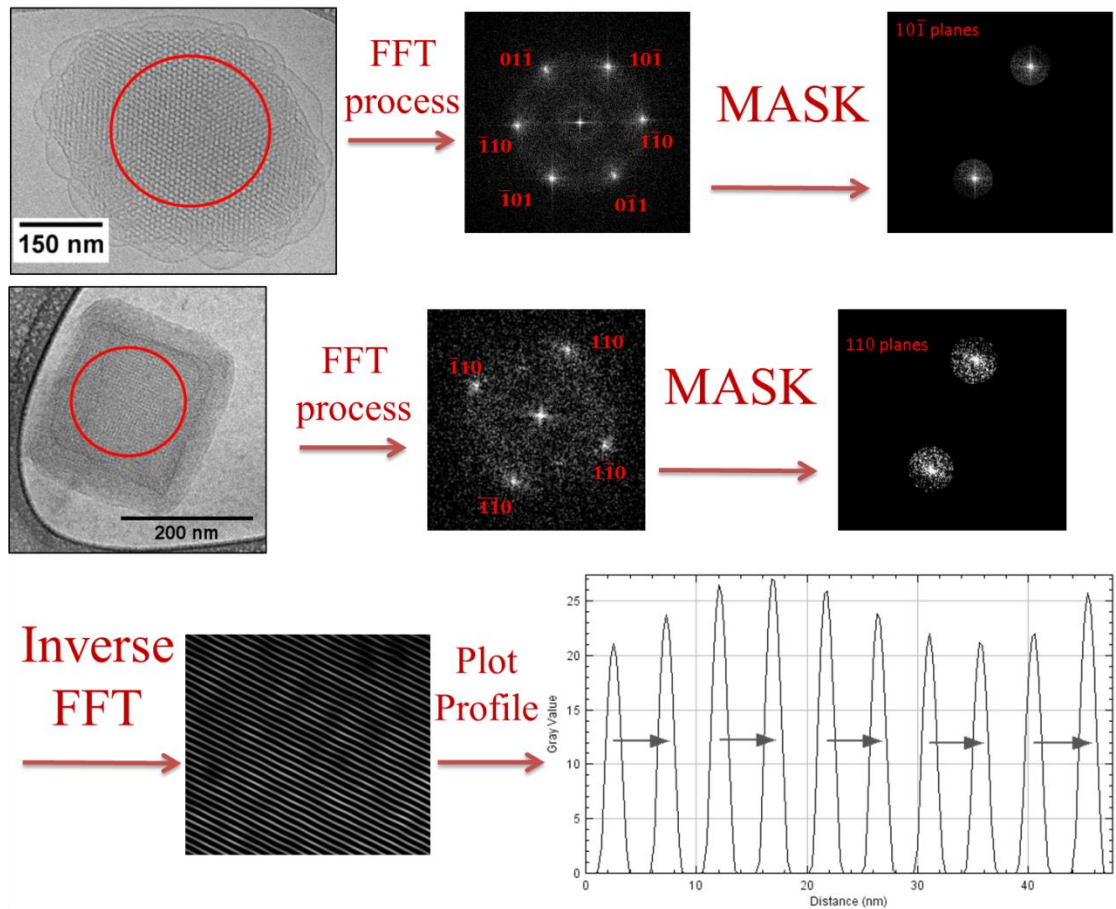


Figure 25. Schematics of the FFT analysis performed for each found particle in cryo-EM micrographs. First, a region inside the particle was chosen, then a FFT of that region was made. After indexing all planes based on Figure 24, a mask containing only one specific pair of planes was made. Subsequently, an inverse FFT was done with the mask and a plot profile reveals the interplanar distance between planes.

Afterwards, knowing the distance, by the relation between interplanar distance and lattice parameter, given in equation 9, one can calculate the lattice parameter a for each found particle.

$$d_{h,k,l} = \frac{a}{\sqrt{h^2 + k^2 + l^2}} \quad (9)$$

It must be noted that cryo-EM gives information about single particles, therefore the found a is particular for each cubosome and must be compared to SAXS information just in order of magnitude.

5. Results and discussion

5.1 Monoolein based cubosomes

Nanoparticles were produced using GMO from an adapted protocol described by Spicer (SPICER et al., 2001). Figure 26 shows the SAXS curve of GMO-based cubosomes (from now on referred as GMO-cub) at ~ 20 mg/mL in ultrapure water. This scattering curve is typical of internally ordered systems, due to the presence of sharp peaks at well-defined positions. Noteworthy, such peaks are due to Bragg diffraction, which arises from the crystallographic inner structure of the scattering particle (see experimental section).

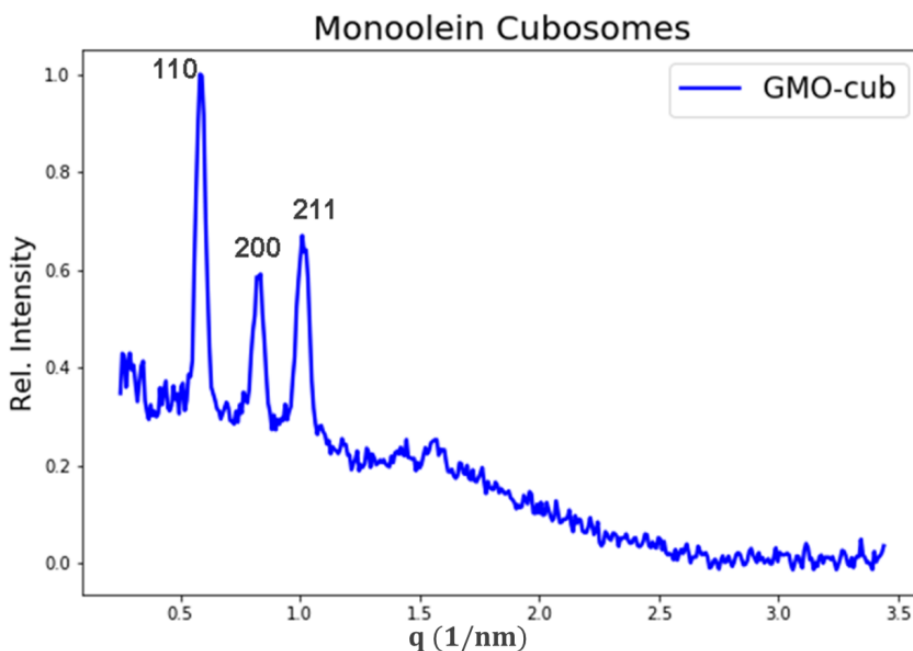


Figure 26. SAXS data for GMO-cubs with indexed diffraction peaks. This plot is typical from nanoparticles with internal structure, peaks indicating the reflections planes and the numbers attributed to them are the Müller indices (MAZZONI et al., 2016).

Figure 26 shows the SAXS data for the GMO-cub dispersions, three peaks are distinguishable from the overall curve, being indexed by the respective diffraction planes. Table 2 shows the peak positions along with the calculated lattice parameter for this sample.

Table 2. Peak positions and the calculated lattice parameter for GMO-cub.

Sample	Peak positions (nm^{-1})			Calculated lattice parameter
	q1	q2	q3	
Reflection Plane	110	200	211	15.3(7) nm
GMO-cub	0.581 ± 0.027	0.830 ± 0.029	1.008 ± 0.028	

GMO alone in water is known to form Pn3m cubosomes with lattice parameter ~ 7 nm, the stabilizer polymer inserts itself into the lipidic moiety, changing both cubosomes crystallographic structure and lattice parameter (MAZZONI et al., 2016).

Comparing data from Table 2 with the study of Spicer et al. (SPICER et al., 2001), who calculated a lattice parameter of 15.0 nm using a probe sonicator, we find that the lattice parameter is compatible with their results even using the bath sonicator instead. This is an indication that the adapted chosen protocol was successfully reproduced.

Comparing our data with others in literature, Gustafsson et al. (GUSTAFSSON et al., 1997) for example used a microfluidizer in his production, in order to reduce particle size, obtaining a lattice parameter between 13.0 nm and 14.0 nm. Murgia et al. (MURGIA et al., 2010) tried a different process by first making the bulk phase (GMO/water) and then adding F127 for break in particles subsequently (using a dispersing tool in homogenizer), obtaining a lattice parameter of 12.6 nm. The slight variations to the calculated lattice parameters depend on the mechanical energy applied to break the nanoparticles from the bulk phase.

Table 3 gives information about the crystallographic symmetry of these nanoparticles. As shown, when comparing with reference values, this GMO-cub have Im3m symmetry (see experimental section), also in good agreement with the chosen adapted protocol (SPICER et al., 2001) and literature (GUSTAFSSON et al., 1997)(MURGIA et al., 2010).

Table 3. Interpretation of SAXS data for determination of cubic space group symmetry.

Sample	Peaks relations		Reference values for $Im\bar{3}m$ symmetry		Reference values for $Pn\bar{3}m$ symmetry	
	q_2/q_1	q_3/q_1				
GMO-cub	1.4286	1.7349	$\frac{q_2}{q_1} = \sqrt{2}$	1.4142	$\frac{q_2}{q_1} = \sqrt{\frac{3}{2}}$	1.2247
			$\frac{q_3}{q_1} = \sqrt{3}$	1.7321	$\frac{q_3}{q_1} = \sqrt{2}$	1.4142

From DLS experiment, a hydrodynamic radius (estimation of particle size) and a polydispersion index (PDI) were measured. Particles revealed size $\sim 300(8)$ nm and PDI $\sim 0.160(20)$.

Literature reports particles with variable sizes depending on the mechanical energy applied to break them from the bulk phase. Nasr et al. (NASR; GHORAB; ABDELAZEM, 2015) reported particles size about 100 nm due to the usage of a probe sonicator. Hinton et al. and Luo et al. (HINTON et al., 2014)(LUO et al., 2015) reported particle in size range 150 nm to 200 nm along with low polydispersion (<0.250).

Figure 27 shows micrographs of GMO-cub sample. All over the grid there were only particles of the shown shape and size, there was no presence of visible vesicles nor aggregates of greater size, in agreement with the low PDI in DLS measurements.

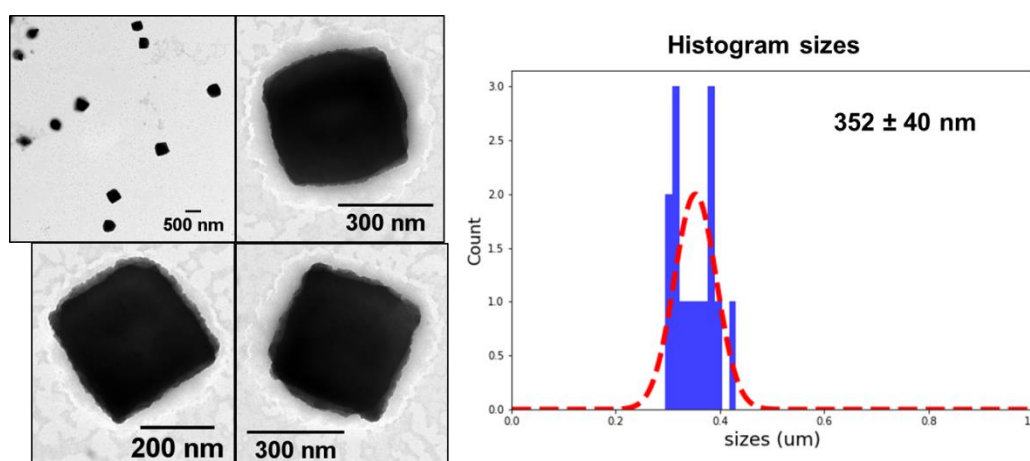


Figure 27. TEM Micrographs at left and a histogram (right) for obtained particle sizes from the TEM experiment. All found particles in the micrographs had sizes ~ 350 nm, compatible with DLS measurements.

Figure 27 also shows the calculated size distribution for particles found in the grid. This distribution was fitted with a Gaussian function in order to estimate medium size and standard deviation. Analysis shows particles with medium size 350(40) nm, TEM experiments reveals slightly bigger size particles than DLS. Very few research groups have tried TEM for cubosomes size analysis, but two recent references (NASR; GHORAB; ABDELAZEM, 2015)(LUO et al., 2015) also report particles with sizes slightly higher than DLS measurements.

GMO-cub sample was also taken to Cryo-EM. In this experiment it was expected to see the internal ordered structure of the nanoparticles. Figure 28 shows details about the internal structure of some nanoparticles. One can see that this sample has particles with internal structure but their sizes are variable, there are small particles (~200 nm) and bigger particles (>500 nm), also they are oriented in different viewing planes, given by the diverse inner structure among nanoparticles.

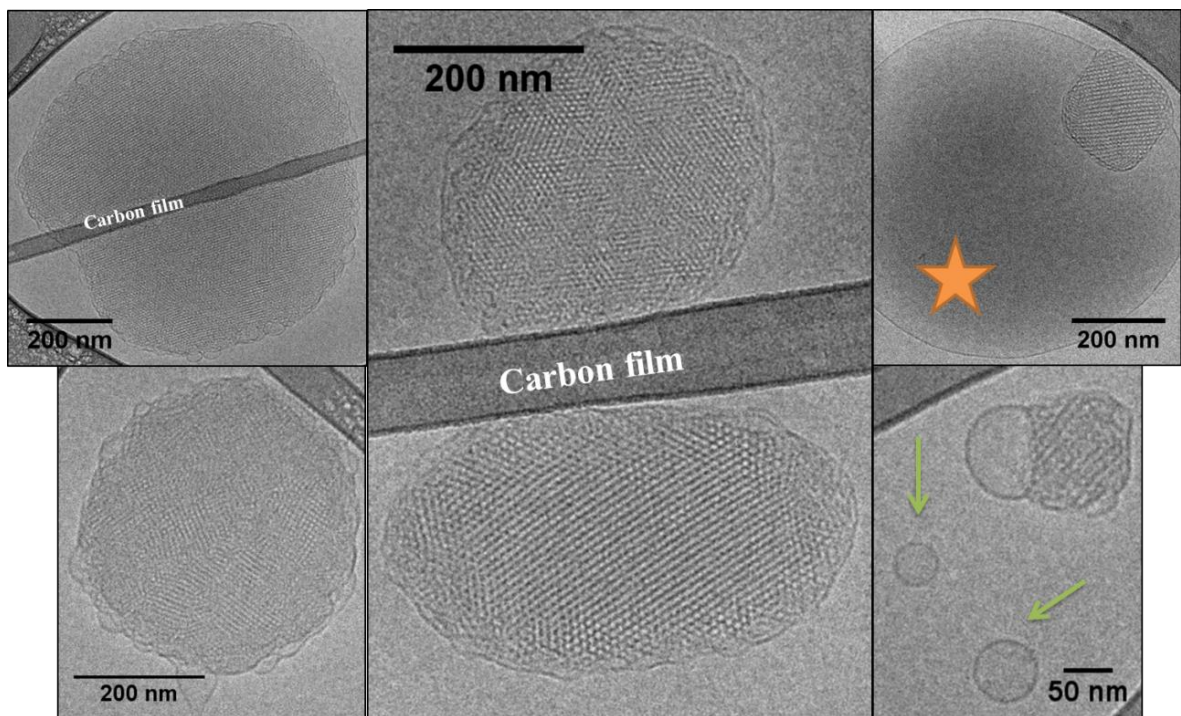


Figure 28. Cryo-EM data for GMO-cubs sample. Micrographs show the internal structure the nanoparticles revealed by the entangled lines seen inside the cubosomes. Green arrows and the orange star point the presence of vesicles and a bigger vesicle which seems to be around the cubosome.

These micrographs are in good agreement with literature in which the patterns for internal structure are shown with more resolution than ours (SPICER et al., 2001). There were also presence of very small vesicles (50 nm) and bigger vesicles (size range 200 nm to 500

nm), also present in many works in literature (SAGALOWICZ et al., 2006)(FERREIRA et al., 2006).

For FFT analysis of these cubosomes found in Cryo-EM, see method section, particles presented the given FFT shapes (see Figure 29), and from there, the lattice parameter for each particle could be calculated.

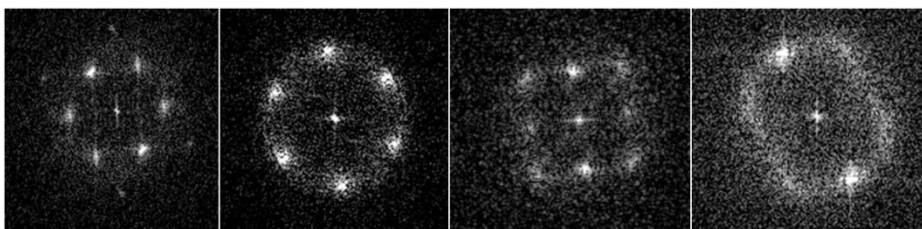


Figure 29. Calculated FFT for some particles in Figure 28. From these, a lattice parameter can be calculated.

The calculated lattice parameters for particles in the micrographs are gathered in the following table:

11.5(5) nm	8.4(5) nm	8.1(5) nm	11.1(5) nm
9.8(5) nm	7.9(5) nm	10.5 (nm)	

It can be seen that the calculated lattices differ slightly from SAXS measurements for the GMO-cubs samples because SAXS gives a general overview of the system, whereas Cryo-EM sees only single particles. Noteworthy, all lattices are in the same order of magnitude as the values calculated by SAXS. Finally, particles presented varied water channel sizes, indicating that each cubosome is somehow a unique nanoparticle. Literature reports cryo-EM calculated lattice parameters for GMO-cubs around from 12 nm to 14 nm, depending on the cubosome formulation (DEMURTAS et al., 2015)(SAGALOWICZ et al., 2006), therefore our results and analysis are in good agreement with them.

5.1.1 Effect of temperature on cubosomal structure

In addition, a study to investigate temperature dependence was performed with GMO-cub sample. Figure 30 shows SAXS results of this study, one can see that the curve are still alike, indicating cubosomes still exist at 37 °C. Peak positions have changed with the increase

of temperature, indicating the cubosomes expel water from their internal structure as temperature is increased. Lattice parameters were calculated: $a_{25\text{ }^{\circ}\text{C}} = 13.6(9)\text{ nm}$ and $a_{37\text{ }^{\circ}\text{C}} = 13.0(6)\text{ nm}$.

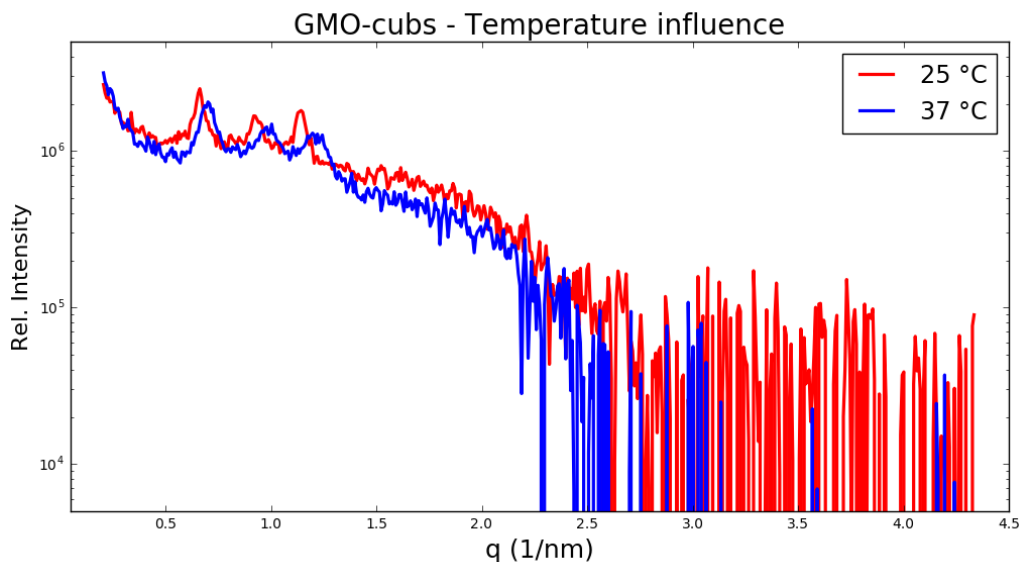


Figure 30. SAXS data for GMO-cub sample in different temperatures. The blue curve shows cubosomes at 37 °C, in which peaks have shifted slightly, indicating that lattice parameter changed and the nanoparticles expelled from its structure as a response to temperature increase.

Peaks shifted for higher q values, resulting in a slight decrease of the lattice parameter a . This induced changes by temperature are also found in literature, Yaghmur et al. showed that lattice parameter decreases when temperature rises (YAGHMUR et al., 2008), a peaks shifting for higher values of q when temperature rises, when measured at 25 °C and at 45 °C.

5.1.2 Miltefosine interaction

To study the influence of miltefosine (MILT) molecule in the cubosomal nanoparticles, the following concentrations were chosen: 0.5%, 1%, 1.5%, 2%, 3%, 4%, 5% w/w, see Table 4 for reference. Samples were named after their percentages. The chosen percentages do not reach the clinical dosage. Only TEM and Cryo-EM were performed with these samples.

Table 4. Calculated quantities of MILT loaded into the cubosomes, both in mass, mg/mL and mol concentrations.

Chosen quantities of MILT loaded into the cubosomes		
Considering a final sample volume of 3mL		
Considering the GMO mass per sample: 46 mg		
% w/w	mg/mL	mM
0.5	0.077	1.9
1.0	0.15	3.8
2.0	0.31	7.5
3.0	0.46	11.3
4.0	0.61	15.1
5.0	0.77	18.8

TEM experiments revealed particles with diverse sizes in the samples. Figure 31 shows a collection of taken micrographs. All samples presented particles of square or rounder shape up to 4% w/w. Sizes varied from a few nm to hundreds. In especial cubosomes loaded with lower amounts of MILT, for instance 0.5% w/w, seem not to have their shape altered by the guest molecule. As MILT content increases, particles can assume rounder shapes, but still resemble to cubosomes. Most particles present a clearer halo around them, this is thought to be a F127 polymer layer on the surface of the cubosomes. For the sample loaded with 5% w/w, only circular and round shapes are distinguishable, evidencing a strong effect of MILT in the GMO-cubs inner structure.

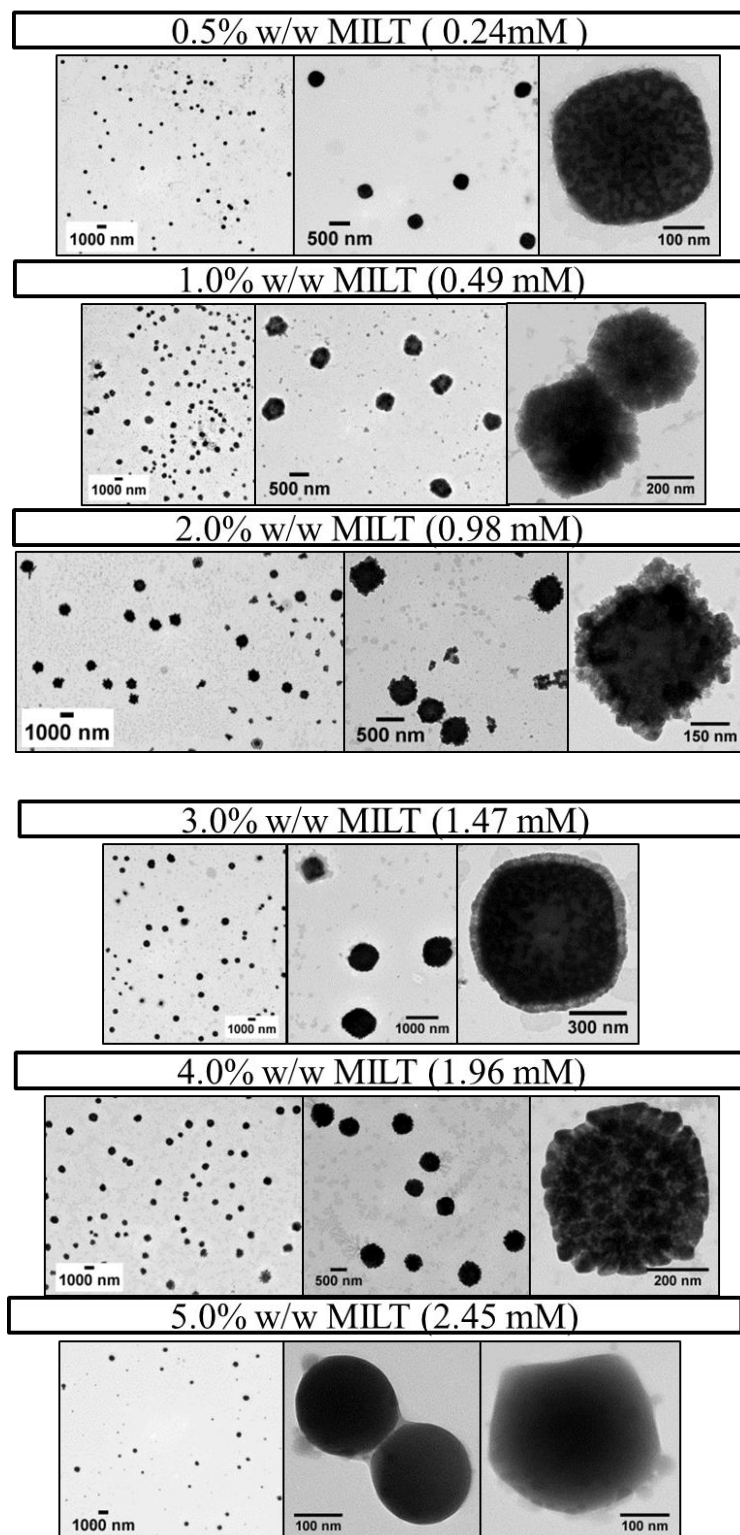


Figure 31. TEM micrographs for cubosomes loaded with MILT at different quantities. It is notable that up to 4% w/w cubosomes in square shapes still exist, only at 5% w/w the nanoparticles lose their shapes, being mostly spherical.

Micrographs were also analyzed with ImageJ® software and the following size dispersions were revealed. TEM is not the best technique for cubosomes characterization, since vacuum could distort the particles by evaporating the water content and deforming the water channels, although it gives an idea of the approximate size and shape of the nanoparticles.

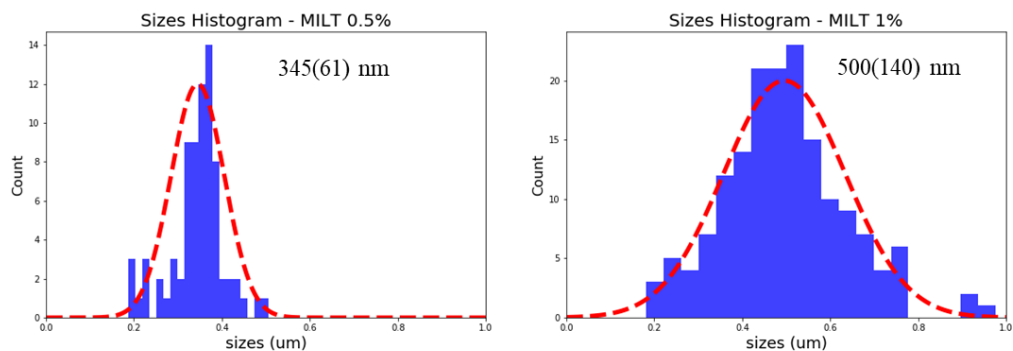


Figure 32. GMO-cubs size distribution histogram from obtained micrographs 0.5% w/w and 1% w/w MILT.

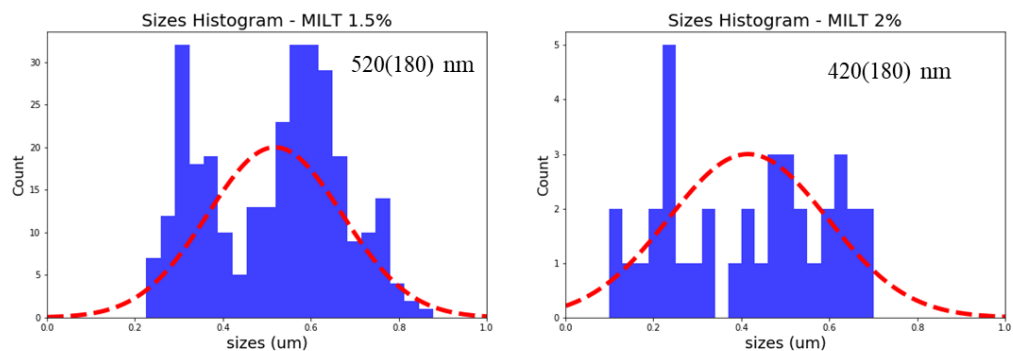


Figure 33. GMO-cubs size distribution histogram from obtained micrographs 1.5% w/w and 2% w/w MILT.

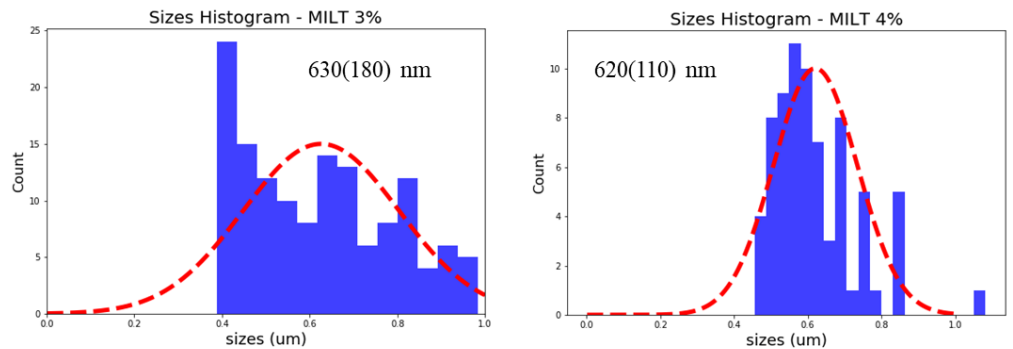


Figure 34. GMO-cubs size distribution histogram from obtained micrographs 3% w/w and 4% w/w MILT.

Gathering information from the size distribution of TEM and ImageJ® analysis, one can compare size distributions. Figure 35 shows an increase in particle size as MILT concentration also increases. Since standard deviation is very high due to the great polydispersion of the samples, it can be considered that only at high amounts MILT influence particle size. Up to 2%, MILT does not influence cubosomes sizes, although for 3% w/w and 4% w/w sizes were increased by 200 nm. No such analysis has been described in literature yet.

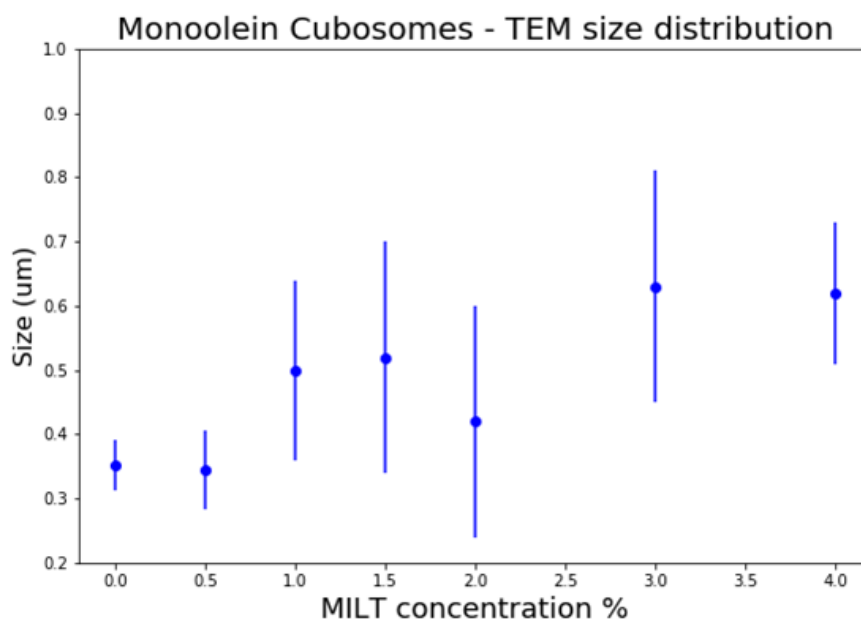


Figure 35. Size distribution from histograms from the TEM micrographs (Figure 31) for the loaded GMO cubosomes. One can say that for concentrations higher than 3% w/w, MILT increases the size of the cubosomes.

Cryo-EM experiments were performed with samples with 5% w/w MILT and 1.5% w/w MILT, see Table 4 for references in mol. 5% w/w MILT sample was very compatible with TEM analysis, as shows Figure 36. One can see that the micrographs shows round shaped particles with no internal structure inside them. The black arrow indicates part of one found particle that shows some inner structure, but the resolution to see it was very poor. Green arrows display vesicles in the sample coexisting with cubosomes. Overall, there is a great compatibility between TEM and Cryo-EM for 5% w/w MILT sample MILT.

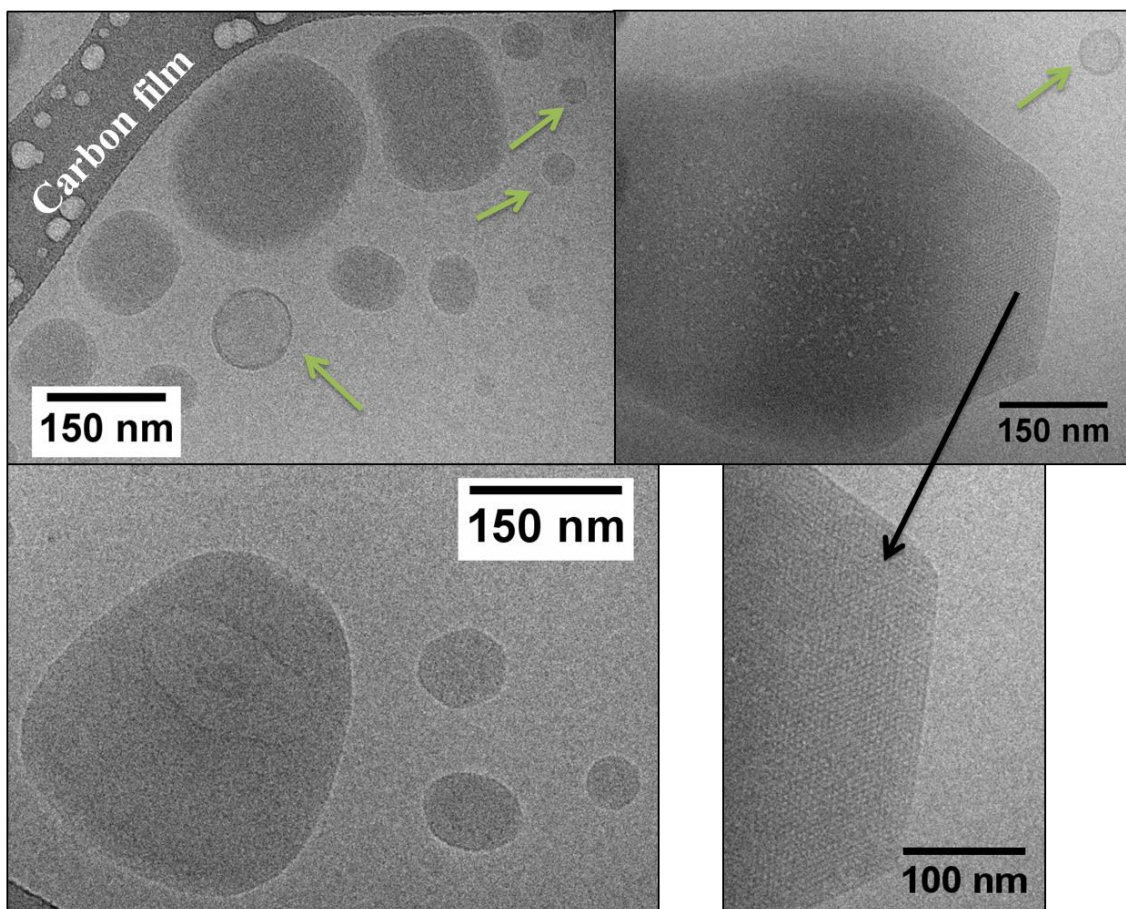


Figure 36. Cryo-EM micrographs for 5% w/w MILT sample. Green arrows display vesicles present in the sample and the black arrow point to the detailed structure of a found particle, which presents some internal structure.

When analyzing 1.5% w/w MILT sample, many particles appeared in different sizes and organizations. As shown in Figure 37, most particles present square shape, some are deformed by the ice formation. But all particles showed well defined inner structure. Sizes vary from 50 nm to ~500 nm and different orientations are seen in their internal structure. Particles viewed from the [111] plane display honeycomb internal structure and particles viewed from other planes had internal linear motif. In addition, most particles present an outer envelope, feature also reported in literature (YAGHMUR et al., 2008)(SAGALOWICZ et al., 2006). This envelope it thought to be the part of the F127 polymer acting on the surface of the cubosomes preventing the aggregation of particles (DEMURTAS et al., 2015)(TRAN et al., 2015).

Vesicle like particles were also found in the sample, as pointed by green and orange arrows, similar to some other studies (TRAN et al., 2015) (GUSTAFSSON et al., 1997).

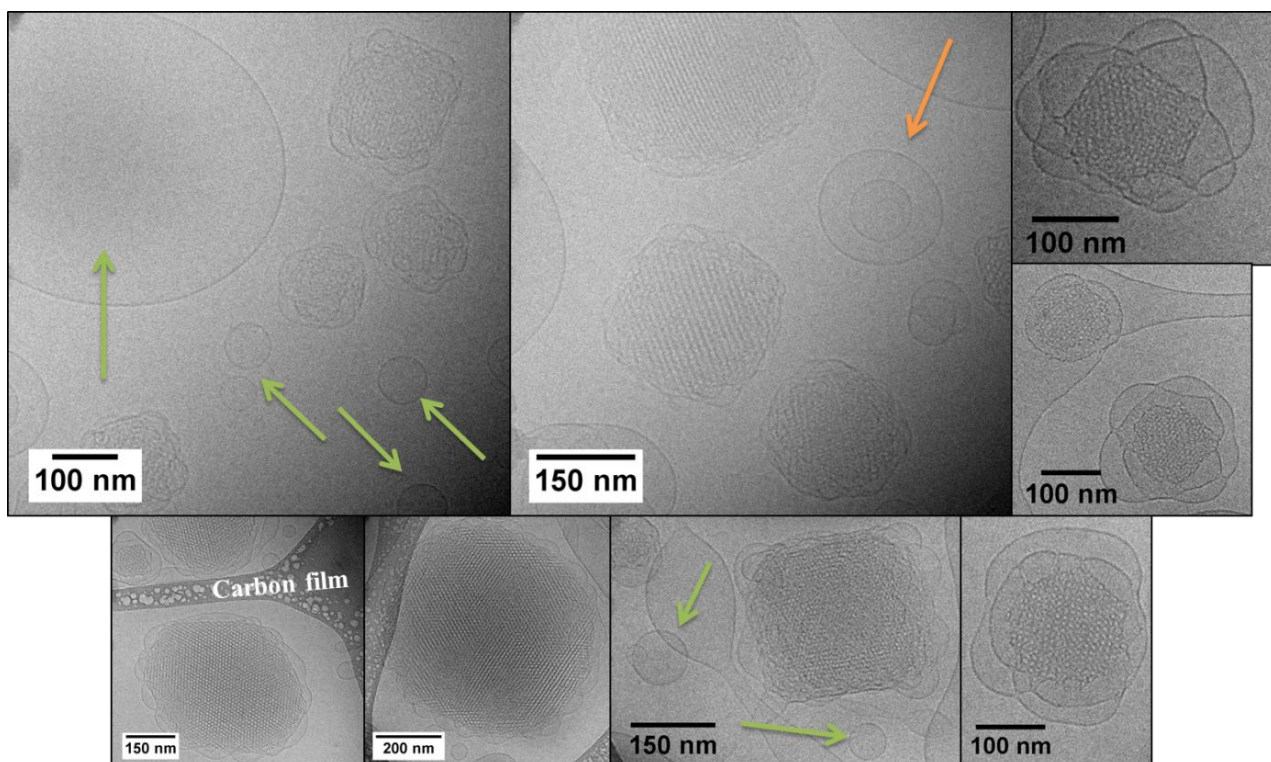


Figure 37. Cryo-EM micrographs for sample 1.5% w/w MILT. Arrows indicate vesicle particles coexisting with the cubosomes. In addition, an envelope is clearly seen around the particles, this is thought to be the F127 polymer acting on the surface of the cubosomes.

When performing the FFT analysis, not all particles could give a clear FFT shape, as shown in Figure 38, therefore, only some particles in the micrographs of Figure 37 were taken into account for lattice parameter calculations.

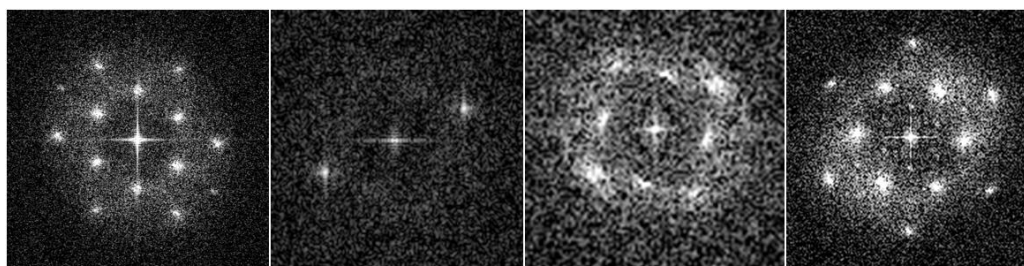


Figure 38. FFT's from some particles in the micrographs of Figure 37. Not all particle could give a clear FFT, therefore, only particles with the given shapes were taken into account for the lattice parameter calculation.

From the found FFT's, one finds the following calculated of lattice parameters:

13.5(5) nm	9.7(5) nm	9.2(5) nm
13.0(5) nm	8.0(5) nm	11.7(5) nm

It is noticeable that a assume a wide range of values for the different particles in the sample. Although this is not different from the blank sample (Figure 29), so that one cannot stake that MILT changes the internal structure of the cubosomes just based on cryo-EM data. An initial conclusion for GMO-cubs is that it does interact with MILT up to a concentration of 4% w/w without destroying the internal organization of the nanoparticle. At 5% w/w MILT begins to be a critical percentage (in mass) for the stability of the cubosomes, since it was difficult to see internal structure in the nanoparticles by cryo-EM.

Due to difficulties in the reproduction of this protocol and the low availability of monoolein, owed to its very high cost, this protocol was abandoned during the first year of the project. A myverol 18-99k was received as a gift from Kerry® and studies of GMO based cubosomes were continued with this product.

5.2 Myverol based cubosomes

Knowing that myverol (MYV) is a mixture of lipids, in which monoolein constitutes at least 60% of the product (DONG et al., 2010). MYV was used as lipid base for the production of Myv cubosomes, from now on referred as Myv-cubs. A new protocol was proposed (see method session) to produce Myv-cubs based on the PHY protocol by Akhlaghi et al. (AKHLAGHI et al., 2016).

First, variable amounts of F127 were added to the formulation in order to see which percentage would give the most stable colloidal dispersion. This evaluation was based in the visual aspect (aggregates in the sample) of the formulation and by SAXS. Results are displayed in Figure 39. The curves are shown in crescent concentration of F127 relatively to the mass of the lipid. It is clear that a small amount of F127 (5% w/w to 8% w/w) makes cubosomes with coexistence of phases (Im3m and Pn3m). For higher amounts only Im3m phase exists, but the dispersions from 10% w/w to 40% w/w presented visible aggregates in

the samples. Therefore it was chosen to continue the myverol cubosomes formulation with 50% w/w (~4 mM) F127.

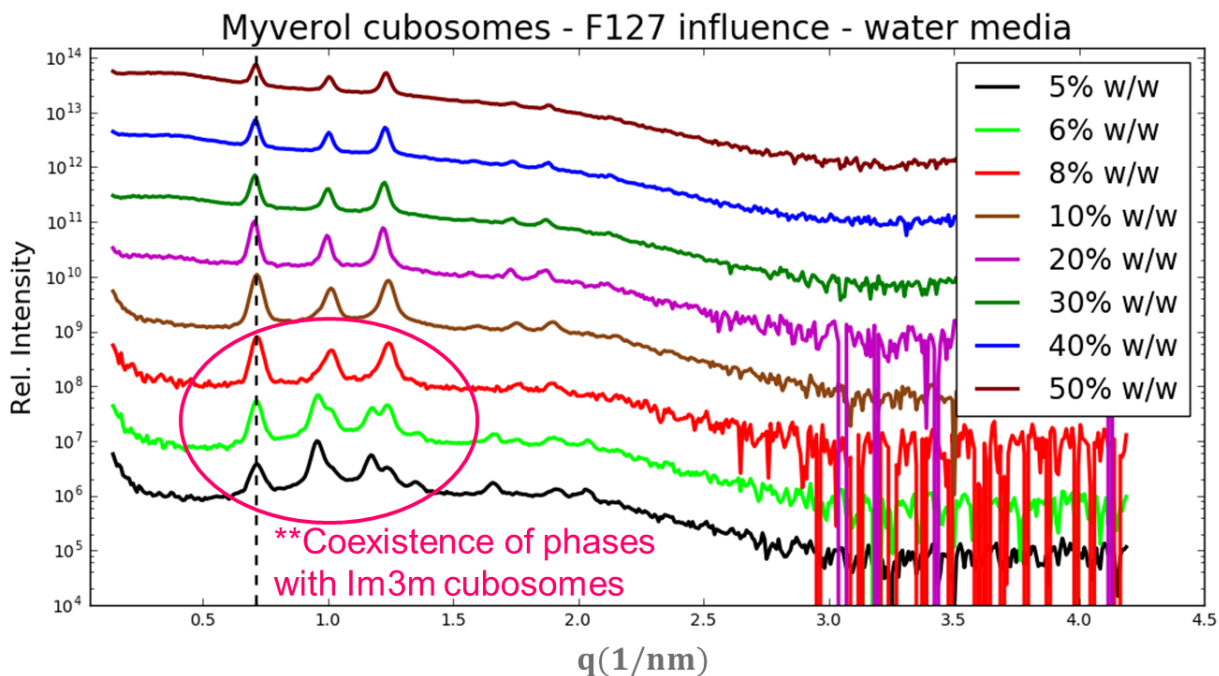


Figure 39. SAXS data for myverol cubosomes at increasing F127 concentration relative to the lipid weight. It can be seen that for low percentages, 5% to 8%, there is coexistence of phases Pn3m and Im3m in the sample. At higher F127 concentrations, only Im3m phase exists.

Myv-cubs were studied by SAXS, TEM and DLS, both in water and in the presence of 2.25% w/v glycerol. Figure 40 displays SAXS data for Myv-cubs in both media. As can be seen, five peaks clearly rise above the overall curve, their indexation based on Table 1, reveals Im3m cubosomes for both media with calculated lattice parameters of $a_{H_2O} = 12.30(12) \text{ nm}$ and $a_{GLY} = 12.23(34) \text{ nm}$. 3

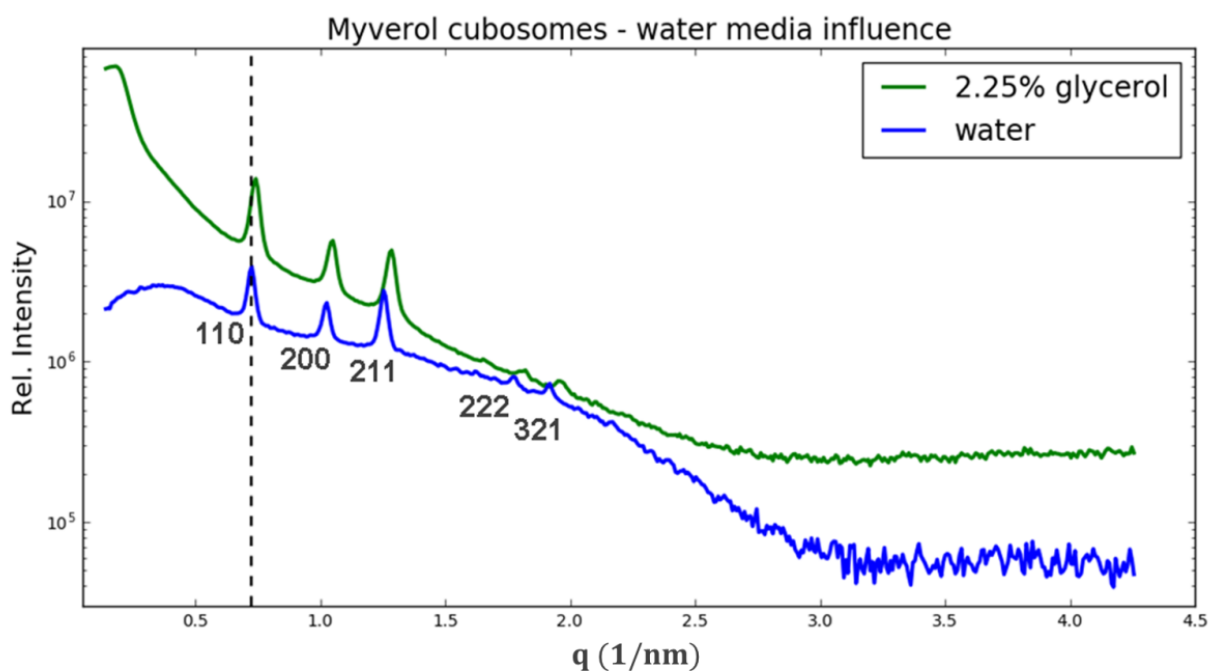


Figure 40. SAXS data for Myv-cubs in both water and glycerol media. Indexed peaks rise in the overall curve, revealing cubic structure for these cubosomes in both media.

Since there are few bottom up (BU) protocols for monoolein/myverol in literature, comparison between top down (TD) and BU protocols could not be made. It is clear that the method of cubosomes production does not significantly alter Myv-cubs lattice parameter, which is in the same order of magnitude as in TD method, see Figure 26. An interesting fact is that, even knowing that MYV is a mixed sample (only 60% GMO), the blank cubosomes production reveals only Im3m cubosomes with no distinguishable interference of the other molecules assembly contribution to the colloidal system.

For BU reported protocols with pure GMO, calculated lattice parameters are in good agreement with the found values for these samples (SHERIF; BENDAS; BADAWY, 2014)(HARTNETT et al., 2015)(TRAN et al., 2017). DLS revealed particles with sizes about 280(5) nm and moderate polydispersion 0.115(52) in water. Literature reports smaller sizes (~150 nm) due to the use of a sonication step in the preparation, in order to diminish particle size (SHERIF; BENDAS; BADAWY, 2014)(HARTNETT et al., 2015).

TEM experiments revealed that this system contains nanoparticles, as displayed in Figure 41 and Figure 42. In these micrographs, when in water (Figure 41) cubosomes present

sizes around ~500 nm and curious shapes. It is thought that the nanoparticles displayed such a leaked shape due to vacuum influence, but their overall look is still square. The same behavior occurs in glycerol medium (Figure 42), where cubosomes are the particles indicated in pink circles, with sizes ranging from 400 nm to more than 1 μ m. Also, other particles were present in the sample, displayed by green arrows. These other nanostructures, that present significant leakage, are thought to be made by other molecules in the myverol sample (only 60% of myverol is GMO).

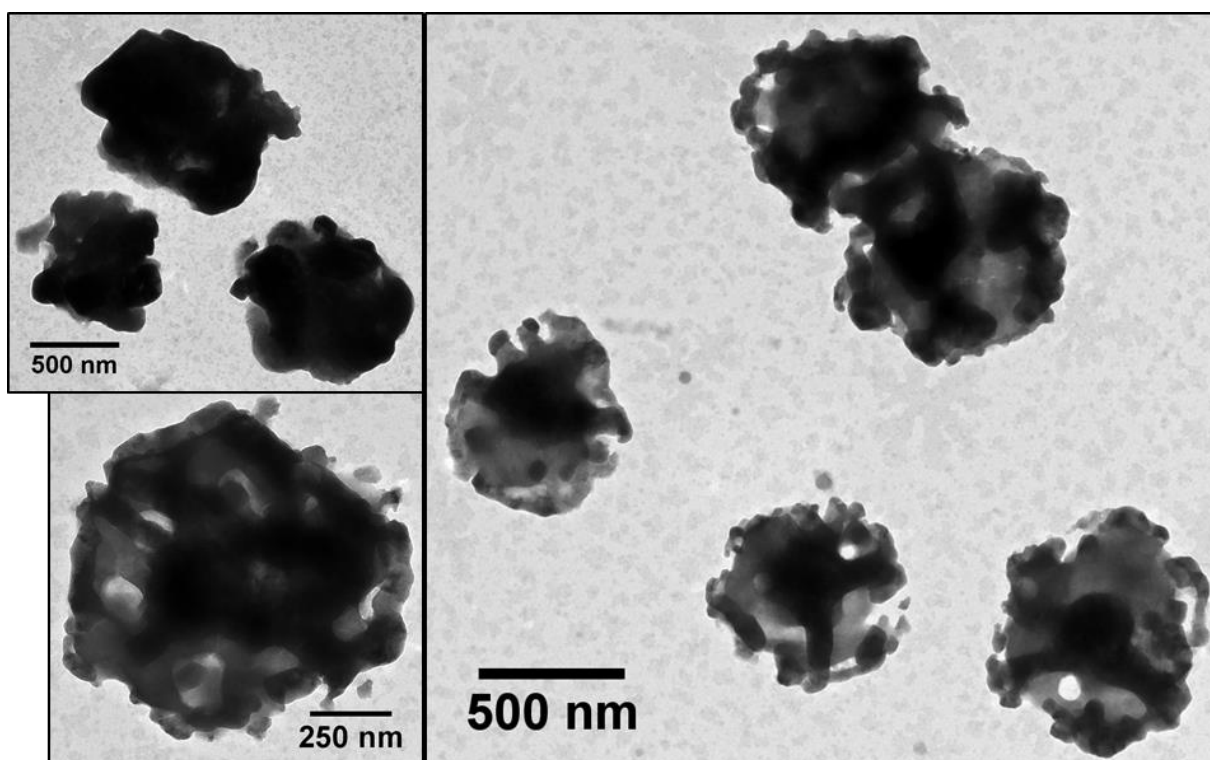


Figure 41. TEM micrographs for MYV-cubs produced by bottom up (BU) method in water medium. Particles have a mean size around ~500 nm and they display leaked shapes, the assumption is that vacuum may have interfered in the overall shape of particles. Although their motifs continue to be square.

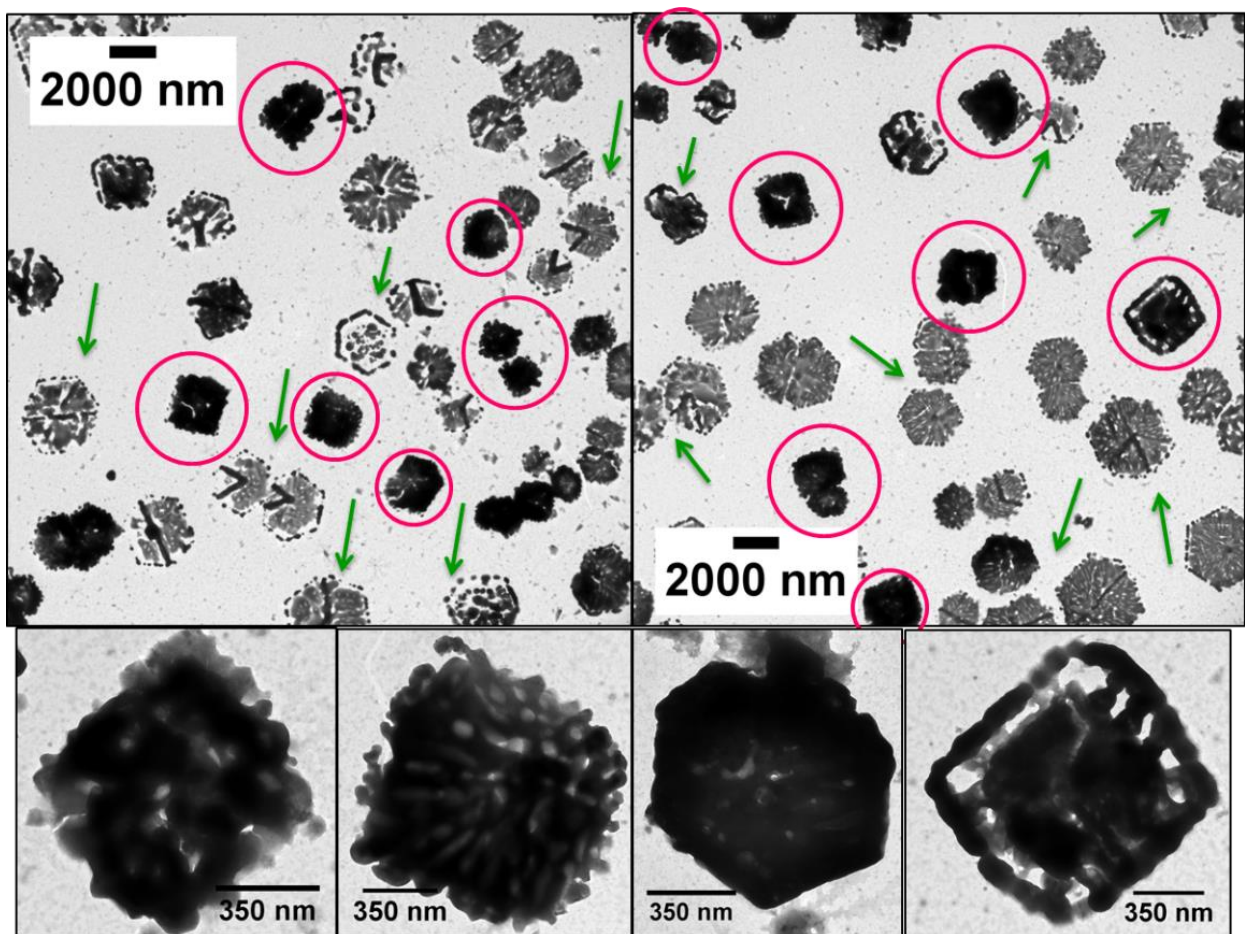


Figure 42. TEM micrographs for MYV-cubs in 2.25% w/v glycerol. Differently from water, in this sample besides cubosomes (pink circles), other particles appear in the sample (green arrows), they present varied shapes and some leakage. These other particles are thought to be formed by the other molecules in myverol.

Since monoolein and the other components (see method section) are glyceryl type lipids, it is reasonable to infer that a glycerol medium influences the interaction between molecules and molecular self-assembly. For blank samples, SAXS does not reveal other structures in the colloidal dispersion, but on TEM micrographs there is a significant presence of unknown particles of varied shape in the sample. In order to better investigate these nanosystems, cryo-EM would be a suitable experiment.

There are few reports of myverol cubosomes in water or PBS media in literature, but the found ones also report lattice parameters ~ 12 nm and $Im\bar{3}m$ cubic symmetry (BYE et al., 2014)(LARKIN et al., 2016)(VAN 'T HAG et al., 2017)

The next step was to evaluate the colloidal myverol system under the influence of temperature. Figure 43 shows SAXS curves for samples studied at 22 °C (room temperature), 40 °C, 50 °C and 65 °C. It is clear from the graphs that only at 22 °C the colloidal system holds the Im3m conformation. When temperature rises, the hexagonal structure begins to appear and at 40 °C there is coexistence of Im3m (blue arrows) and hexagonal (green arrows) phases given by the other visible peaks in the curve. At 50 °C almost all particles present hexagonal structure, Im3m peaks can be seen in the curve but with very low intensity. At 65 °C only the hexagonal phase exists. This phase transitions over temperature are thought to be due to the presence of other molecules in the MYV mixture, since GMO phase diagram reveals hexagonal phase only at very high temperatures (80 °C above), see Figure 5.

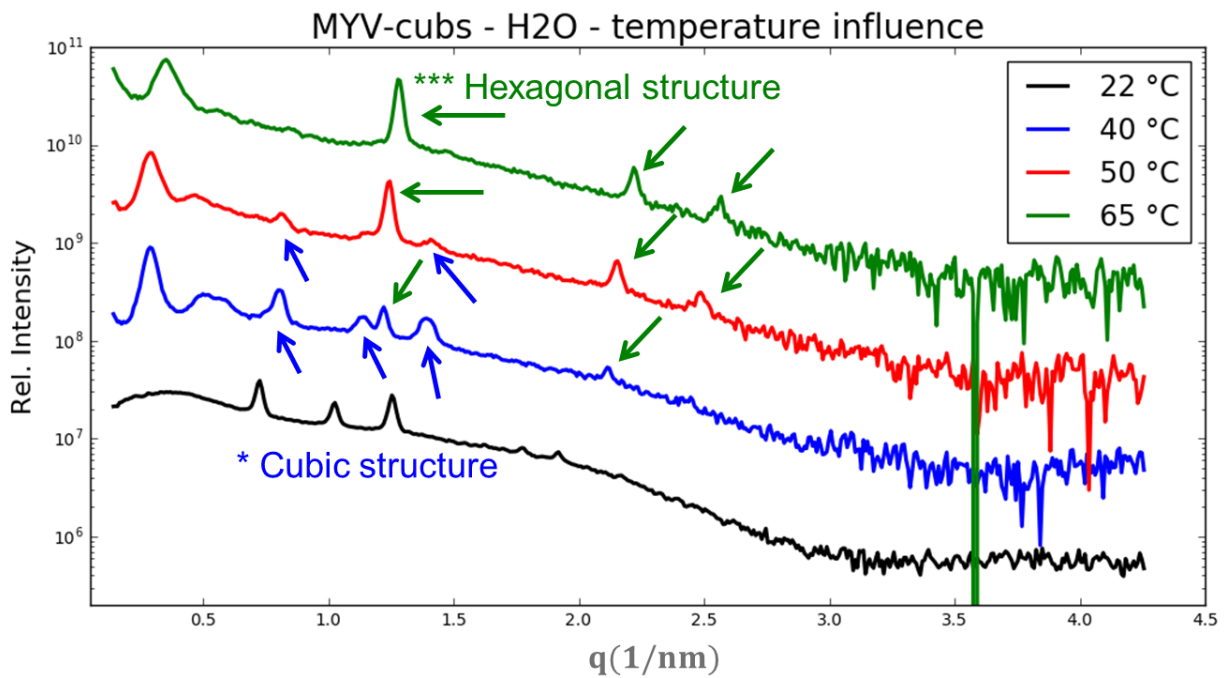


Figure 43. Myverol blank cubosomes SAXS data over temperatures. It is clear that over the influence of higher temperatures, the cubosomes go under phase transition from cubic phase (blue arrows) to hexagonal phase (green arrows). This feature is probable to happen due to the other molecules present in the myverol mixture.

5.2.1 Myverol based interaction with miltefosine

It was chosen to work with the same quantities of MILT for the Myv-cubs, as it was for the GMO-cubs. The calculated molarities for each sample are displayed in Table 5, for a sample with final volume of 4 mL.

Table 5. Calculated masses and concentrations of incorporated MILT for Myv-cubs.

Chosen quantities of MILT loaded into the cubosomes		
Considering a final sample volume of 4mL		
Considering GMO 60% of Myverol total mass		
Considering the GMO mass per sample: 100 mg		
% w/w	mg/mL	mM
0.5	0.13	3.1
1.0	0.25	6.1
2.0	0.50	12.3
3.0	0.75	18.4
4.0	1.00	24.6

SAXS and TEM were performed with these samples in both water and 2.25% glycerol medium. Figure 44 and Figure 45 display the SAXS results for loaded Myv-cubs. In Figure 44 cubosomes in water media still hold their Im3m crystallographic symmetry with the addition of MILT given by the five visible peaks in the curve. Interestingly, lattice parameters (a) are altered due to the peak shifting for lower q values, indicating that a increasing as more MILT is loaded in the cubosomes.

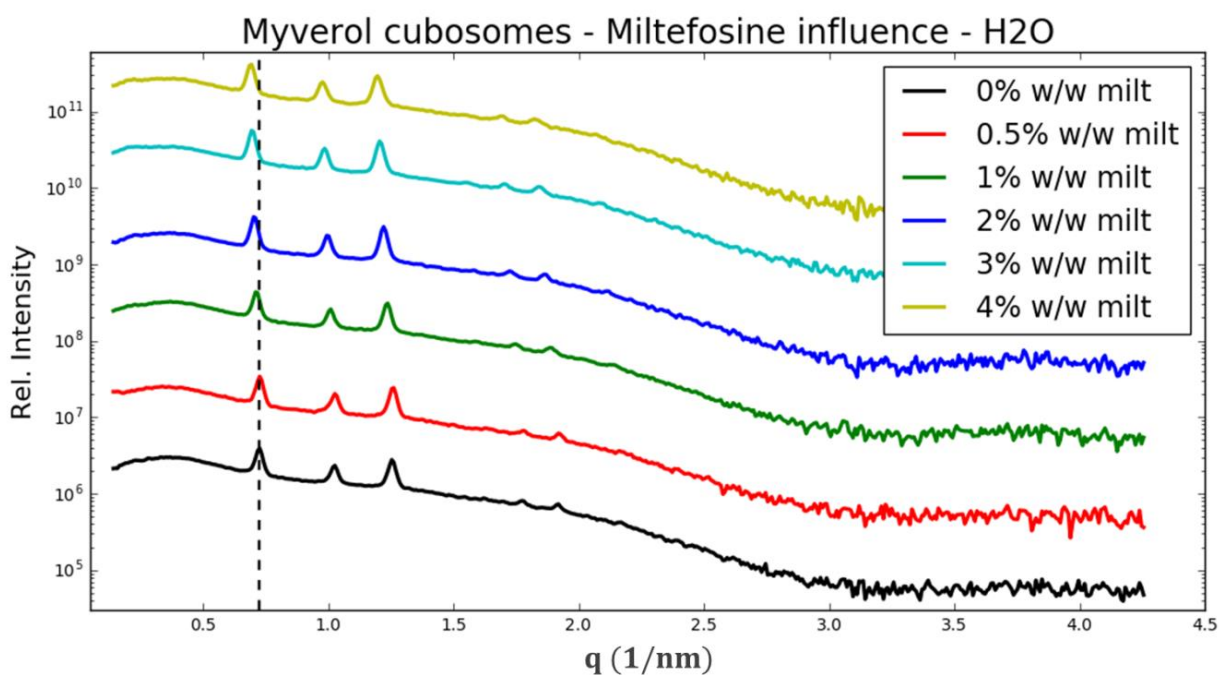


Figure 44. SAXS results for loaded Myv-cubs in water medium. The addition of MILT to the cubosomes does not destroy the crystallographic $Im\bar{3}m$ symmetry of the nanoparticles but alters its lattice parameter, given by the shifts in the peaks positions.

Similar effect was observed for cubosomes in 2.25% glycerol medium. The loading of MILT into the nanoparticles also changed the lattice parameters for higher values without changing the crystallographic symmetry of the nanoparticles. Curiously, for 0.5% w/w, 1% w/w and 2% w/w MILT other inner structures appear in the colloidal system, see pink circle in Figure 45. Two main possibilities are proposed, or glycerol molecules in the aqueous media induce the formation of other phases in the presence of MILT, or the other molecules in the myverol mixture are responsible for that. No further SAXS experiments were performed to investigate these possibilities.

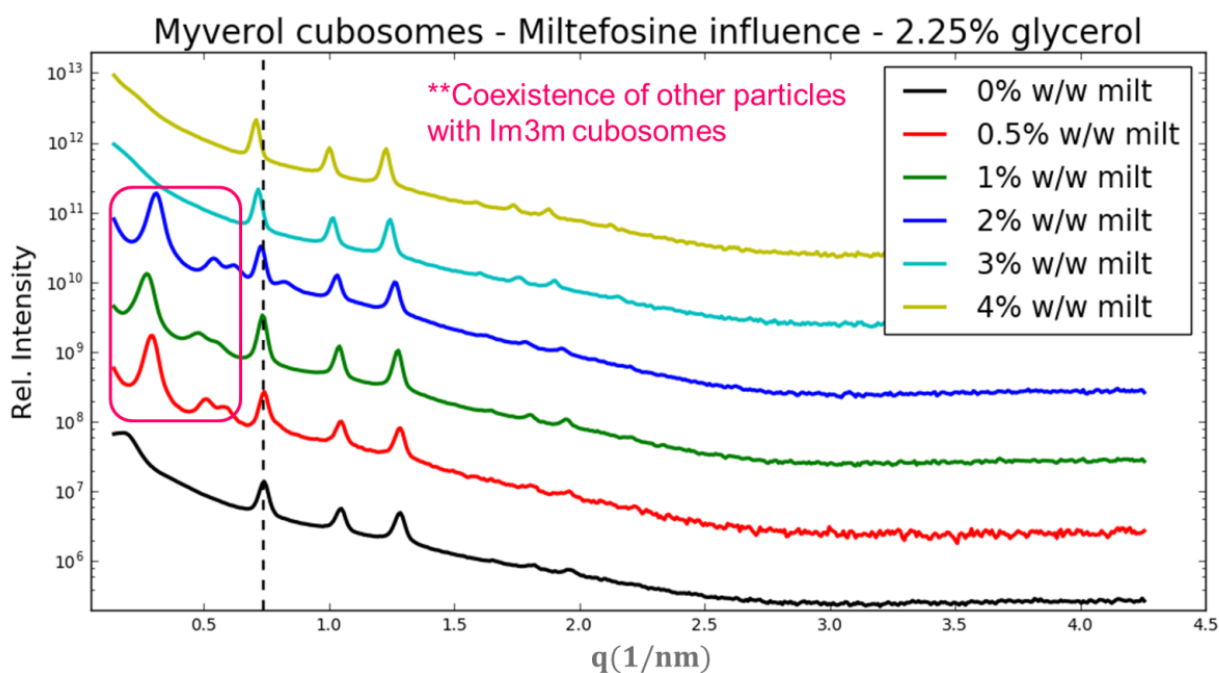


Figure 45. SAXS results for loaded Myv-cubs in 2.25% glycerol medium. The addition of MILT to the cubosomes does not affect particle crystallographic symmetry but at 0.5%, 1% and 2% there are other unknown particle structures in the sample, given by the peaks at low q values. Overall, for Im3m cubosomes, MILT only affects the lattice parameter inflicted by the first peaks shift for lower q values.

Considering only the Im3m cubosomes phase in the samples, the calculated lattice parameter values for both aqueous media are displayed in Figure 46. Overall, both aqueous media (water or 2.25% glycerol) produce cubosomes with the same lattice parameters in presence or absence of MILT, given by the statistical z -test analysis between a values. In water medium, MILT only changes significantly the lattice parameter at 4% w/w loading. Interestingly, in 2.25% glycerol medium, there were no significant changes in lattice parameter for all MILT loaded concentrations, therefore no conclusion can be made about MILT interaction with cubosomes in this aqueous medium.

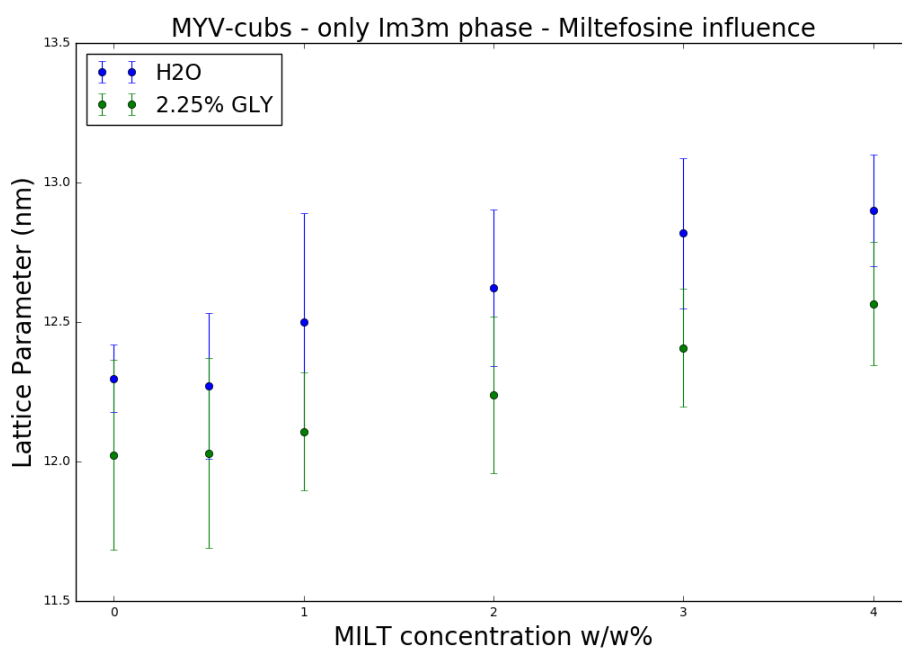


Figure 46. Calculated lattice parameters for Myv-cubs loaded with MILT in both water and glycerol aqueous media. Comparing values through statistical methods, MILT only significantly alters the lattice parameter of the cubosomes when in 4% w/w.

TEM measurements were performed with Myv-cubs loaded with 2% and 3% w/w MILT in water medium. Results are shown in Figure 47 and Figure 48. All micrographs revealed particles in square shapes in varied size, for sample 2% w/w MILT, Figure 47, particle size fluctuated between ~400 nm and ~2 μ m indicating a large polydispersion on the sample. For sample 3% w/w MILT, Figure 48, particle size fluctuated much less, going from ~400 nm to 1 μ m only.

In addition, comparing the loaded MILT samples with the blank Myv-cubs, see Figure 41, MILT does seem to affect particle size since for blank cubosomes particles presented sizes no bigger than ~600 nm and with loaded MILT particles reached 1 μ m. Further DLS measurements should be made to confirm this hypothesis.

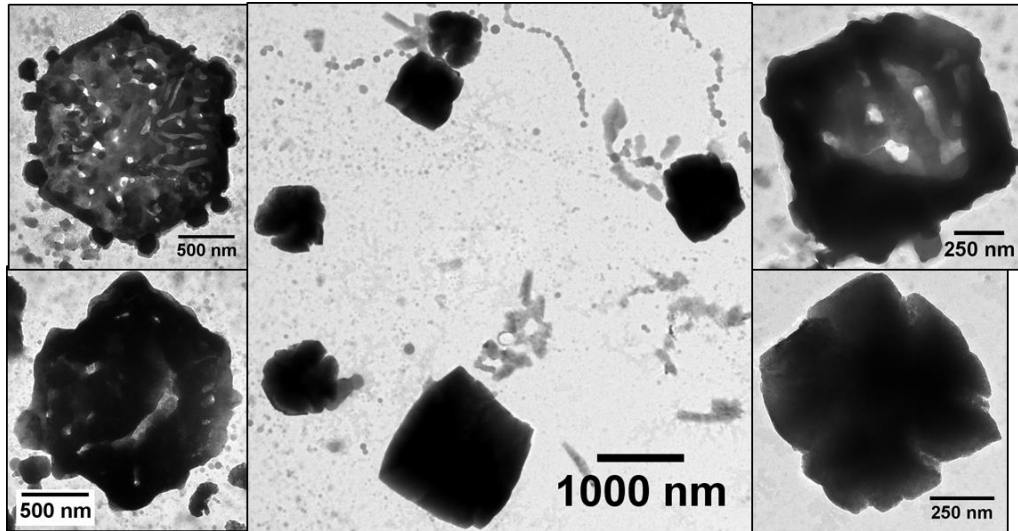


Figure 47. TEM micrographs for Myv-cubs loaded with 2% w/w MILT. Most particles presented square shapes with irregular surface. Significant size polydispersion is revealed since particles present varied sizes from ~400 nm to 2 μ m.

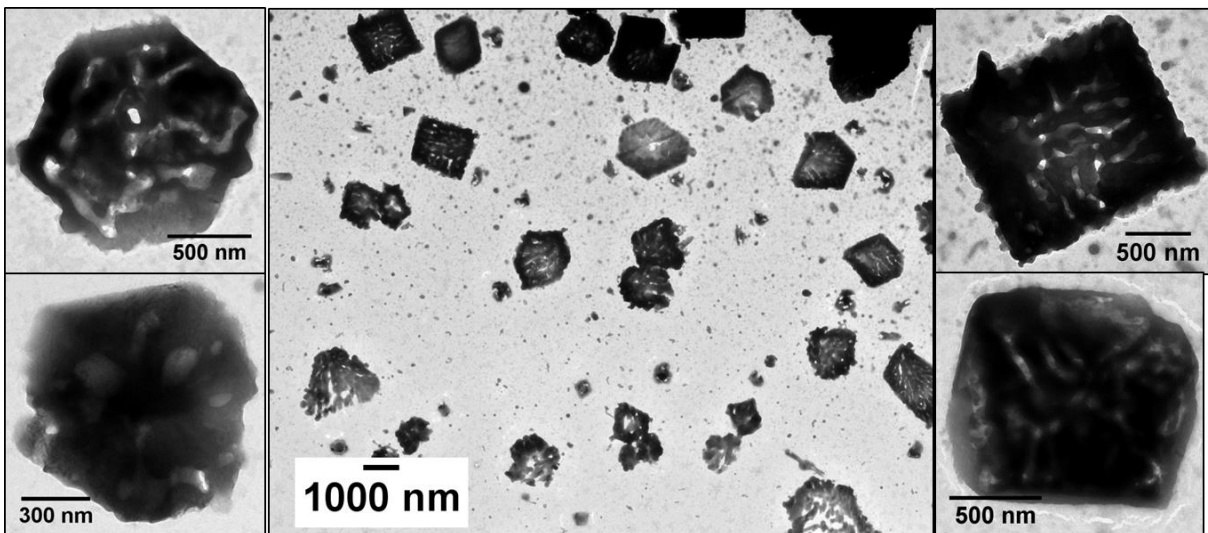


Figure 48. TEM micrographs for Myv-cubs loaded with 3% w/w MILT. Particles revealed square shapes and similarly to sample 2% w/w, polydispersion is also very present in these samples, where sizes fluctuate between ~400 nm to 1 μ m.

Finally, due to the unknown effects of other lipid molecules in the myverol mixture, this proposed protocol should be more investigated in order to fully understand the influence of a non-pure GMO mixture in the cubosomal production. Besides, separation methods could be proposed in order to make the colloidal system more pure.

5.3 Phytantriol based cubosomes

Cubosomes manufactured with phytantriol (PHY) were successfully reproduced using the protocol proposed by Akhlagui et al. (AKHLAGHI et al., 2016). PHY is known to have higher structural stability, due to the presence of saturated bonds and the lack of ester groups (AKBAR et al., 2017), it is also cheaper than GMO. PHY nanocarriers research is advantageous, once it can lead to more stable nanoparticles that suffers less from digestion processes, like cleavage and degradation, for instance (BARRIGA; HOLME; STEVENS, 2018). Phytantriol based cubosomes (from now on referred as PHY-cubs) were produced in water, 2.25% w/v glycerol media and PBS buffer.

The percentages of MILT to be incorporated into the cubosomes were chosen from very small amounts to higher quantities. Table 6 shows the calculated quantities going from 0.5% w/w (~0.24 mM) to 20% w/w (~9.8 mM), these values were estimated based on the structure of MILT. The chosen concentrations did not reach the clinical dosage.

Table 6. Calculated chosen percentages of MILT incorporated into the cubosomes.

Chosen quantities of MILT loaded into the cubosomes		
Considering a final sample volume of 5mL		
Considering the PHY mass per sample: 100 mg		
% w/w	mg/mL	mM
0.5	0.1	0.24
1.0	0.2	0.49
2.0	0.4	0.98
3.0	0.6	1.47
4.0	0.8	1.96
5.0	1.0	2.45
10.0	2.0	4.91
15.0	3.0	7.36
20.0	4.0	9.81

Both co-solubilization and addition after prepared blank cubosomal dispersion methods were tested for MILT encapsulation. All systems were characterized by SAXS, TEM, cryo-EM and DLS.

5.3.1 PHY - cubosomes in the absence of MILT

Figure 49 shows SAXS data for Phy-cubs in water media at 22°C (room temperature), where six well defined peaks clearly arise, indicating periodicity in the inner structure of the nanoparticles. Each peak, corresponds to a crystallographic plane and it also corresponds to a given square root, for instance, peak 110 = $\sqrt{2}$, 111 = $\sqrt{3}$, 200 = $\sqrt{4}$, 211 = $\sqrt{6}$, and so on, see methods section and Table 1 for further references. This information leads to the calculation of a lattice parameter, which gives an indication of water channel size of the cubosomes.

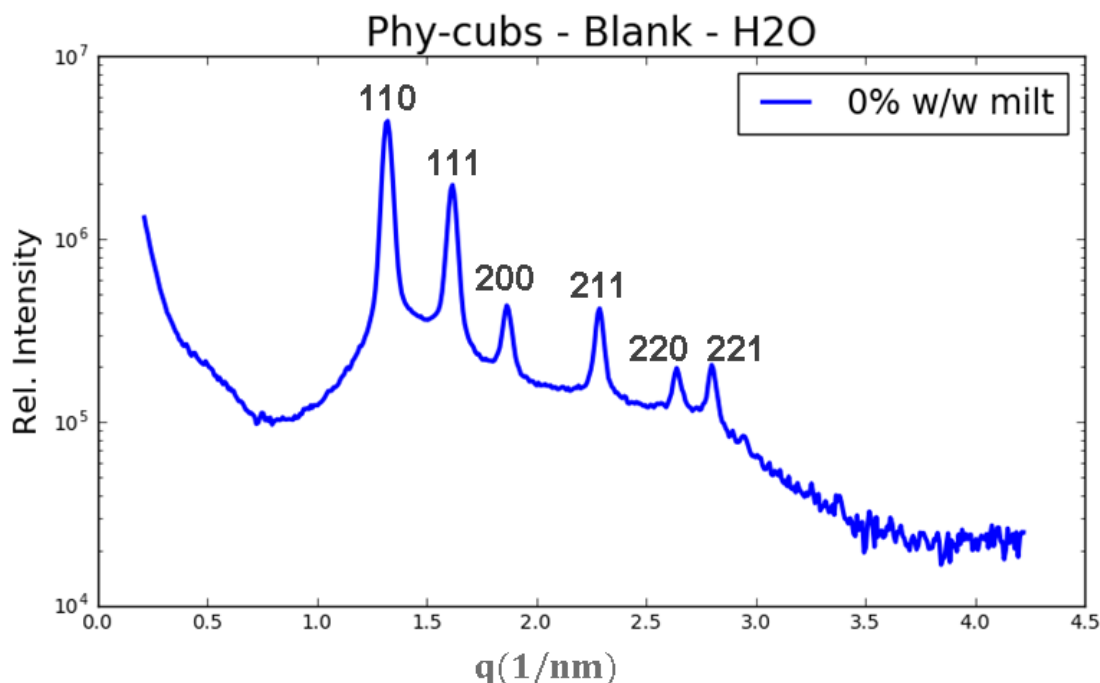


Figure 49. SAXS curve for cubosomes in water media with indexed crystallographic peaks. Each number refers to a crystallographic index, the Muller indices, which indicates the reflection planes in the diffraction peaks.

Cubosomes were also produced in PBS buffer and 2.25% w/v glycerol media. Figure 50 shows data for cubosomes in different water media. It is clear from the graph that different media did not affect the inner structure of the nanoparticle, neither the calculated lattice parameters, as shown in Table 7.

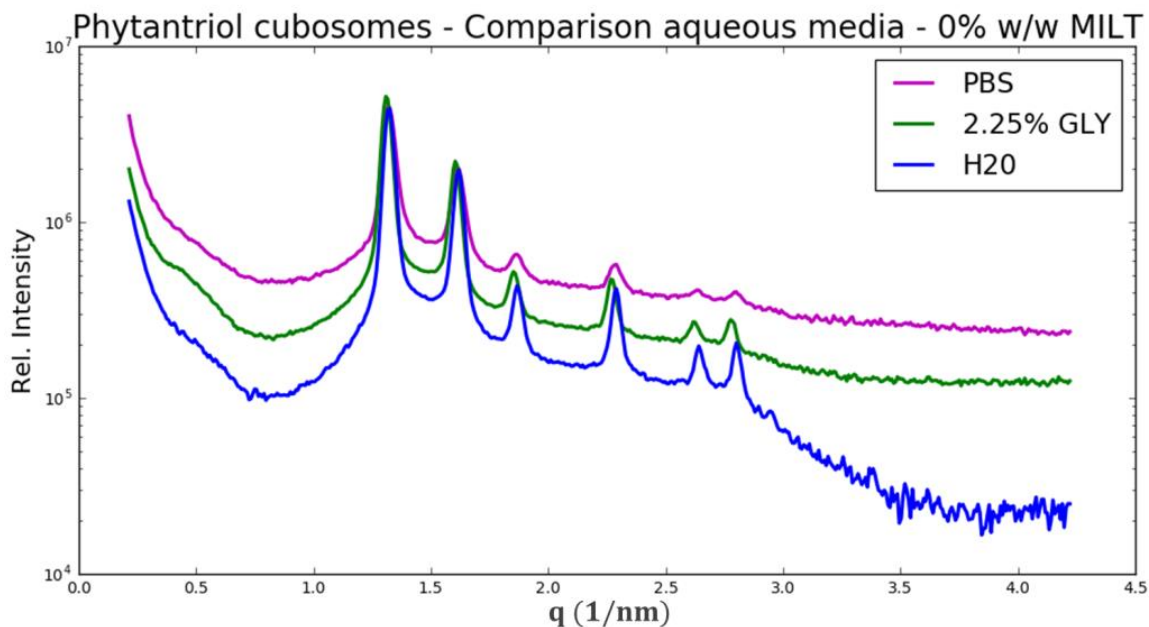


Figure 50. SAXS curves for cubosomes in different media (PBS, glycerol and water). It is clear that the change in aqueous media does not affect the cubosomes inner structure, once all curves were analogous. The difference in intensity only refers to a slight variation in the concentration of the samples (~25 mg/mL).

Table 7. Calculated Lattice parameters of cubosomes in different aqueous media. There is no change in the water channels of the nanoparticles prepared in water, PBS or glycerol.

Blank Phy-cubs in different water media					
Sample	Peak positions (nm^{-1})				Calculated Lattice Parameter (nm)
medium	q1	q2	q3	q4	
Water	$1.322 \pm$	$1.616 \pm$	$1.863 \pm$	$2.286 \pm$	6.74(07)
	0.023	0.025	0.029	0.028	
PBS	$1.317 \pm$	$1.610 \pm$	$1.862 \pm$	$2.285 \pm$	6.75(10)
	0.026	0.028	0.031	0.031	
2.25% Glycerol	$1.309 \pm$	$1.601 \pm$	$1.847 \pm$	$2.264 \pm$	6.79(06)
	0.023	0.026	0.030	0.029	

In order to determine the crystallographic symmetry of the cubosomes, the peak ratio was analyzed. Each structure holds a different peak ratio regarding the first peak, in

Table 8, one can see the first three peak ratios for both Im3m and Pn3m crystallographic symmetries. When calculating these ratios for samples in Figure 50, the found symmetry was Pn3m. These results are in good agreement with those reported by Akhlaghi et al. (AKHLAGHI et al., 2016), where a lattice parameter of ~6.4 nm for the chosen protocol for cubosomes with Pn3m crystallographic symmetry. Literature also reports blank PHY-cubs with lattice parameters in the order of 6 nm to 7 nm, where different protocols were used (ALCARAZ et al., 2018)(ASTOLFI et al., 2017)(SHI et al., 2015).

Table 8. Peak positions and ratios for cubosomes samples in different aqueous media. Showing that Phy-cubs have Pn3m crystallographic symmetry.

Sample	Peaks positions and ratios			Reference values		Reference values	
				Im3m symmetry	ratio	Pn3m symmetry	ratio
Phy-cubs (medium)	q2/q1	q3/q1	q4/q1				
Water	1.2223	1.4092	1.7291	$\frac{q2}{q1} = \sqrt{2}$	1.4142	$\frac{q2}{q1} = \sqrt{\frac{3}{2}}$	1.2247
PBS	1.2224	1.4138	1.7350	$\frac{q3}{q1} = \sqrt{3}$	1.7321	$\frac{q3}{q1} = \sqrt{2}$	1.4142
2.25% Glycerol	1.2230	1.4110	1.7296	$\frac{q4}{q1} = \sqrt{4}$	2.0000	$\frac{q4}{q1} = \sqrt{3}$	1.7321

Cubosomes were also submitted to extrusion and lyophilization treatments, both in water and PBS media. Extrusion was performed in a mini extruder from Avanti Polar Lipids Inc. using polycarbonate membranes in 0.4 μm , 0.2 μm , 0.1 μm , 0.05 μm and 0.03 μm pore sizes. For lyophilization, where samples were plunged into liquid nitrogen at -70°C overnight, and the evaporation process was performed in a Liotop® L101 equipment at -53°C for 22h in low pressure (0.120 mBar). For sample analysis, they were re-hydrated with the respective medium in a water bath at 45°C prior to measurements.

Results in Figure 51 and Figure 52 are quite interesting. Samples only loose concentration (due to the difference in measured intensity), but the inner structure of the nanoparticles remains the same. In water, Figure 51-A, only two peaks appear in the overall curve, it is possible that other peaks were lost in the noise due to the great loss in

concentration for this lyophilized sample. When extruded, Figure 51-B, some concentration is lost but all peaks still appear.

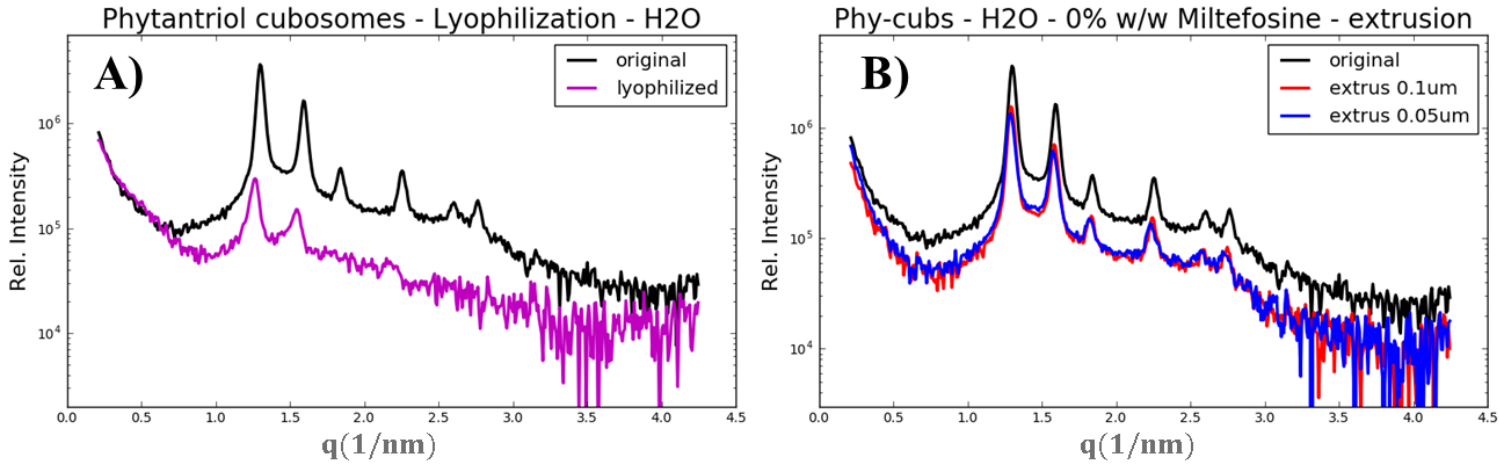


Figure 51. Lyophilized A) and extruded B) cubosomes in water medium. In both procedures the sample loses concentration, but when lyophilized this feature is far more evident. Although there is no change in the inner structure of the cubosomes after both processes.

In PBS medium, Figure 52-A, the lyophilized colloidal system seems to have favorable assembly into cubosomes when re-hydrated, because of the little loss in concentration and all four peaks appearance. The same happened for extrusion, Figure 52-B. When calculating the lattice parameters of the nanoparticles, before and after treatments for both media, the values remained the same (~6.8 nm). This indicates that Pn3m cubosomes are versatile nanoparticles, once they can be lyophilized and extruded without loss of morphological properties. This information is important for pharmaceutical applications, once the cubosomal dispersion can be lyophilized for conservation purposes and extruded for size control purposes as well.

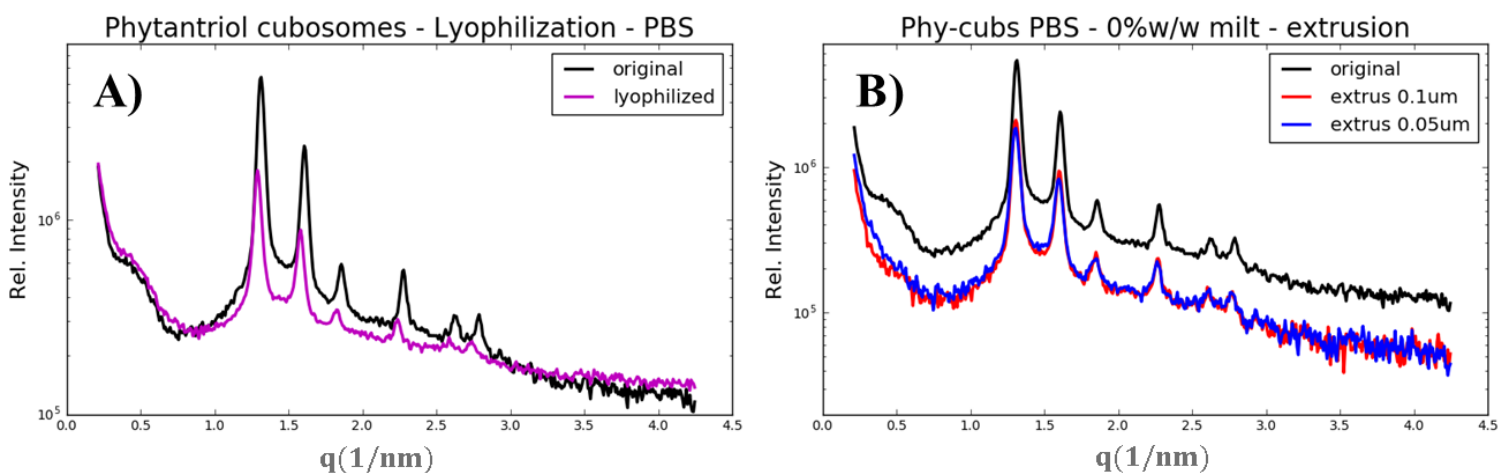


Figure 52. Lyophilized A) and extruded B) cubosomes in PBS medium. Four peaks clearly rise in the lyophilized sample, showing that PBS seems to be a favorable environment for cubosomes formation after re-hydration. In the extruded sample, cubosomes also lose some concentration but all diffraction peaks are still visible.

In literature, little is known about extrusion and lyophilization process for cubosomes. The latest work mentioning extrusion dates back from 2013, where Nilsson et al. (NILSSON et al., 2013) produced radiolabeled cubosomes for theranostic purposes using extrusion as a way of controlling particle size. In their work, they mention that extruded cubosomes still hold the Pn3m symmetry after the process. Lyophilization have been explored in 2015 in a study by Shi et al. (SHI et al., 2015) where samples were submitted to this process for conservation purposes, after re-hydration of the powder, the cubic structure also remained Pn3m.

DLS experiments were also made to explore the extrusion influence on particle size both with PBS and water samples. An additional study of size stability over time was performed in a total of 4 weeks. For water samples, extrusion was tested with all available filters in the laboratory (0.03 μm to 0.4 μm) and the results are displayed in Figure 53. Raw DLS data is shown in Figure 53-A, where the correlation functions shift to lower time values as the sample is extruded in smaller filters, indicating cubosomes of smaller sizes. This is confirmed by the calculated mean diameters in Figure 53-B, the sample starts with ~ 450 nm, when extruded at the 0.4 μm filter and after extrusion in a 0.03 μm filter, the size dropped to ~ 200 nm. Polydispersion (PDI) of the samples was also reduced when extruded over all filters, going from 0.198(25) to 0.082(14) in the 0.05 μm filter. Our results are in good agreement with those reported by Nilsson et al. (NILSSON et al., 2013), where they extruded

samples in filters going from 800 nm to 100 nm, obtaining particle sizes around ~160 nm and PDI 0.18(2).

For PBS medium, the original sample revealed medium diameter 341(9) nm and PDI 0.104(29) for the original sample, revealing smaller cubosomes than in water. After extrusion in a 0.05 μm pore filter, the nanoparticles presented sizes 217(5) nm and PDI 0.079(19) indicating that extrusion also improved the polydispersity of the system. Samples in PBS medium were not studied over time.

Throughout the four weeks of experiment, sizes remained stable, as can be seen in Figure 53-B, showing that extruded cubosomes did not aggregate back into bigger particles. For lyophilized samples, DLS was also performed, revealing that after re-hydration particles presented mean diameter of 278(4) nm and PDI 0.127(17), for sample in water media, and 308(6) with PDI 0.206(19), for sample in PBS media. Curiously, sizes and PDI were slightly lower than the original sample. These are interesting features that demonstrate cubosomes as remarkable nanoparticles that can resist to extreme processes such as lyophilization and extrusion. These informations are very important for pharmaceutical applications, since keeping small particle size is a requirement for intravenous administration route along with a way of conserving and sterilizing samples through both lyophilization and extrusion.

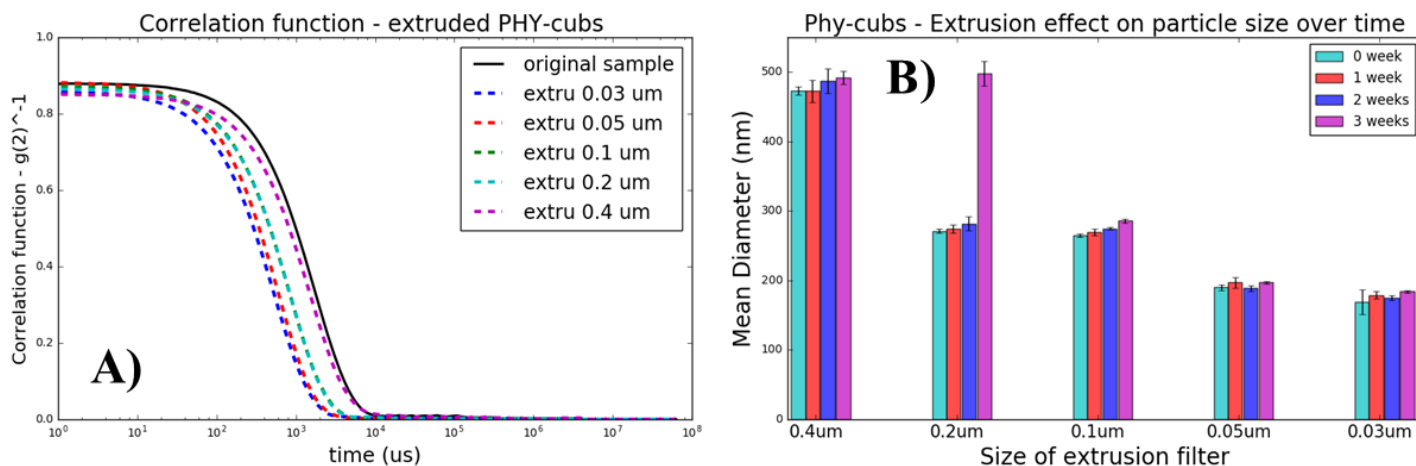


Figure 53. Extruded samples in water media. A) Raw data from DLS, as can be seen, when extruded over the filters the particles have their correlation functions changed, moving toward smaller sized. B) Compilation of size stability over time: overall, the samples in all four weeks have shown to be very stable with no major fluctuations in the mean diameter.

When no extrusion is made, literature reports Phy-cubs particle size ranging from 150 nm to 250 nm due to the use of a probe sonicator along with a top-down technique to produce cubosomes (ALCARAZ et al., 2018)(ASTOLFI et al., 2017)(FRASER et al., 2013)(HINTON et al., 2014). Our results differ from these studies because of the different preparation methods. Although, Akhlagi et al. (AKHLAGHI et al., 2016) reported cubosomes with sizes ~300 nm for the chosen protocol, making our samples in good agreement with their work.

Samples prepared in both water and PBS media were also taken to NTA. Figure 54 and Figure 55 display the results of these experiments. In water medium, Figure 54, cubosomal nanoparticles (blue curve) presented a broad size distribution with mean values of ~353(9) nm and total particle concentration $\sim 3.4(1) \times 10^{12}$ particles/mL. This total particle concentration is calculated from the software estimation of particles in the measured diluted sample, therefore it takes into account the dilution factor. These results are slightly lower than DLS. This small discrepancy is well explained by the limitations of DLS measurements that are highly influenced by the light scattering of bigger particles, while NTA measures single particles instead (RIBEIRO et al., 2018).

When extruded into 0.05 μm pore filters (red curve in Figure 54), the sample reveals mean particle size ~200(3) nm and total particle concentration $\sim 5.0(3) \times 10^{12}$ particles/mL, a concentration higher than the original sample, indicating that through the extrusion process, bigger particles were broken into smaller ones. NTA results for the extruded samples were in good agreement with DLS measurements.

In addition, a rough calculation can be made in order to estimate the concentration in mg/mL of the samples. Taking for instance the results from the extruded cubosomes, considering only cubic nanoparticles of size 200 nm and cubosomes made only of lipid, the rough mass of a unique cubosome can be calculated as:

$$m_{cubosome} = \rho_{cubosome} \cdot V_{cubosome} \quad (10)$$

Where $\rho_{cubosome}$ indicates the estimated cubosome density of ~1 g/mL (the lipids and polymer have densities similar to water, see materials section) and the $V_{cubosome}$ is the volume of a cubic particle of 200 nm. From equation 10, it follows:

$$m_{cubosome} = 1 \frac{g}{10^{-3}L} \cdot 8 \cdot 10^6 \cdot 10^{-27} \cdot 1000L = 8 \cdot 10^{-15}g \quad (11)$$

Therefore, gathering this information (equation 11) with the particle concentration from NTA measurements:

$$\text{concentration of the sample} = 8 \cdot 10^{-15} g \cdot 5.0 \cdot 10^{12} \frac{\text{particles}}{\text{mL}} = 40 \text{ mg/mL} \quad (12)$$

Reaching the final value of 40 mg/mL for an extruded cubosomes sample.

In literature, little is known about NTA measurements for cubosomes. A study by Azmi et al (MAT AZMI et al., 2015) characterized the PHY cubosomes made by a TD protocol using a sonicator, and reported particle mean size ~157(22) nm without mentioning about the particle concentration.

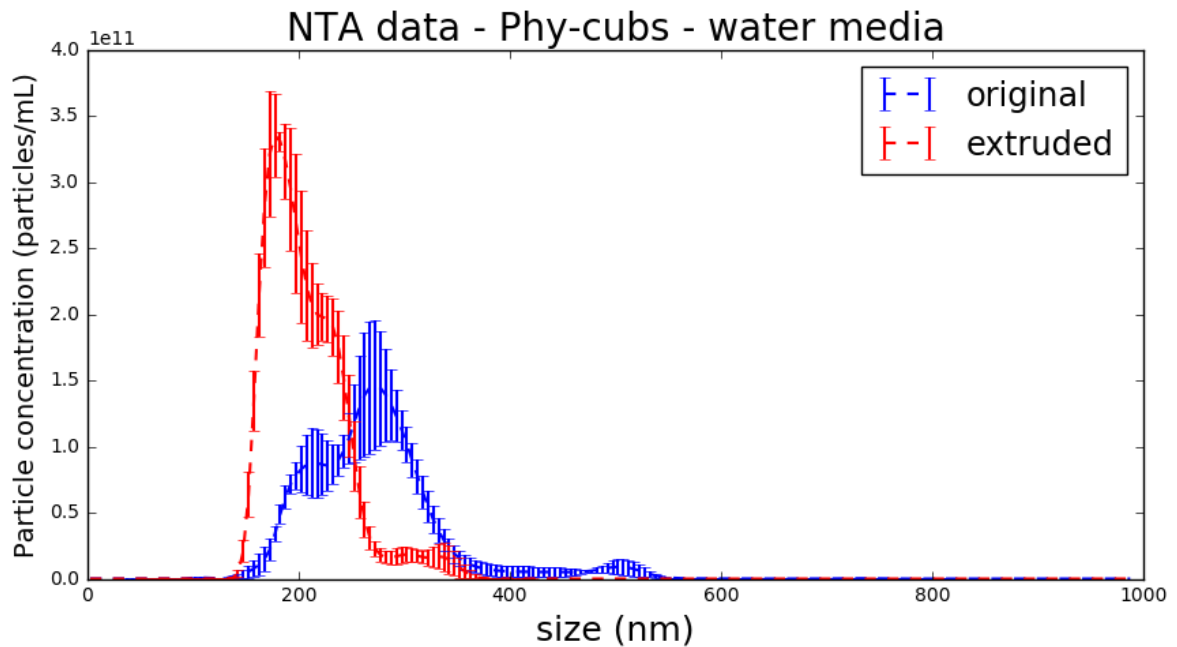


Figure 54. NTA data for Phy-cubs in water medium. Cubosomes presented a wide size distribution before extrusion in a 0.05 μm pore filter (blue curve), with mean value ~353(9) nm, after extrusion (red curve) the particles revealed mean size ~200(3) nm. Interestingly, concentration of particles also increased when extruded, indicating that bigger particles were broken into smaller ones.

Figure 55 displays the NTA results obtained with Phy-cubs in PBS medium. Similarly to water medium, the original dispersion (blue curve) also presented a broad size distribution with mean value ~330(2) nm and total particle concentration $\sim 6.4(3) \times 10^{12}$ particles/mL. NTA results also present sizes smaller than DLS measurements in this case. The extruded in a 0.05 μm pore filter sample (red curve in Figure 55) revealed mean particle size ~217(4) nm

and total particle concentration $\sim 4.3(5) \times 10^{12}$ particles/mL. Differently from water, when extruded the particle concentration slightly diminished, from this one can infer that in PBS cubosomes are less malleable than when in water medium, nonetheless, extrusion makes a shorter particle size distribution.

The lyophilized sample (black curve in Figure 55) reveals a significant reduction in total particle concentration $\sim 1.8(3) \times 10^{12}$ particles/mL and medium calculated size $\sim 303(7)$ nm. From this, one can infer that lyophilization destroy part of the cubosomes in the process of lyophilization. Sizes measured from NTA are in good agreement with DLS measurements.

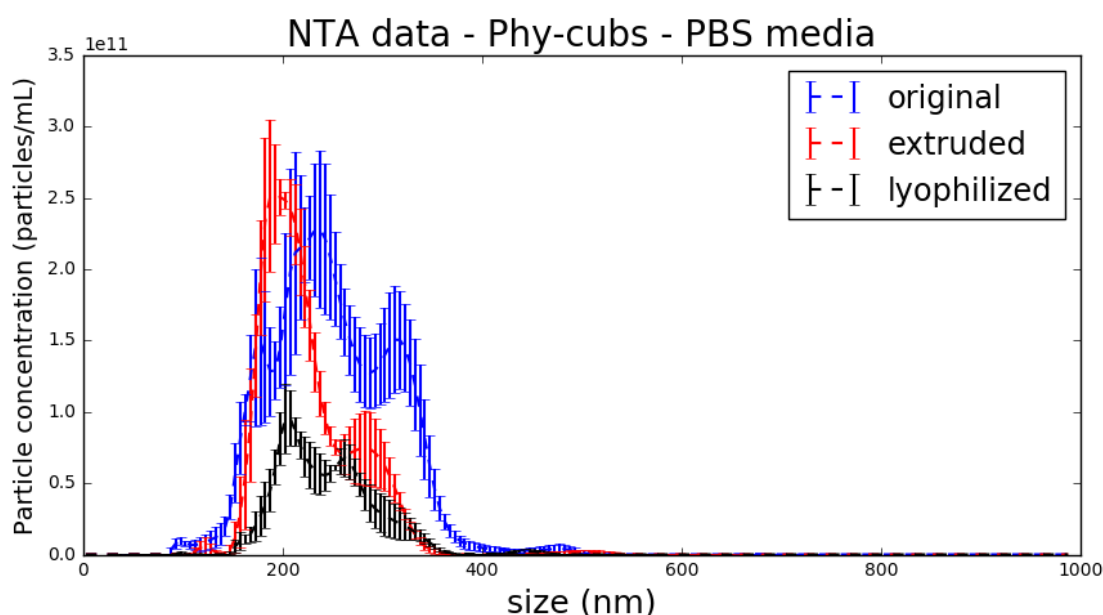


Figure 55. NTA data for Phy-cubs in PBS medium. The original sample (blue) also presented a broad size distribution with mean size $\sim 330(2)$ nm, the extruded sample (red) revealed particles with mean size $\sim 217(4)$ nm but no significant changes in particle concentration in the sample. The lyophilized sample (black) presented mean size $\sim 303(7)$ nm with great loss in particles concentration.

Samples were also analyzed by TEM and Cryo-EM. Figure 56 shows a collection of TEM micrographs that reveals cubosomes with sizes bigger than 500 nm. The micrographs marked with an orange star show peculiar cubic structures, these are thought to be cubosomal nanoparticles as seen by different planes related to the electron beam (as micrographs in Cryo-EM can be seen by different crystallographic planes, see methods section). Their sizes were greater than 1 μm . Sizes accessed in TEM differ a lot from DLS measurements, this is to be thought due to vacuum distortions that the TEM apparatus may cause in the nanoparticles.

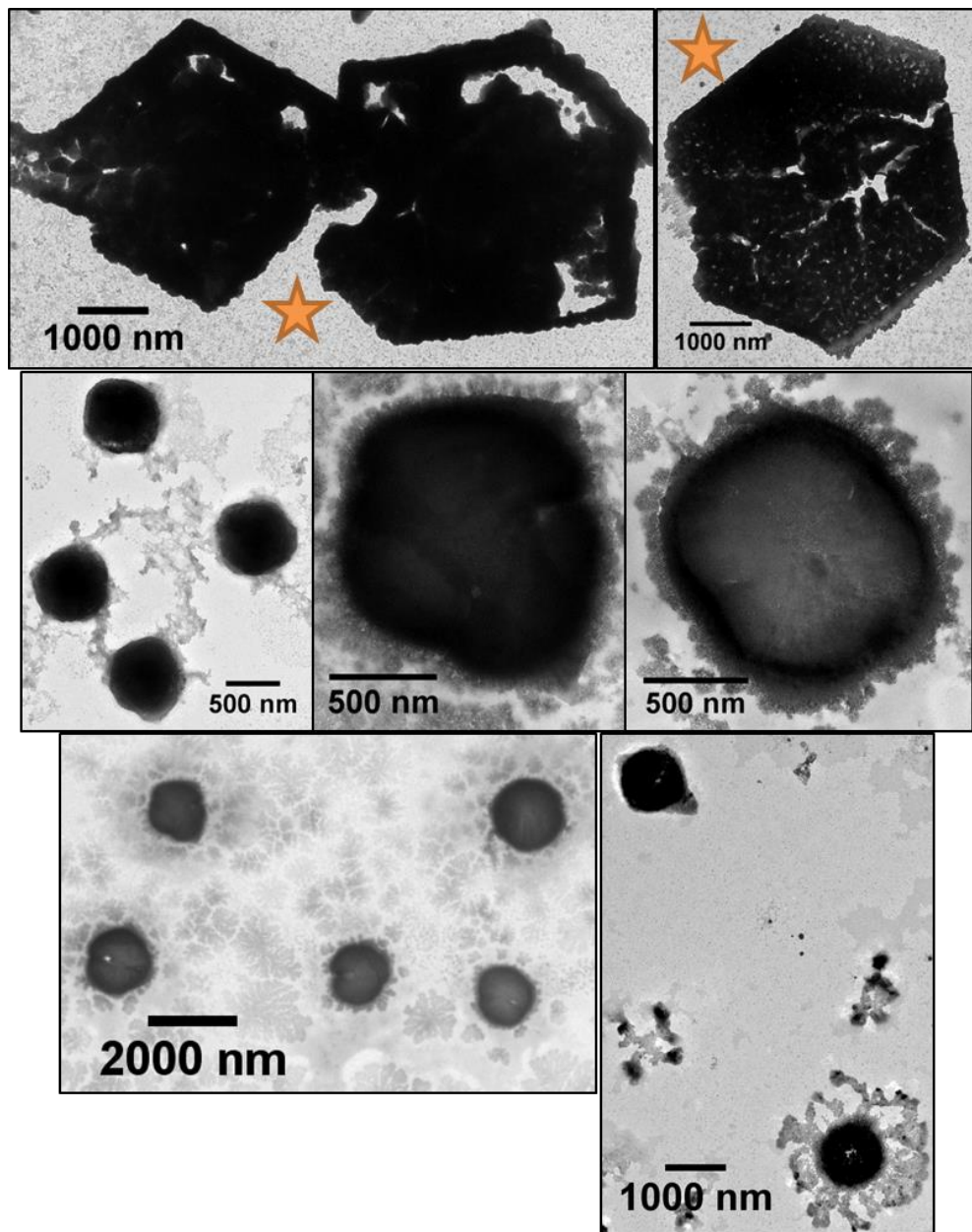


Figure 56. TEM micrographs of blank cubosomes in water. All found particles had sizes bigger than 500 nm. The micrographs with the orange star marking shows peculiar cubic structure in the sample, these structures are thought to be cubosomes, as seen by different planes in the electron microscope.

In literature, there is no much TEM data for cubosomes, although, two recent works presented micrographs for GMO cubosomes, as can be seen in Figure 57. Both works reported particle size bigger than those measured by DLS (LUO et al., 2015)(NASR; GHORAB; ABDELAZEM, 2015).

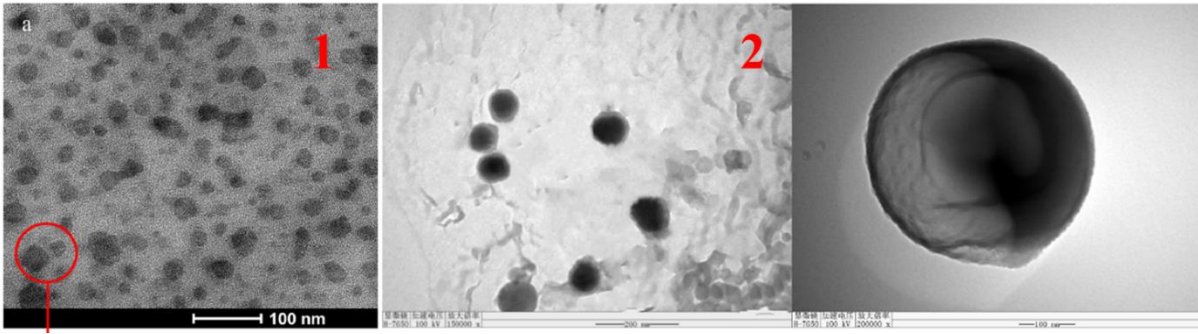


Figure 57. TEM data from literature. 1) Results from (NASR; GHORAB; ABDELAZEM, 2015) where the circle represents a GMO cubosome. 2) Results from (LUO et al., 2015) Both blank and with the studied drug, respectively. Both papers report sizes in TEM bigger than DLS.

Figure 58 shows TEM micrographs for cubosomes in PBS media. One can notice that there is no change in the shape of the nanoparticles when cubosomes are produced in PBS, although, the found particles were significantly smaller than those prepared in water. The biggest particles present ~500 nm in size, whereas in water there are cubosomes at the micrometer order of magnitude. This corroborates with DLS measurements, showing that in PBS cubosomes tend to be smaller than in water.

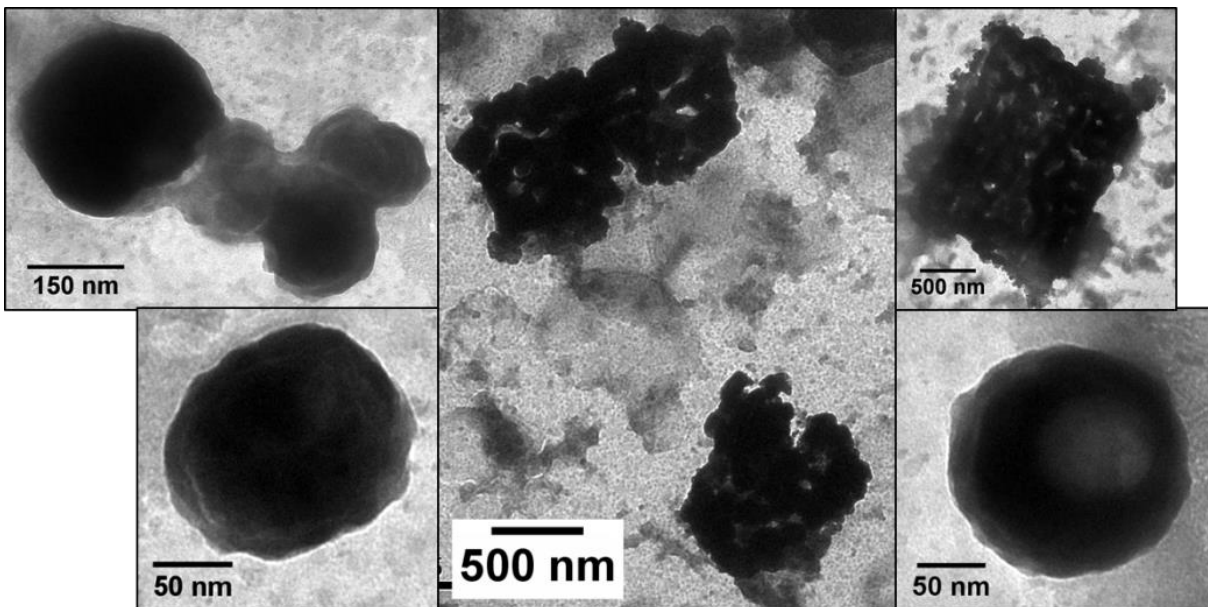


Figure 58. TEM micrographs for Phy-cubs in PBS media. Comparing these particles with the ones in Figure 56, there is no difference in the shape of cubosomes, although, all found nanoparticles in PBS presented smaller size than those prepared in water.

TEM micrographs were also made for lyophilized and extruded cubosomes. Figure 59 presents cubosomes in water media extruded in a 0.05 μm pore size filter, where one clearly see particles in the system, mostly with a square shape. Sizes were variable, most particles presented sizes around ~ 300 nm, and overall this is compatible with DLS measurements. On the other hand, Figure 60 displays lyophilized cubosomes in PBS media where particles have similar sizes and shapes as in Figure 56 (original sample). As it can be seen, sizes are also in the order of ~ 400 nm, compatible with DLS measurements. TEM data reinforces that Phy-cubs can go through extreme processes such as lyophilization and extrusion without loss of their morphology.

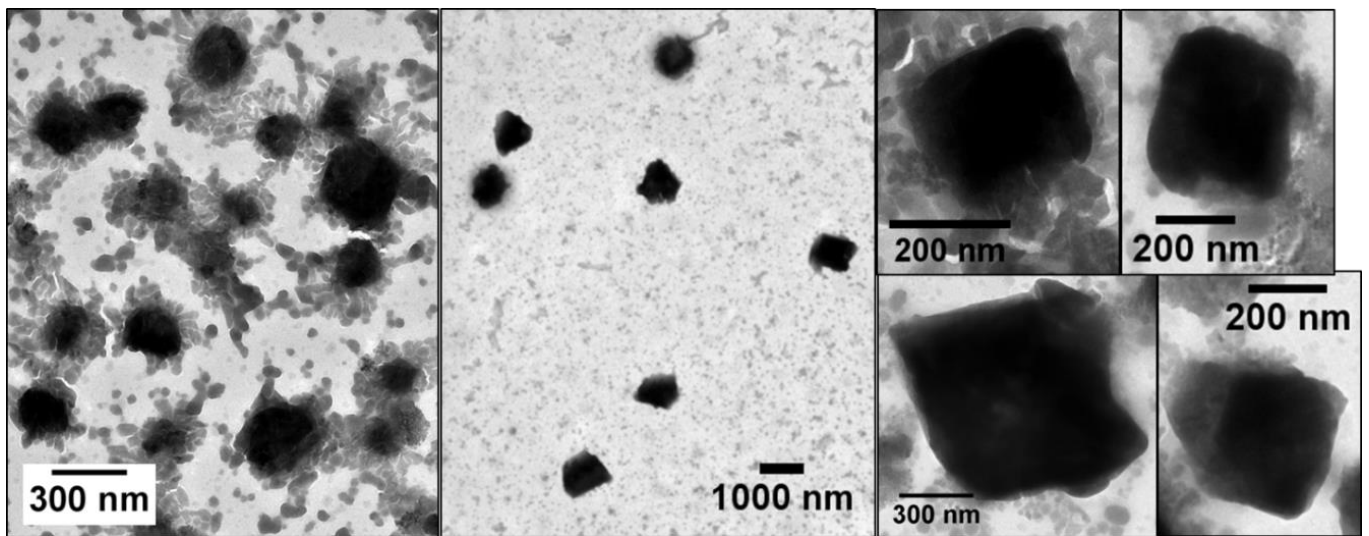


Figure 59. Extruded cubosome in a 0.05 μm pore filter. Micrographs present nanoparticles in varied size, most of them particles reveal sizes ~ 300 nm, compatible with DLS measurements.

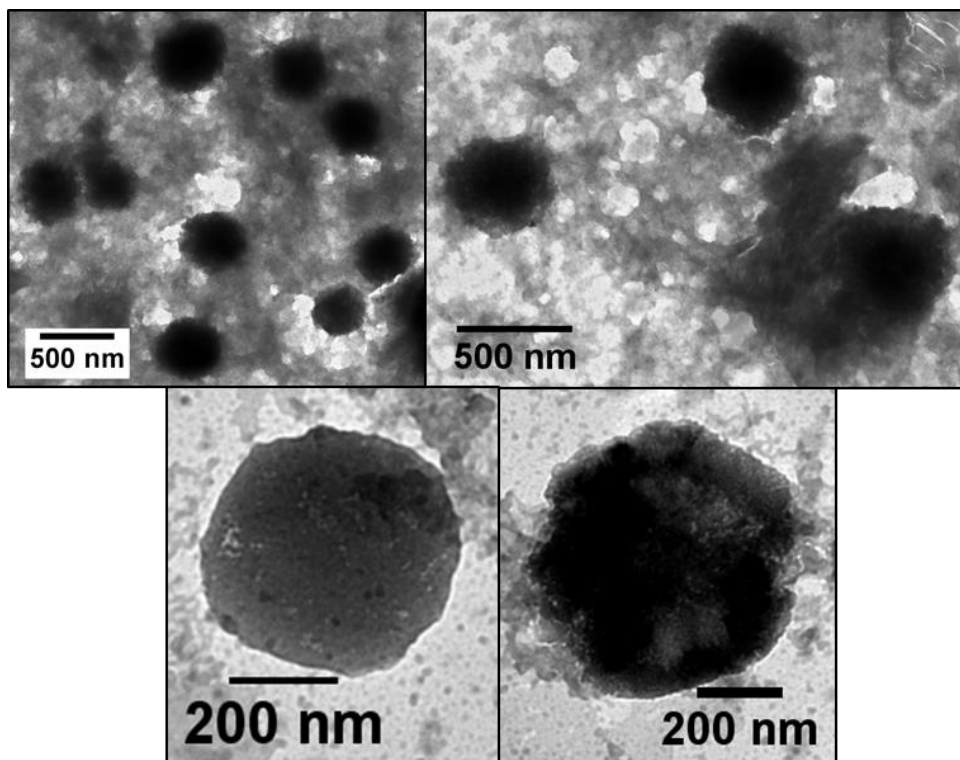


Figure 60. Lyophilized cubosomes in PBS media. Cubosomes present sizes similar to the original sample (see Figure 58). These data reinforces that cubosomes still hold cubic structure after lyophilization and rehydration.

Figure 61 shows cryo-EM data for blank samples of Phy-cubs. As one can see, a variety of particle sizes and shapes are found, from 100 nm to 400 nm, indicating considerable polydispersion in the sample. Most particles displayed internal structure, given by the net draw inside their shapes. Also, there was presence of micelles and uni and multi lamellar vesicle were observed in the sample, as can be seen in Figure 62. Green arrows show unilamellar vesicles and orange arrows show multilamellar vesicles coexisting with Phy-cubs.

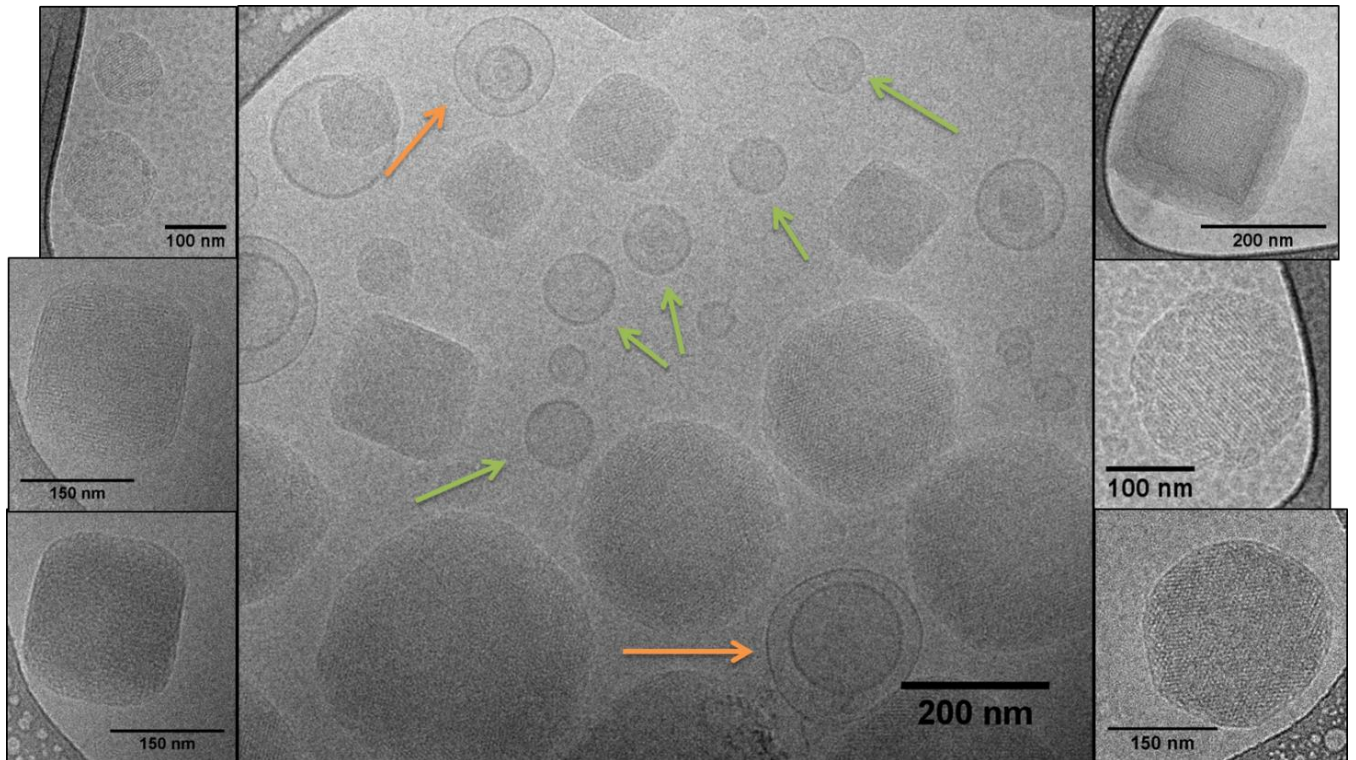


Figure 61. Cryo-EM data for PHY cubosomes in water medium. Many particles were found with diverse sizes, indicating considerable polydispersion. Most particles present internal order given by the structure in their morphologies. Green arrows also display unilamellar vesicles and orange arrows display multilamellar vesicles

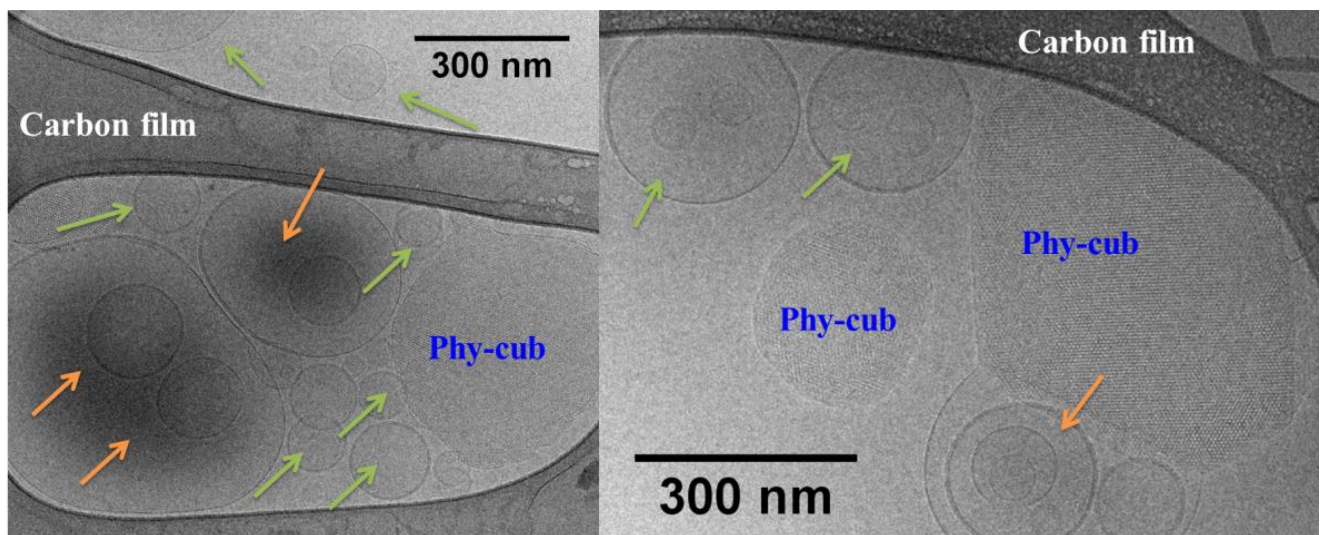


Figure 62. Cryo-EM micrograph of Phy-cubs showing the presence of vesicles in the sample coexisting with cubosomes. Green arrows display unilamellar vesicles and orange arrows display multilamellar vesicles.

These micrographs are in good agreement with the results from Akhlagi et al. study (AKHLAGHI et al., 2016), who also report presence of vesicles in the samples and particles

in varied sizes from 50 nm to 300 nm. In general, literature reports cryo-EM data for cubosomes with internal structure and coexistence with other phases (vesicles) in the colloidal system (DEMURTAS et al., 2015)(SAGALOWICZ et al., 2006)(SPICER et al., 2001). One possible reason for the presence of vesicles is the polymer added to stabilize the colloidal system, these other structures could be made from polymer molecules that did participate on cubosomal formation, and in addition, some of the lipid molecules could also find thermodynamic equilibrium in small micelles and vesicles rather than into the cubosomes.

Besides size and internal structure evaluation, FFT analysis (see method section) was also performed in order to find an estimation for the lattice parameter for some particles. For some particles in Figure 61 this FFT analysis was done and the resulting FFT shapes were found. The calculated FFT's for some particles are displayed in Figure 63, one can see many hexagonal motifs and other shapes. Only the particles with a clear FFT shape were taken into account for the lattice parameter calculation.

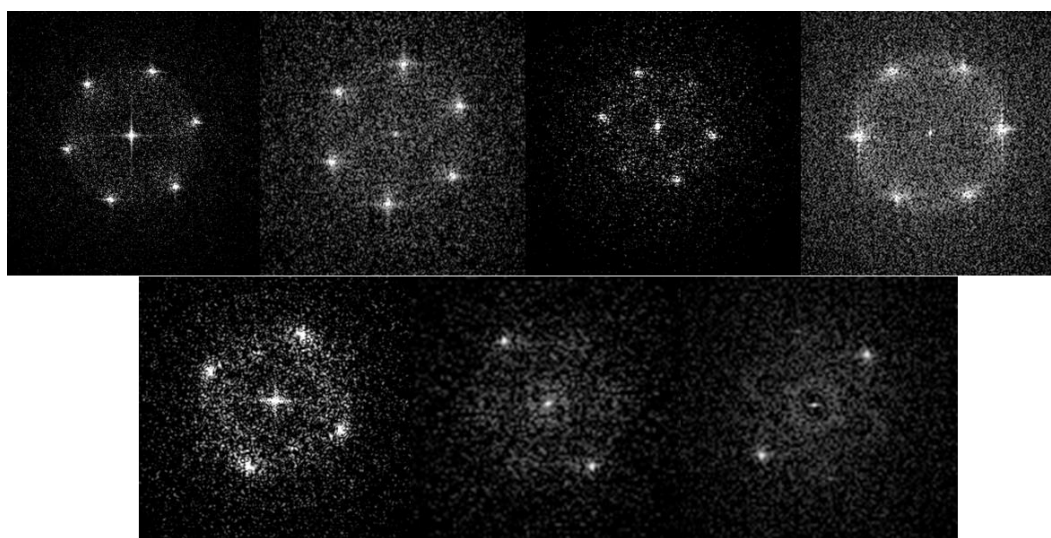


Figure 63. Some calculated FFT's from particles in Figure 61. Some particles presented clearer FFT patterns than others, given by the easiness to recognize a pattern in the FFT.

The calculated lattice parameters are presented bellow:

6.1(5) nm	6.2(5) nm	6.2(5) nm	6.9(5) nm
7.0(5) nm	7.5(5) nm	7.2(5) nm	

These found values are compatible with the lattice parameters found by SAXS, as seen in Table 7. Once more, cryo-EM gives information about single particles, therefore only the

order of magnitude of these found lattice parameter should be compared to SAXS experiments. Interestingly, it is clear that the samples presented cubosomes with varied lattice parameter ranging from 6 nm to 7.5 nm.

5.3.2 Temperature influence – blank cubosomes

Cubosomes were also studied at 45 °C, 50 °C and 65 °C in order to understand the effects of temperature over the nanoparticle system. These values were chosen based on the PHY phase diagram (Figure 6), knowing that at the chosen temperatures there is phase transition of the bulk lipid phase. Both water and PBS medium were investigated.

SAXS curves are displayed in Figure 64 and Figure 65. For water medium (Figure 64) it is clear that the cubosomes hold their internal structure up to 50 °C and the only change is the peak shifting to higher q values, that can be explained by the nanoparticle expelling water from its structure. This indicates the lattice parameter decreases over temperature. At 65 °C the colloidal system becomes isotropic, giving the L_2 phase. Curiously, in PHY phase diagram the bulk phase undergoes at least two phase transitions, hexagonal and lamellar phases, over these temperatures, but the nanoparticles do not. This suggests that F127 (stabilizer polymer) acts on the nanoparticles preventing the lipid to change phases.

Our results are in good agreement with literature. For cubosomes produced in a TD method, Fraser et al. (FRASER et al., 2013) reported that Phy-cubs at 60 °C are in isotropic L_2 phase. Nilsson et al. (NILSSON et al., 2014) reported mixed hexagonal and L_2 phases at 50 °C. Recently, in a detailed work by Tran et al. (TRAN et al., 2018), also reported Phy-cubs in hexagonal and isotropic L_2 phases at 60 °C.

When in PBS medium (Figure 65) cubosomes have similar behavior as in water medium. Up to 50 °C the nanoparticles retain their internal Pn3m structure expelling water from the channels, as seen by the peak shifting. At 65 °C the colloidal system also changes to isotropic L_2 phase.

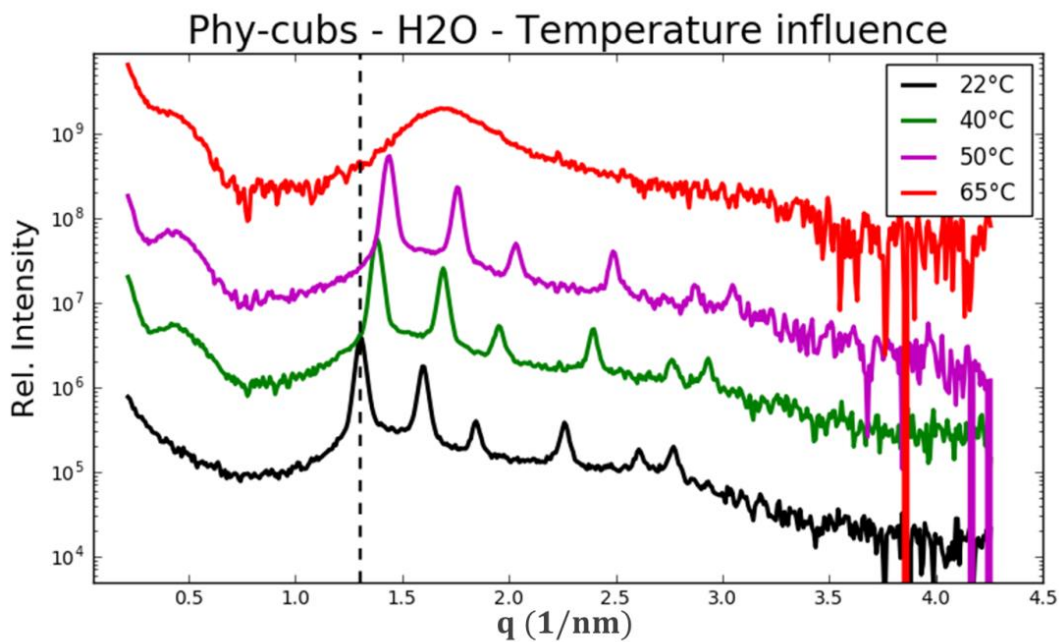


Figure 64. SAXS data for Phy-cubs in water medium over temperature. Up to 50 °C cubosomes hold their internal structure, only expelling water, given by the peak shifting for higher q values. At 65 °C the system entered an isotropic phase.

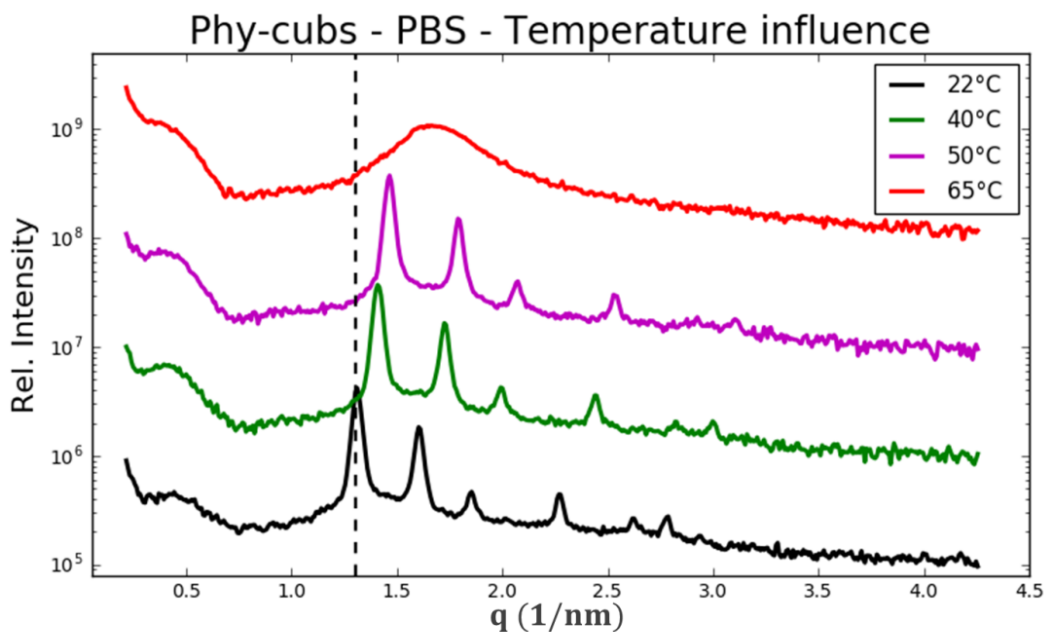


Figure 65. SAXS data for Phy-cubs in PBS medium over different temperatures. Similarly to water, up to 50 °C cubosomes hold their internal structure Pn3m, the peak shifting for higher q values indicates that cubosomes expel water as the temperature rises. At 65 °C the system also became isotropic.

5.3.3 Miltefosine interaction with Phy-cubs

Following the loaded quantities in Table 6, two types of loading were tested: co-solubilization and addition after cubosomal dispersion was prepared. Samples were studied in water, PBS and 2.25% w/v glycerol media by SAXS, DLS, TEM and cryo-EM.

5.3.3.1 Co-solubilization method

For this study, MILT was added together with the lipid solubilization in ethanol, see methods section. First, up to 4% w/w MILT loading was assessed in order to investigate the influence of the molecule in the internal structure of the nanoparticles. SAXS results are shown in Figure 66. It is clear that MILT does not destroy the cubosomes internal structure, since all curves presented all six peaks, although a peak shifting is evident, indicating that MILT enlarges the lattice parameter of the cubosomes. It is hypothesized that MILT is located into the bilayer of the water channels.

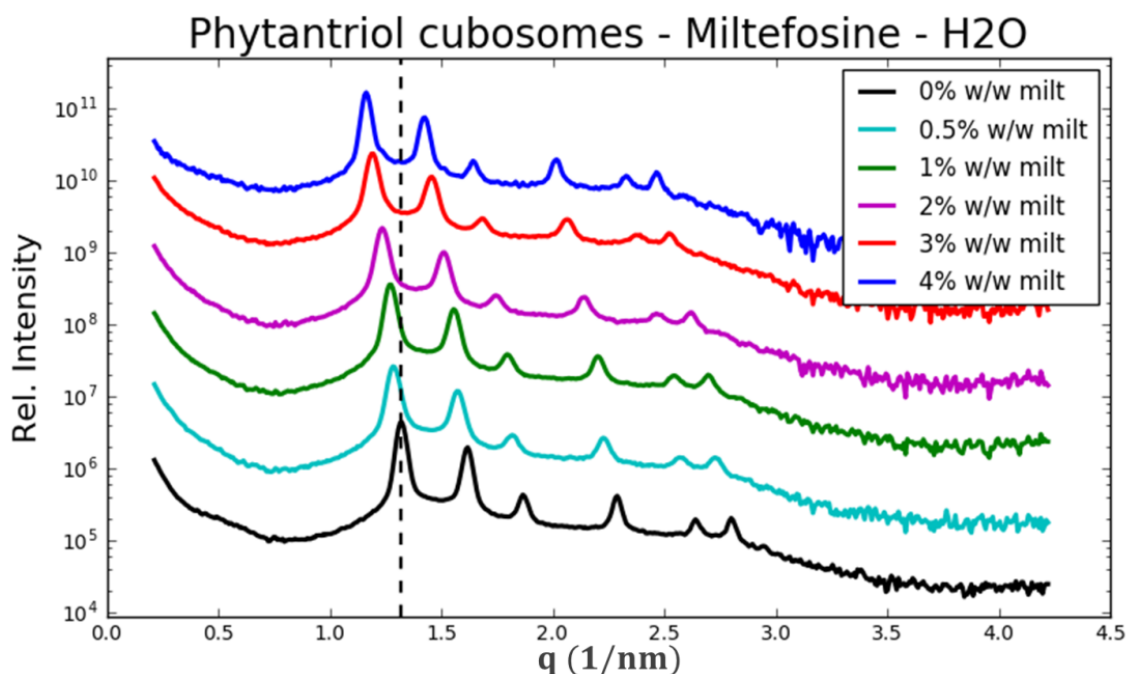


Figure 66. SAXS data for MILT loaded Phy-cubs at room temperature. From the curves, it is clear that MILT does not destroy the cubosomes internal structure, but it changes the diameter of the water channels, given by the peak shifting to lower q values. MILT enlarged the lattice parameter.

Similar results are obtained in 2.25% w/v glycerol and PBS media (Figure 67).

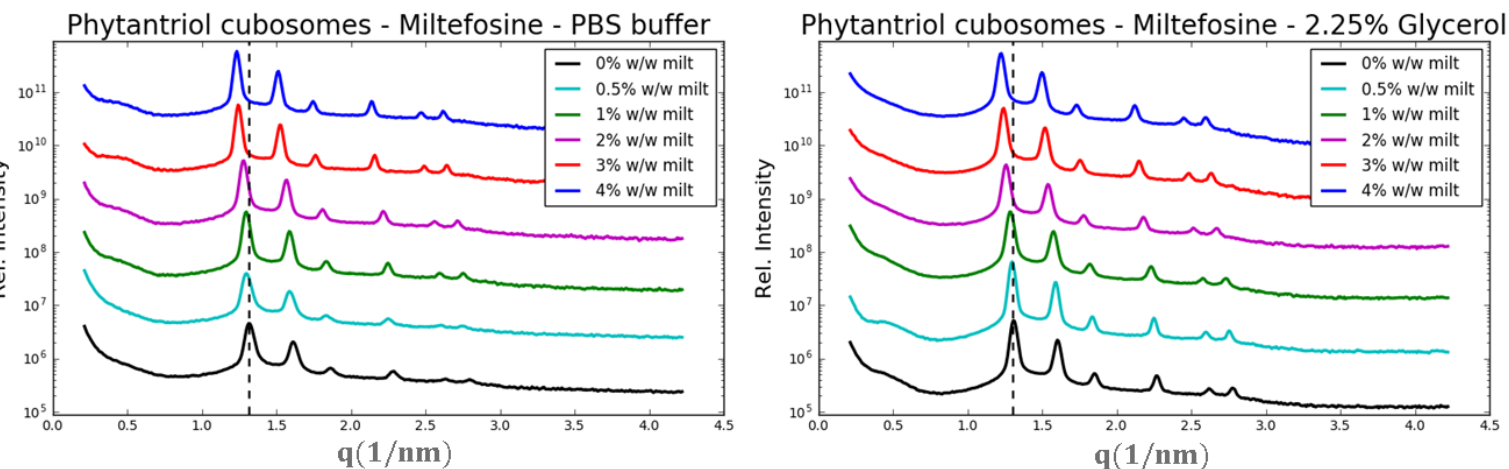


Figure 67. SAXS results for MILT loaded Phy-cubs in PBS (left) and glycerol (right) media. Similarly to water, MILT did not destroyed cubosomal internal structure but it shifted the peaks, indicating that an enlargement in the lattice parameters.

Figure 68 compares the calculated lattice parameter for all aqueous media analyzed. It is evident that as more MILT is incorporated into the cubosomes, more the lattice parameter increases for all aqueous media. An increase of ~ 1 nm is seen for water and ~ 0.8 nm for PBS and glycerol compared to the blank sample, for the 4% w/w MILT. Interestingly, the water medium seems to affect how MILT interacts with cubosomes, for concentrations up to 1% w/w, similar lattice parameters are calculated for all three aqueous media. For 2% w/w beyond values begin to deviate when calculated for water and PBS or glycerol. A hypothesis for this fact is that the presence of the salt molecules in PBS case and glycerol molecules can exert some influence over the MILT molecule, not letting it insert completely into the lipidic moiety, as in water case.

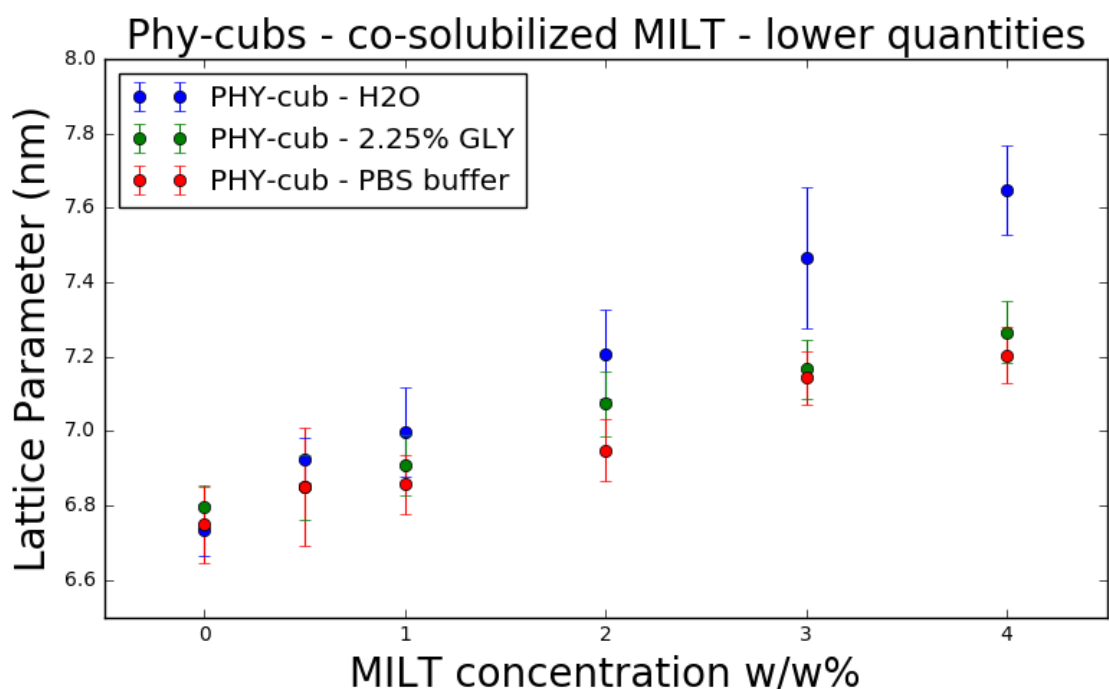


Figure 68. Calculated SAXS lattice parameters Phy-cubs in water, glycerol and PBS media. For all aqueous media, MILT increased the lattice parameter of the cubosomes. Taking for instance blank cubosomes vs 4% w/w MILT, a significant difference of ~1.0 nm was shown. Another interesting feature is that up to 1% w/w MILT has the same effect on lattice parameter for all three aqueous media, but for 2% w/w beyond, slight changes could be seen from water to PBS and glycerol.

Literature reports varied results regarding the influence of molecules in the cubosomes morphology, some hydrophobic drugs do change the inner structure of the cubosomes, but others just change the lattice parameters, like MILT. Yang et al. (YANG et al., 2011) incorporated amphotericin B (AmB) into Phy-cubs in various amounts finding that the cubosomes remained in the Pn3m arrangement but the lattice parameter was changed. Also, as more AmB was loaded, diffraction peaks were losing scattering intensity, explained as a result of AmB to be inserted on the surface of the nanoparticle, therefore interfering with the detection of the scattered light. Jain et al. (JAIN et al., 2015) loaded docetaxel into cubosomes, reporting mixed dispersion of cubic and hexagonal nanoparticles at given amounts of the incorporated drug. Qin et al. (QIN et al., 2016) encapsulated small amounts of hydroxycamptothecin into cubosomes and reported no changes in the inner structural parameters also. Ali et al. (ALI et al., 2016) encapsulated 7-Ethyl-10-hydroxyl camptothecin, low soluble cancer drug, into cubosomes, finding that the drug did not change the

crystallographic structure of the cubosomes, with no mention about the lattice parameter. Shi et al. (SHI et al., 2015) incorporated oridonin, a very low soluble anti-cancer drug, into cubosomes reporting that the drug changed the lattice parameter of the nanoparticles but they remained in Pn3m symmetry.

On the other hand, when MILT is loaded into other nanostructures, morphology alterations due to the drug incorporation may happen. In one hand, when loading MILT into liposomes, Teymouri et al. (TEYMOURI et al., 2015) found that the drug did not change significantly the morphology of the nanoparticles up to 4% w/w drug encapsulation, particle size and polydispersion remained the same with and without the drug. In addition, when loaded into lipid nanocapsules, Eissa et al. (EISSA et al., 2015) found that MILT also did not alter the colloidal properties of the lipid nanocapsules when incorporated between 25 to 100 μM , keeping the same size and polydispersion. On the other hand, when encapsulated into solid lipid nanoparticles, Bitencourt et al. (DA GAMA BITENCOURT et al., 2016) found that as more MILT was loaded, up to 40 mg/ml encapsulated, the appearance of the colloidal system changed, in addition, MILT also disturbed particle size and polydispersion, making a second population of particles to be detected by DLS measurements.

DLS measurements were performed with fresh samples and over time. Figure 69 displays results for samples in water medium, no clear influence on particle size is seen when loading different amounts of MILT, neither polydispersion changes significantly. Samples presented great stability over the month measured, sizes fluctuated minimally with no significant changes.

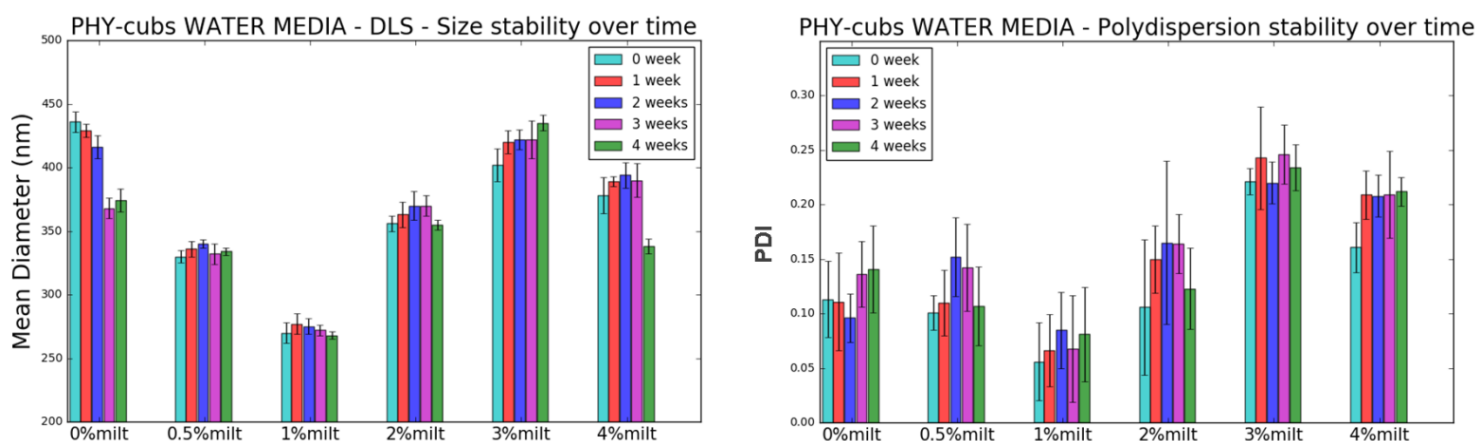


Figure 69. DLS results for samples in water medium over a period of four weeks. MILT does not seem to influence particle size (left) neither polydispersion (right). Samples presented great stability over a month measured.

For samples in PBS medium, similar results were obtained, MILT did not seem to influence particle size either, although, for samples 3% w/w and 4% w/w MILT, sizes significantly diminished by 50 nm. In addition, except from sample 2% w/w MILT, polydispersion was similar to all samples. Over the three week measured, samples also presented great stability with small fluctuations in size and PDI.

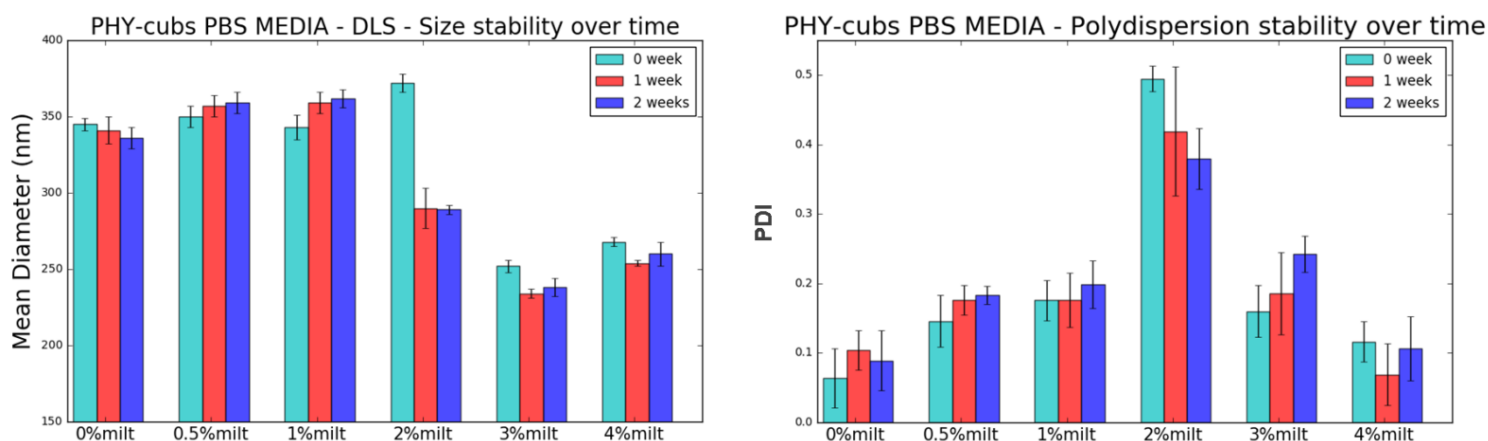


Figure 70. DLS results for Phy-cubs samples in PBS medium, followed over three weeks. Similarly to water, MILT does not seem to influence particle size (left), although, for 3% w/w and 4% w/w there is a significant reduction in particle size. Except from sample 2% w/w, polydispersion (right) was compatible between all samples.

Literature reports cubosomes of smaller sizes due to the different methods of production, which in general involves a tip sonicator probe that breaks particles into smaller ones. Yang et al. (YANG et al., 2011) report no significant changes in particle size nor PDI when loading amphotericin B. Ali et al. (ALI et al., 2016) also reported Phy-cubs with ~250 nm and 0.3 PDI when incorporated with 7-Ethyl-10-hydroxyl camptothecin. Astolfi et al. (ASTOLFI et al., 2017) reported that after loading 5- fluorouracil, particle size diminished from ~220 nm to ~180 nm with no significant changes in PDI. Shi et al. (SHI et al., 2015) reporting cubosomes with ~230 nm and ~0.115 PDI for oridonin loaded nanoparticles.

TEM experiments were performed with samples 3% w/w MILT, both in PBS and water. Figure 71 presents the micrographs of found particles in water medium, particles reveal sizes smaller than 250 nm, deviating from DLS measurements. They have rounder shapes and blurred identification due to the background. Figure 72 displays results for sample in PBS medium, curiously, the found particles were no much bigger than ~300 nm, compatible with DLS measurements. In addition, these particles have square and hexagonal shapes, indicating that some cubosomes were not affected by vacuum distortions. The hexagonal shaped particles are thought to be cubosomes seen by the [111] plane, while the squared ones are thought to be seen by the [110] plane, see methods section for further references.

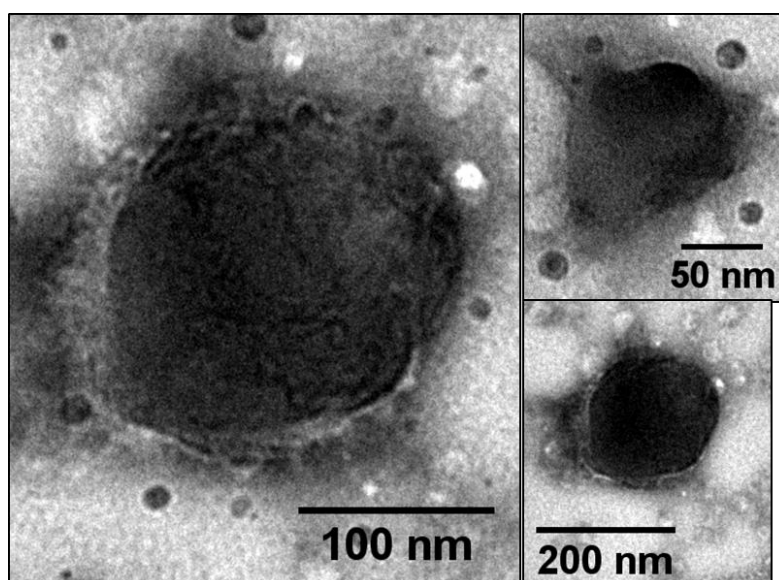


Figure 71. TEM micrographs for Phy-cubs sample with loaded 3% w/w MILT in water medium. The found particles revealed sizes smaller than those detected by DLS.

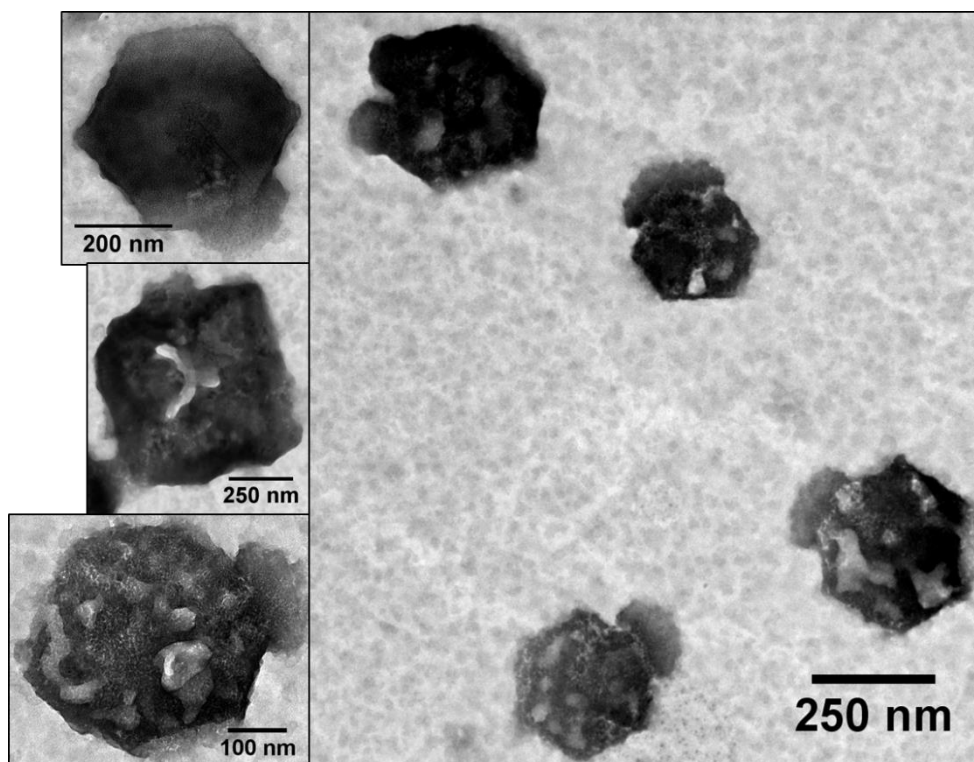


Figure 72. TEM micrographs for Phy-cubs samples loaded with 3% w/w MILT in PBS medium. Curiously, the found particles presented sizes similar to DLS measurements. In this samples, cubosomes presented square and hexagonal shapes, indicating that nanoparticles were seen in different axis regarding the electron beam.

Once MILT did not affect particle inner structure up to 4% w/w, it was decided to investigate higher quantities in order to estimate at what amount MILT would change the cubosomal inner structure. For this, the chosen percentages were 5% w/w, 10% w/w, 15% w/w and 20% w/w, for both water and PBS media. SAXS results are displayed in Figure 73 and Figure 74. In the water medium, Figure 73, MILT did not affect cubosomal inner structure up to 10% w/w, but an indication of a phase transition can be seen with a small peak in low q value, indicated by the green arrow. For 15% w/w MILT, cubosomes have changed phases for the Im3m symmetry, and almost no Pn3m nanoparticles in the system. For 20% w/w, only Im3m phase exists in the colloidal system.

In this concentration (20% w/w), there are eight molecules of lipid per molecule of drug, explaining why the nanoparticle had to change its phase in order to better accommodate the drug within its structure. It is well known that for Im3m cubosomes (from the GMO cubs study), the lattice parameter increases (~ 10 nm), giving more space for MILT molecules to coexist in the lipid PHY bilayer.

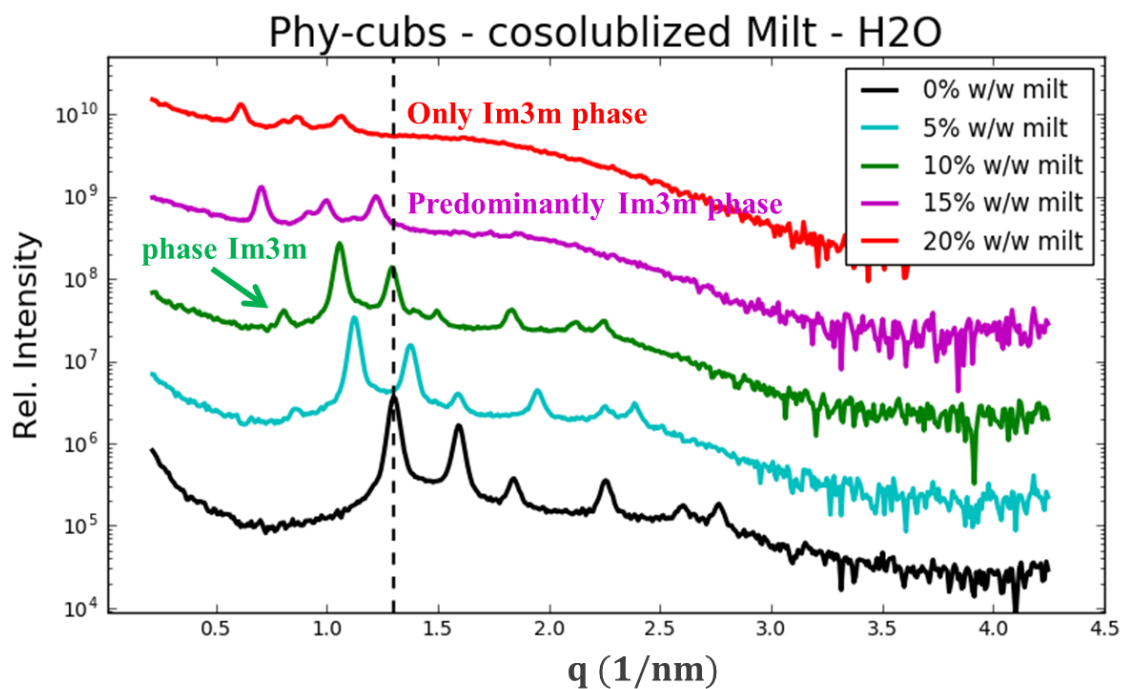


Figure 73. SAXS results for Phy-cubs loaded with higher amounts of MILT, through co-solubilization method, in water medium. MILT does not affect the cubosomal structure up to 10% w/w, but in this concentration, there is an indicative of a new phase forming (green arrow). For 15% and 20% w/w cubosomes assume the Im3m symmetry.

Similar effect happens for PBS medium, Figure 74, MILT did not altered cubosomes Pn3m structure up to 5% but at 10% there is already strong coexistence of Pn3m and Im3m phases, given by the existence of more peaks in the curve. For 15% and 20% w/w only Im3m phase exists in the colloidal system.

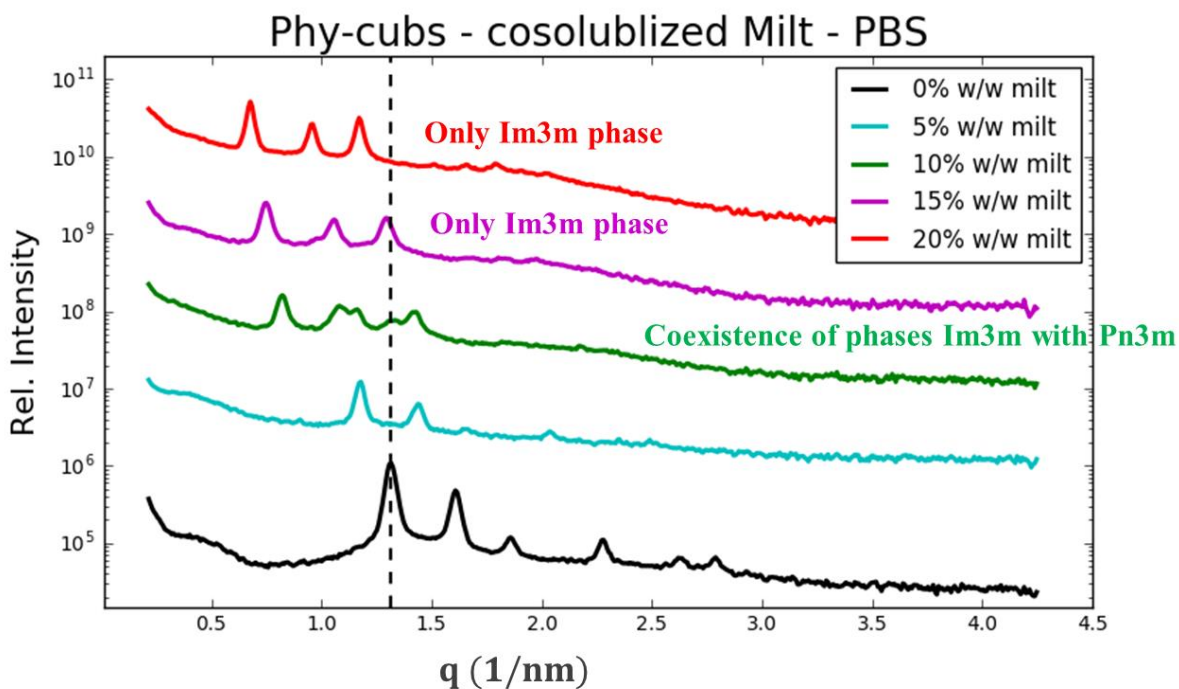


Figure 74. SAXS results for sample in PBS medium. Differently from water medium, in PBS the phase transition of cubosomes begins at 10% w/w with coexistence of phases. For both 15% and 20% w/w only Im3m cubosomes are seen in the colloidal dispersion.

Comparing these results with literature, in a recent work, Astolfi et al. (ASTOLFI et al., 2017) incorporated 5- fluorouracil in order to improve the efficacy of low doses, reporting that for low quantities (3% mol) the system was unaltered from Pn3m, but for 5% mol and 8% mol, phase Im3m coexisted with phase Pn3m in the colloidal dispersion. Fong et al (FONG et al., 2014) reported the encapsulation of an antimicrobial peptide into GMO-based cubosomes demonstrating also a phase transitions of the cubosomes as higher quantities (10% and 20% mol) of the peptide were loaded into the nanoparticles.

Calculating the lattice parameter for both Pn3m and Im3m phases (Figure 75), it can be seen that for Pn3m cubosomes, both in water and PBS, as more MILT is incorporated into cubosomes, the lattice parameter increased by ~ 1.5 nm, going from 6.833(53) nm in the blank sample (0% w/w) to 8.42(15) nm for 10% w/w loaded MILT. For higher amounts of MILT, the Im3m phase presents lattices ranging from 10.85(36) nm to 13.16(17) nm.

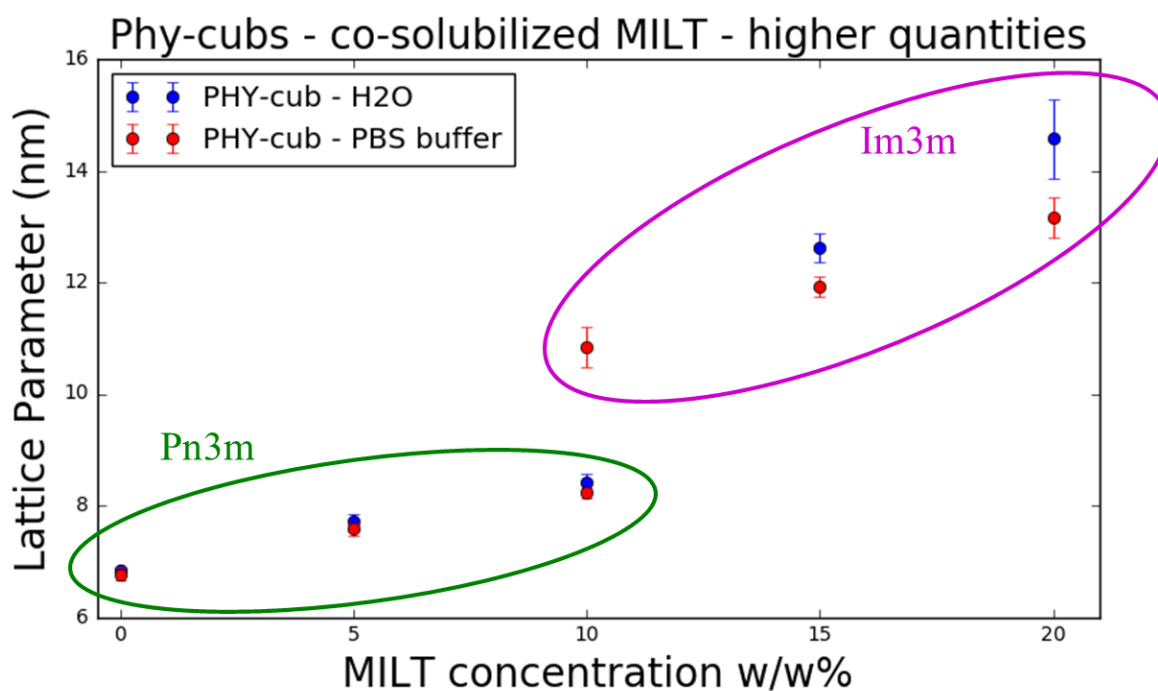


Figure 75. Calculated lattice parameters for Phy-cubs in both Pn3n and Im3m phases. The green circle displays the calculated lattices for the Pn3m nanoparticles showing an increase as more MILT is encapsulated into cubosomes. The purple circle displays the calculated lattices for the Im3m phases, showing a great difference with the blank sample (0% w/w).

DLS measurements were also performed with these samples. Figure 76 displays the results for MILT loaded nanoparticles in water medium. It is clear that even with higher amounts of incorporated MILT, the mean diameter (left graph) does not seem to be altered by the presence of higher concentration of the drug. On the other hand, polydispersion (right graph) seems to be affected for 15% and 20% w/w MILT, which is very compatible with SAXS measurements, once there were two populations of cubosomes, Im3m and Pn3m were present in the samples. Regarding temporal stability, samples revealed compatible sizes and PDI over the 4 weeks studied.

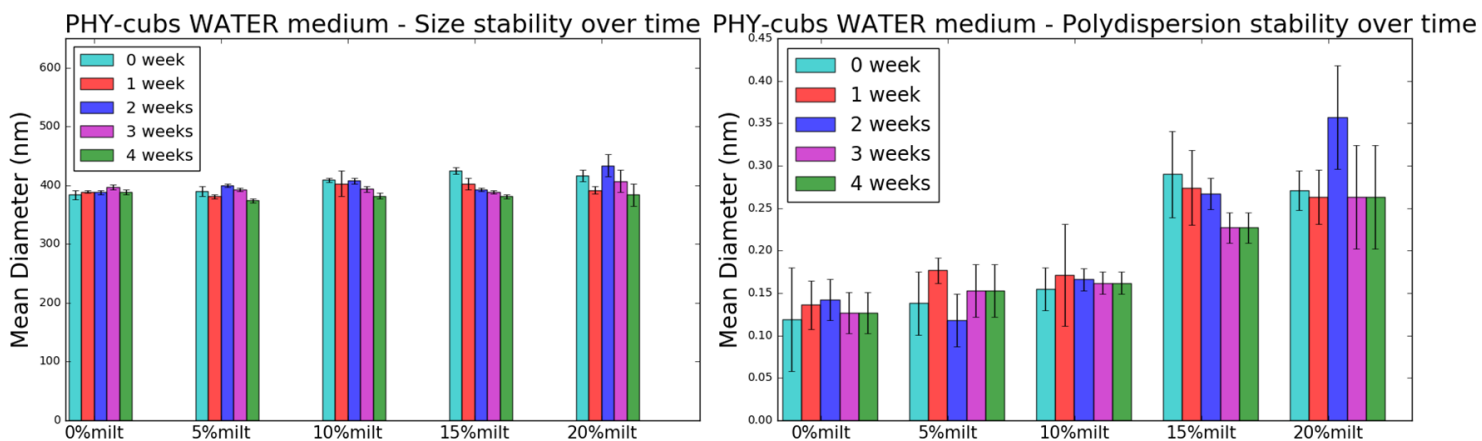


Figure 76. DLS measurements for samples with higher MILT quantities loaded in water medium. Sizes (left graph) do not seem to be altered by the higher quantities of loaded MILT, note that for 15% and 20% w/w, the mean diameters reflect sizes for the Im3m populations included. For PDI (right graph), the 15% and 20% w/w increases the polydispersion of the colloidal system due to the coexistence of different populations, Im3m and Pn3m.

Interestingly for PBS medium, see Figure 77, particle size (left graph) at 20% w/w loaded MILT is much higher than the blank samples or 5%, 10% and 15% w/w MILT loaded samples. Also, particle size at 20% w/w reflects Im3m cubosomes sizes because in PBS there is no coexistence of phases at this concentration. In addition, for polydispersion (right graph), cubosomes loaded with the highest MILT concentration presents the higher polydispersion index too, while all other samples have compatible values of measured PDI within error bars. Once more, temporal stability over the 3 weeks studied was seen, since all measured values for size and PDI were compatible.

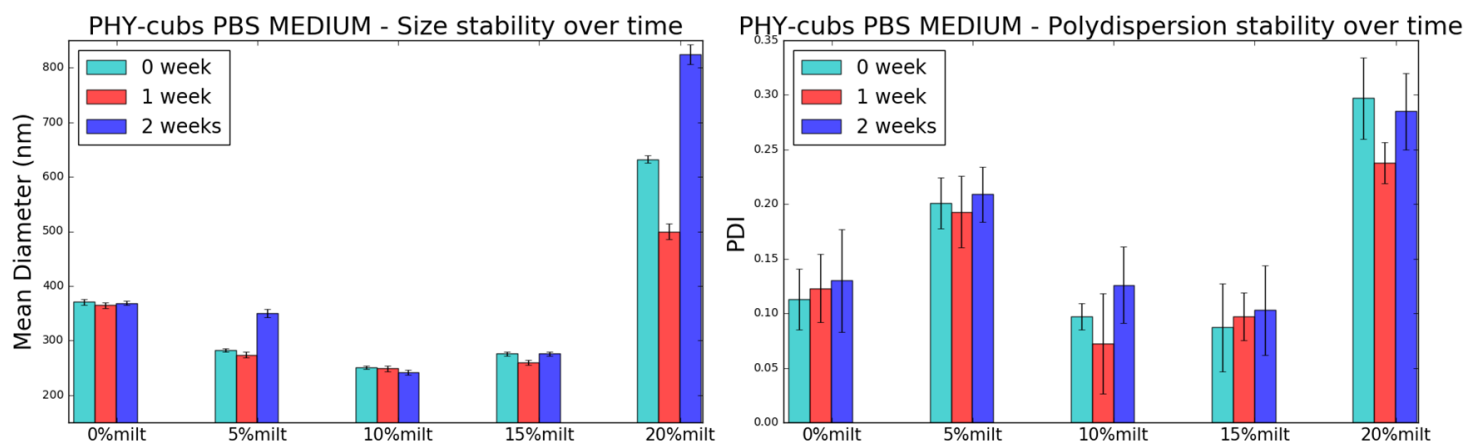


Figure 77. DLS measurements for higher quantities loaded MILT cubosomes in PBS medium. Curiously, when loaded with the highest concentration of MILT, sizes (left) are much bigger than other samples and also PDI (right) is higher, note that this measurements reflect only the Im3m cubosomes in the sample. For all other loaded amounts (5%, 10% and 15% w/w) neither particle size or PDI values were altered by the presence of the drug.

5.3.3.2 Temperature influence for loaded cubosomes

Phy-cubs samples 1% w/w and 3% w/w MILT were studied over temperatures (22 °C, 40 °C, 50 °C and 65 °C) in order to investigate if MILT would exert some influence on particle phase transition as seen in Figure 64. Figure 78 displays the SAXS results for sample 1% w/w MILT, in this concentration MILT does not prevent the colloidal system to undergo phase transition to L_2 at 65 °C. Below 65°C, the system remained cubic and as temperature rises, the cubosomes also expel water from its structure, given by the peaks shifting for higher q values.

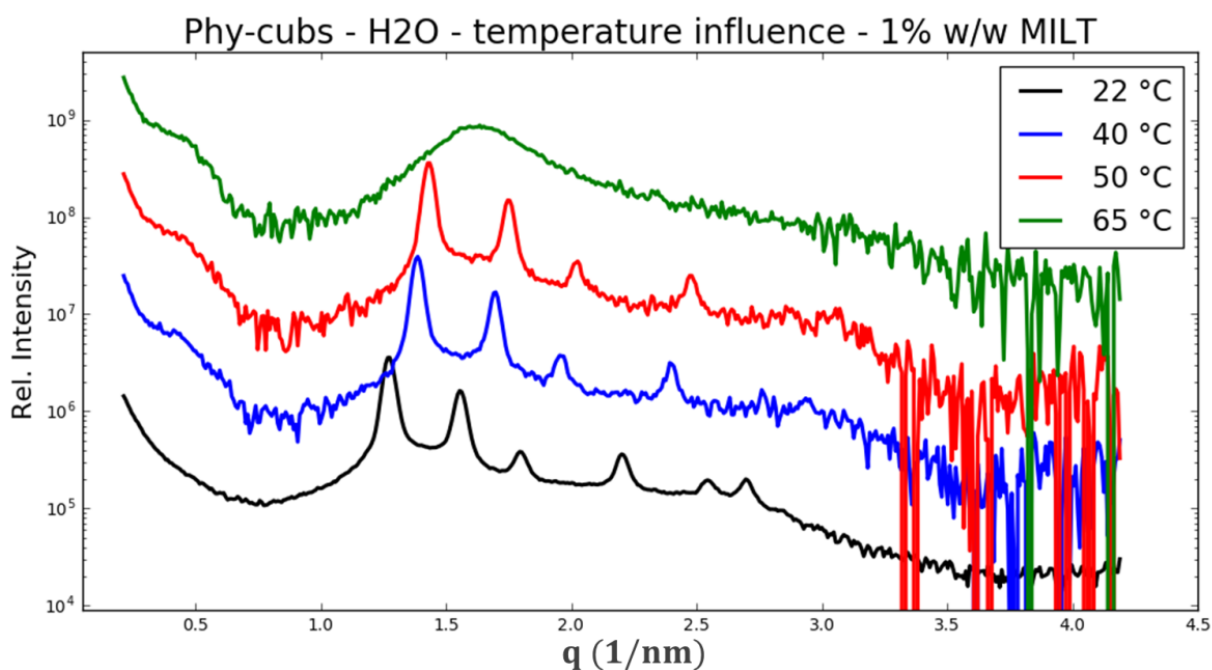


Figure 78. SAXS data for sample 1% w/w MILT at different temperatures. In this concentration, MILT does not prevent cubosomes from undergoing phase transition at 65 °C.

Curiously, at 3% w/w, Figure 79, the nanoparticle suspension holds the cubic structure even at 65 °C, for this concentration, MILT molecules hold the nanoparticles inner structure intact. It can be hypothesized that because MILT is inserted into the lipid moiety, it is strongly linked with the lipid molecules, preventing the disruption of the cubosomes morphology. In addition, as temperature rises, water is also expelled from the nanoparticles, given by the peaks shifting for higher q values.

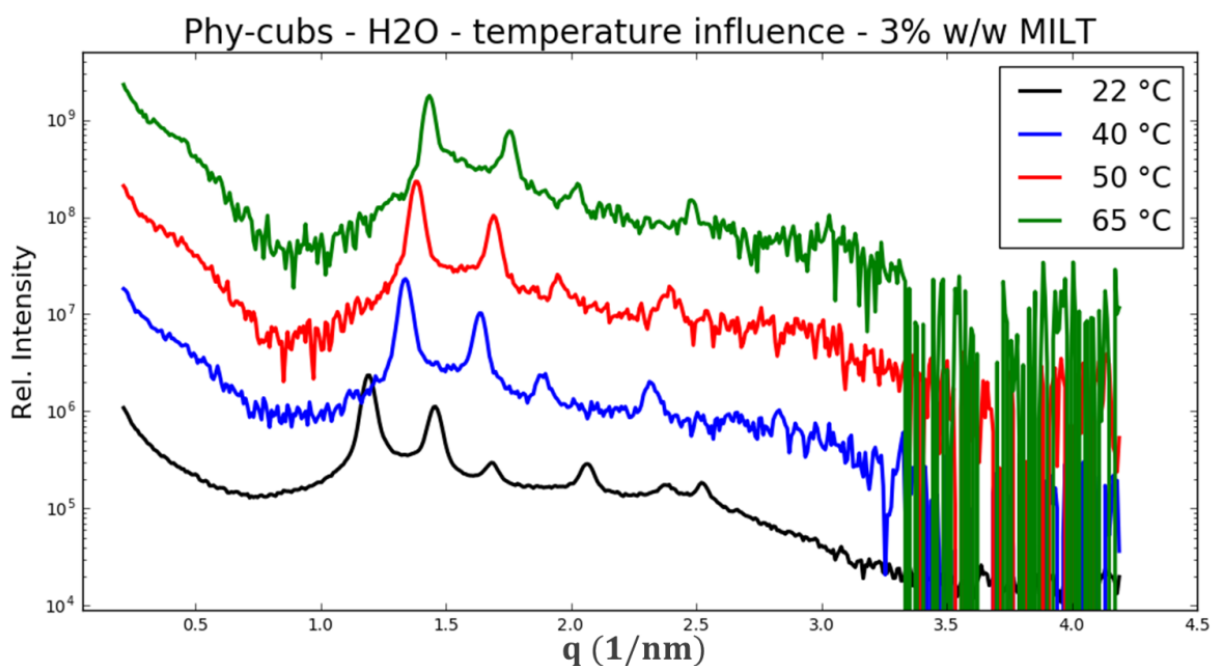


Figure 79. SAXS data for sample 3% w/w MILT. Curiously, at this concentration cubosomes still exist at 65 °C . It can be inferred that MILT holds the structure together because it is inserted into the lipid moiety.

DLS measurements were also performed in order to investigate temperature influence over particle size, since the nanoparticles expel water from the channels as temperature rises, evidenced by SAXS. Figure 80 displays results for blank cubosomes (0% milt) and 1% w/w and 3% w/w loaded MILT. Interestingly, particle size does not seem to be affected by temperature, all measurements are compatible between themselves, both for mean diameter and polydispersion. Moreover, for blank and 1% w/w MILT samples, the found sizes and PDI at 65 °C reflect the estimated sizes for the isotropic L_2 phase.

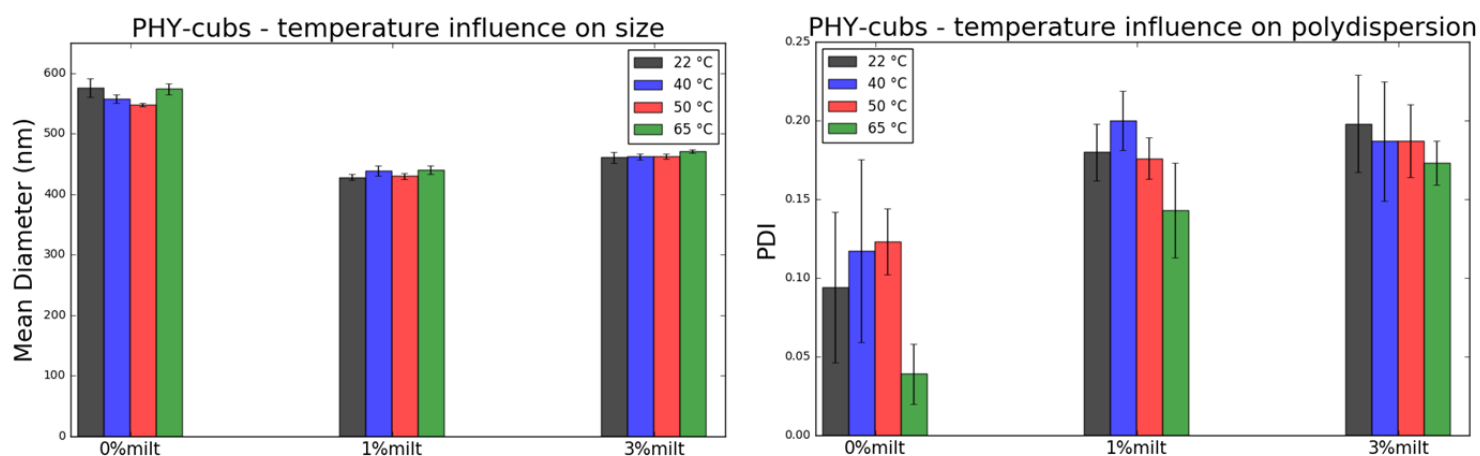


Figure 80. DLS measurements for size (left graph) and PDI (right graph) over temperatures. Curiously, temperature did not influence particle size or polydispersion. For samples 0% and 1% w/w MILT, sizes and PDI at 65°C reflect the measurements for the isotropic phase L_2 (see PHY phase diagram, Figure 6).

5.3.3.3 Addition of MILT after cubosomal dispersion was prepared

Knowing that MILT is a very hydrophobic molecule (CMC $\sim 50 \mu\text{M}$ - (BARIONI et al., 2015) and LogP 6.7 (From Pubchem)), it was hypothesized that even after addition to the blank cubosomes, the molecule would prefer to stay in the lipid moiety of the nanoparticles. For testing this assumption, MILT was added from a stock solution to the blank cubosomal dispersion in the same quantities as the co-solubilized samples, see Table 6 and methods section for references.

Figure 81 displays SAXS results for MILT added into the blank cubosomes in water medium. One can see that even from a stock solution, when MILT is in contact with cubosomes, it interacts with the nanoparticles. The peak shifting indicates that as more MILT is added to the blank samples, more the cubosomes have their lattice parameter changed. Curiously, even at higher amounts (5% to 15% w/w) MILT still enters on the lipid moiety of the nanoparticles, although it does not modify the crystallographic structure Pn3m. A big difference can be seen in these cases from the co-solubilization method (see Figure 73) and the addition after preparation.

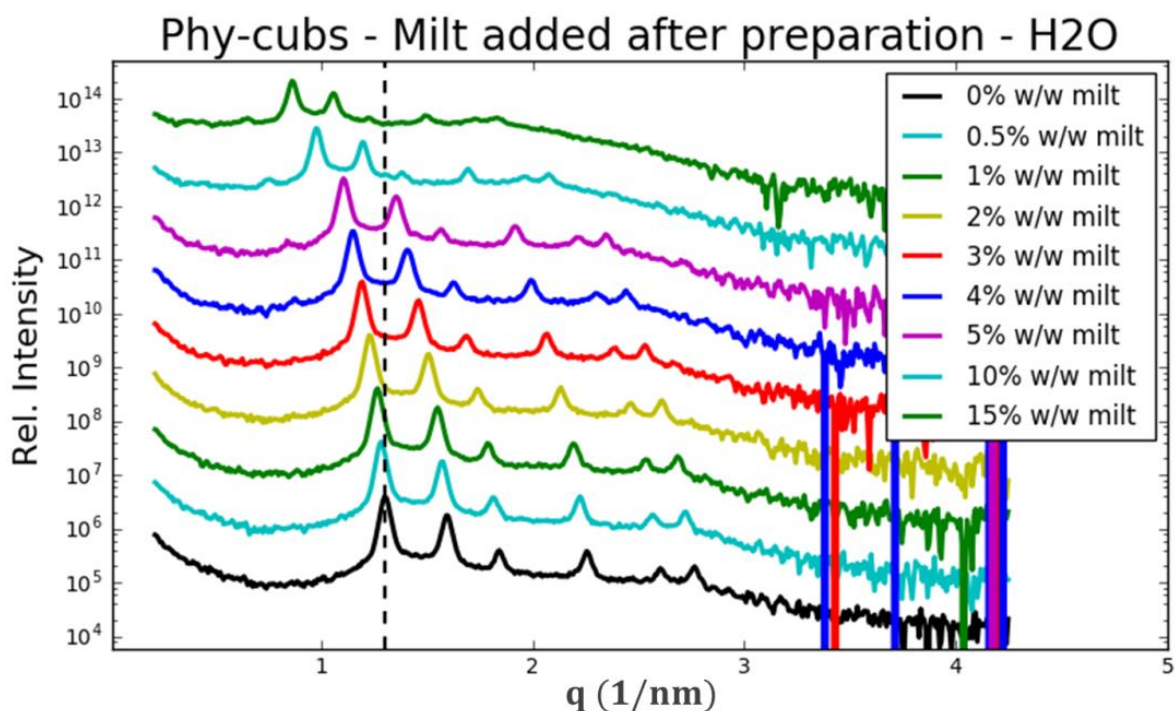


Figure 81. SAXS results for cubosomes loaded with MILT from a stick solution after the dispersion was prepared. Interestingly, even for higher amounts of MILT (5% to 15%), the molecule did not change the structure of the cubosomes as in the co-solubilization case (see Figure 73).

Figure 82 presents the results for PBS and 2.25% w/v glycerol media. Similar to water, MILT also enters the lipid moiety of the cubosomes when added after the preparation process. Differently from water, at the higher concentrations (10% and 15% w/w), the first peak of the Im3m crystallographic symmetry can be seen in the curves, see purple arrows in Figure 82, all other peaks in the curve belonging to the Pn3m symmetry.

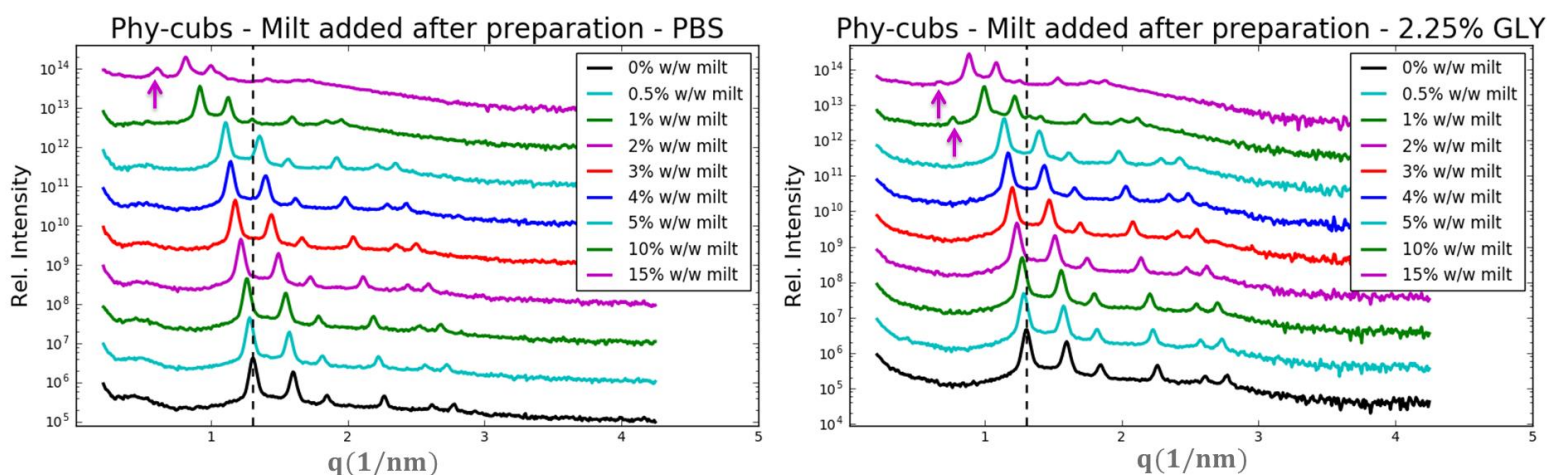


Figure 82. SAXS results for samples in PBS (left graph) and glycerol (right graph) media. Similarly to water, for low concentrations of added MILT, the molecules also inserts itself into the lipid moiety of the cubosomes. Interestingly, for higher quantities (10% and 15% w/w), the first peak from the Im3m structure also appears.

Considering now only the Pn3m cubosomes, calculating the lattice parameters for all aqueous media, as more MILT is loaded into the cubosomes, more it changes the lattice of the nanoparticles (Figure 83). Notice that up to 5% w/w MILT, the lattice parameter is increased by ~1 nm only, similar to the results by the co-solubilization method (see Figure 68). On the other hand, for higher MILT concentrations (10% and 15% w/w) the lattice parameter is increased by almost 3.5 nm compared to the blank sample, in PBS medium, this increase in lattice parameter is much more evident.

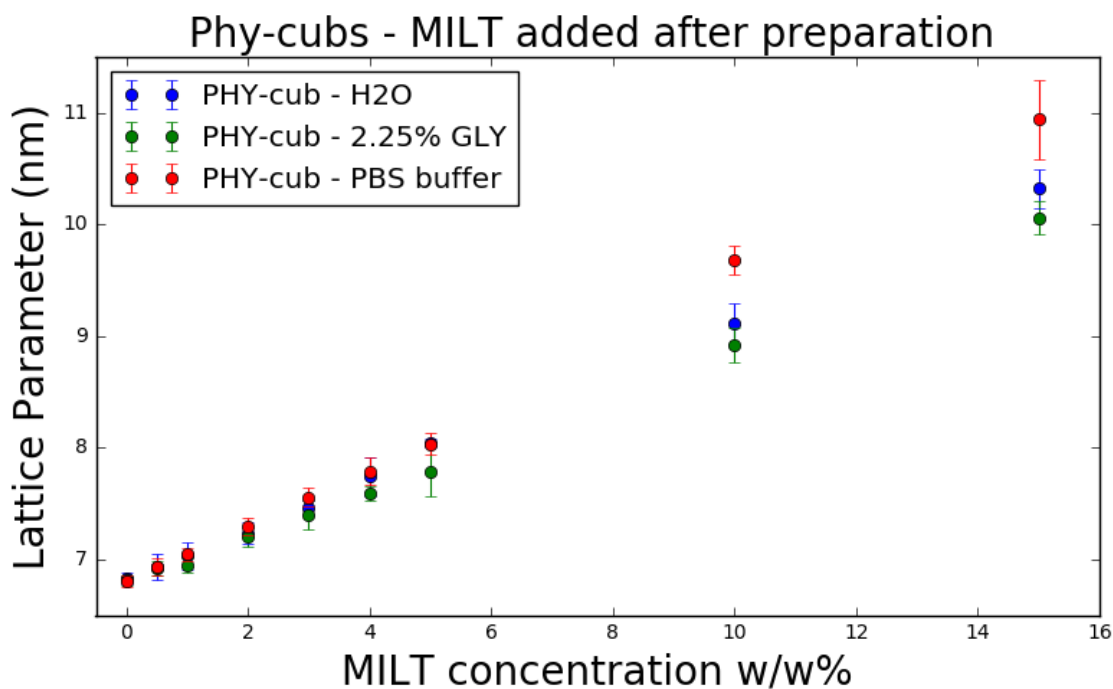


Figure 83. Calculated lattice parameters for cubosomes loaded with MILT after preparation. Up to 5% w/w loading, the lattice parameter was shifted by ~1 nm, but for higher concentrations (10% and 15%), an increase of almost ~3.5 nm was revealed.

Comparing the calculated lattice parameters from the co-solubilization method with the addition after preparation, interesting facts are revealed. Considering only the concentrations that do not induced phase transitions (up to 4% w/w), Figure 84 displays the comparison for MILT loading methods. Results show that for water medium, both co-solubilization and addition after preparation have the same effects over the cubosomes. All calculated lattice parameters were compatible between themselves within error bars.

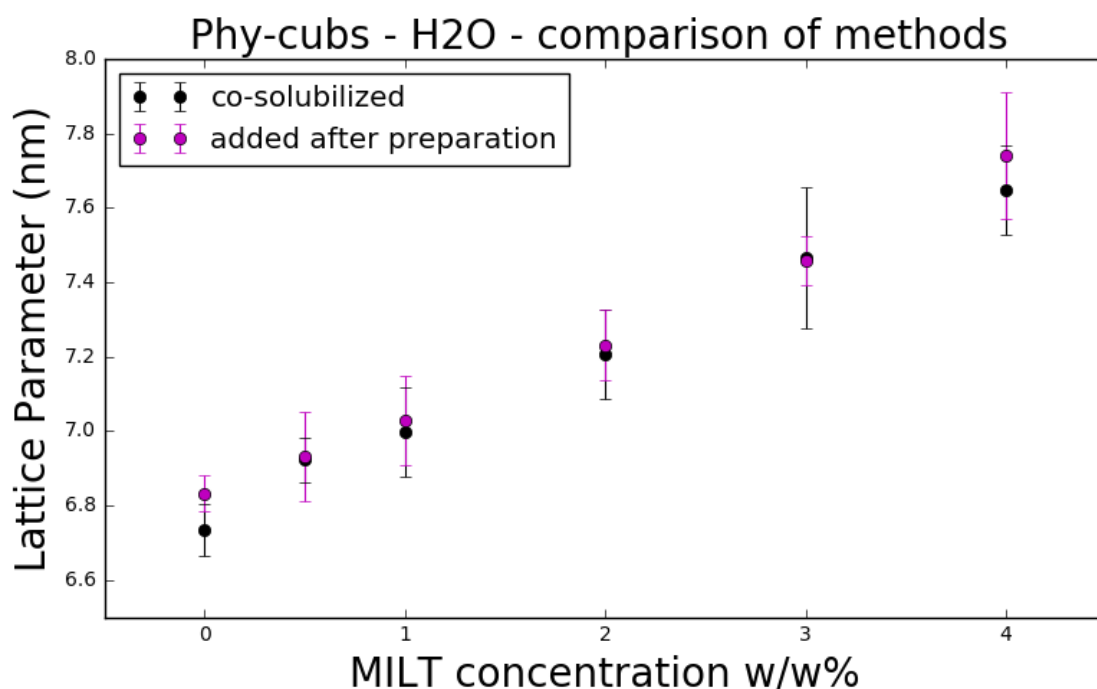


Figure 84. Lattice parameter comparison for both co-solubilization and addition to already prepared cubosomes MILT loading methods. For water medium, both methods were proven to exert the same effect on the cubosomes.

When comparing the same data for PBS and glycerol medium, a few differences are evidenced. In PBS medium (left graph in Figure 85), the calculated lattice parameters for the MILT loaded after preparation were significantly different from the lattices calculated by the co-solubilization method. For glycerol medium (right graph in Figure 85), these differences are much less evident. A possible explanation for these results are that molecules (salt in PBS case or glycerol molecules in the other case) in the aqueous medium, may exert some interaction with MILT competing for it or disfavoring its transfer from the aqueous phase to the cubic phase.

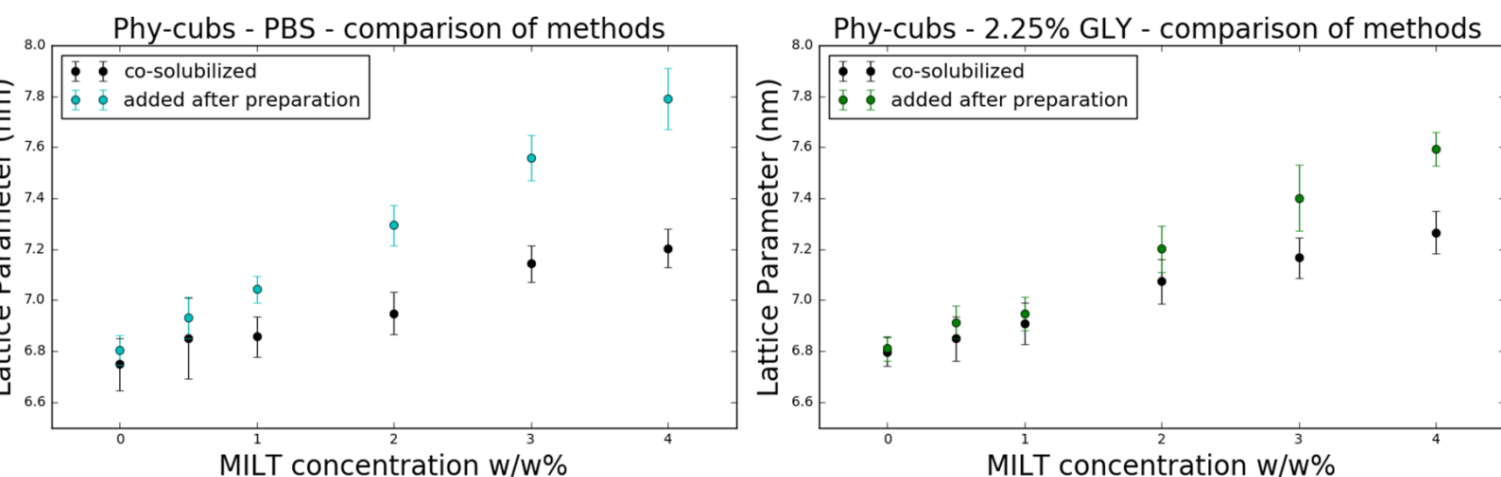


Figure 85. Lattice parameter comparison for MILT loading methods in PBS and glycerol media. As can be seen, in PBS (left graph) the calculated lattices are higher when adding MILT after the nanoparticles preparation. For glycerol medium (right graph) this deviation is lower but still happens.

DLS was also performed for these samples in order to investigate if MILT would influence particle size, once it was added to the formulation after the cubosomal nanoparticles were formed. Figure 86 displays size and polydispersion results for water, PBS and glycerol media. Interestingly, MILT did not seem to affect particle size or PDI when added to the cubosomes dispersion, for any of the tested aqueous media. This indicates that MILT can be loaded into the nanoparticles without any damage to the cubosomes biophysical properties.

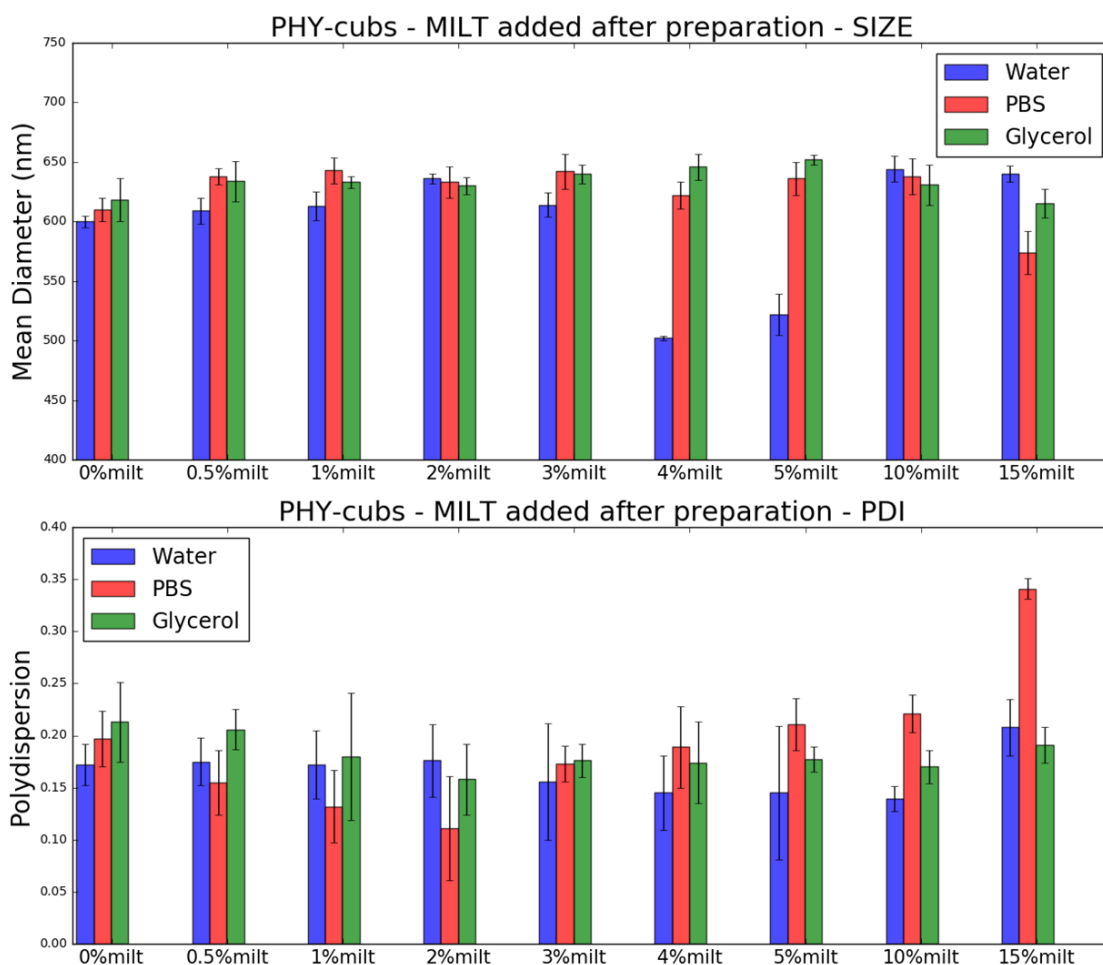


Figure 86. DLS measurements of size (upper graph) and PDI (down graph) for cubosomes loaded with MILT after preparation. Interestingly, MILT also does not seem to influence neither particle size or polydispersion.

Cryo-EM was performed to sample 4% w/w, water medium, in order to investigate if there could be traces of MILT in the surface of the particles, not noticed by DLS measurements. Figure 87 presents the obtained micrographs for this sample. Overall, all found particles are cubosomes due to the well evidenced internal structure, their surfaces do not present any features differently from the blank sample (see Figure 61), therefore, MILT must be inserted into the cubosomes inner structure.

Particles shapes displayed square or round motifs, similar to blank samples, and size was variable (~200nm to ~900 nm), confirming the moderate polydispersion measured on DLS. The orange arrow points out a curious structure, a cubosome that seems to be linked to a large vesicle, and inside it other smaller vesicles and a very small cubosome can be found.

From the 2D micrograph there is no way to say if all these structures are on top of each other or if they are inside each other, this would require a cryo-tomography (DEMURTAS et al., 2015). This curious structure was the only one found in the sample, such structures were not seen in the blank sample (Figure 61).

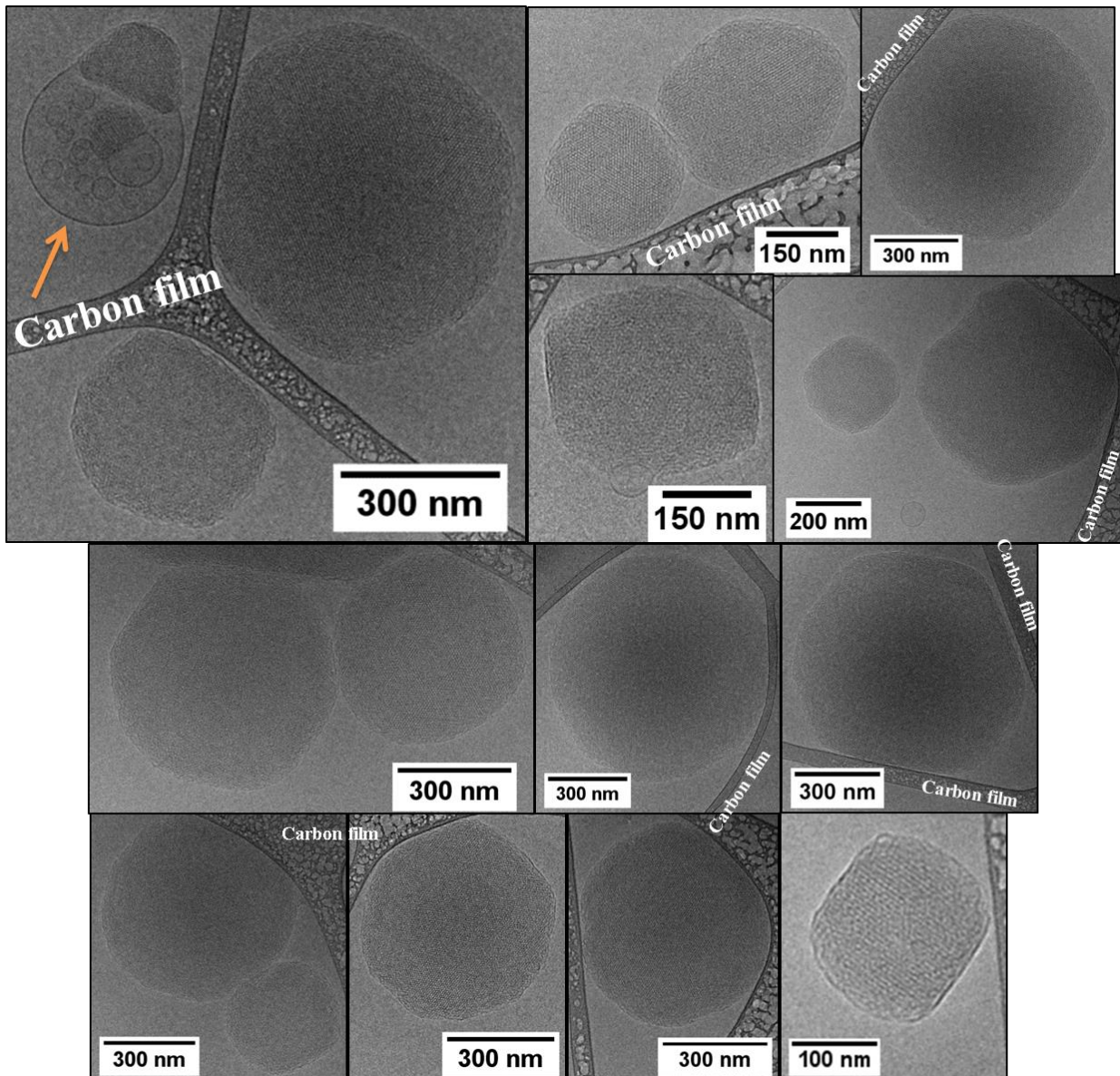


Figure 87. Cryo-EM micrographs for sample 4% w/w MILT in water medium. In all micrographs, the internal structure of the cubosomes is well defined, the particles surface showed no features differently from the blank samples (Figure 61). Cubosomes in this sample have both rounder and square shapes and varied size, confirming the DLS measured polydispersion. The orange arrow points out a curious particle structure, in which the cubosome seems to be linked to a big vesicle, in addition, inside this structure other smaller vesicles and cubosomal particles can be found.

FFT analysis was also done for the found particles in Figure 87. Curiously, almost all particles in this sample were frozen in the same axis, as can be seen by their FFT shape. Figure 88 displays the FFT's for some of the particles in Figure 87, one can see that almost all FFT's present a hexagonal shape, indicating that all these particles were frozen in the same direction, relatively to the electron beam. The blue star exhibits a FFT in a square shape, suggesting that this cubosome in particular was frozen in a tilted position related to the others.

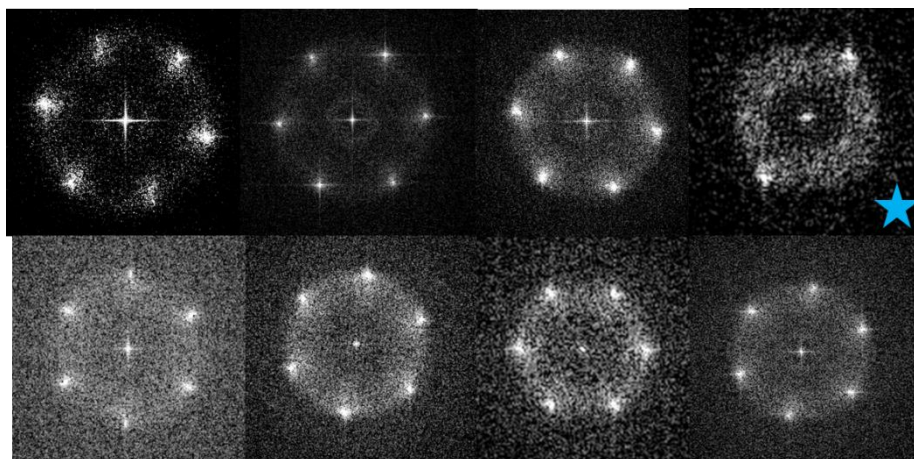


Figure 88. FFT of some particles from Figure 87. Notice that almost all FFT's have a hexagonal motif, while only one (blue star) displays a square motif, indicating that this particle alone was frozen in a tilted angle.

When calculating the lattice parameters for the particles in Figure 87, the following values ranging from 6.4(5) nm to 7.6(5) nm were found:

7.2(5) nm	7.2(5) nm	6.9(5) nm	7.4(5) nm	7.6(5) nm	7.2(5) nm	7.4(5) nm
6.4(5) nm	6.9(5) nm	7.0(5) nm	7.2(5) nm	7.6(5) nm	7.4(5) nm	7.0(5) nm
7.3(5) nm	7.0(5) nm	7.0(5) nm	7.3(5) nm			

These found lattice parameter values are compatible with the ones calculated from SAXS experiments (see Figure 84), in addition, most particles also present higher lattices than the blank sample (see table on page 88). From this, we conclude that MILT can be loaded into cubosomes both via co-solubilization or added after the cubosomal dispersions is prepared, since there are no huge changes in both loading methods.

5.3.3.4 Temperature effect on cubosomes for MILT added after preparation

Samples with 1% w/w, 3% w/w, 5% w/w and 10% w/w MILT were submitted to SAXS measurements at 22 °C, 40 °C, 50 °C and 65 °C in order to investigate if MILT added after the cubosomal preparation would have any effect over the phase transition of the cubosomes in comparison to blank samples (Figure 64 and Figure 65). Figure 89 presents the results for loaded cubosomes in water. For the lowest MILT concentration, 1% w/w (Fig 82-A), up to 50 °C the colloidal system is only made by Pn3m cubosomes, and the peak shifting indicates that water is being expelled from the nanoparticles, as in the blank cubosomes case (see Figure 64). Interestingly, at 65 °C there is coexistence of hexagonal phase (red arrows) and Pn3m cubosomes. Comparing the co-solubilized sample at the same temperature (see Figure 78), one can hypothesize that MILT loading after the cubosomes were prepared, induced the system to undergo from cubic to hexagonal phase. When co-solubilized, the system changed from cubosomes to L_2 phase.

For intermediate concentrations, 3% w/w (Fig. 82-B) and 5% w/w (Fig. 82-C), as in the co-solubilized case (see Figure 79), the cubosomes dispersion held the cubic structure over all temperatures, indicating that MILT helped the nanoparticles to keep the Pn3m structure. At the highest concentration, 10% w/w (Fig.82-D) most part of the cubosomes have Pn3m symmetry, but as temperature rises, the first peak from the Im3m crystallographic symmetry (blue arrows) becomes more evident in the curves, although there is no phase change in the system. The appearance of this Im3m peak is also compatible with the results by the co-solubilization method (see Figure 79).

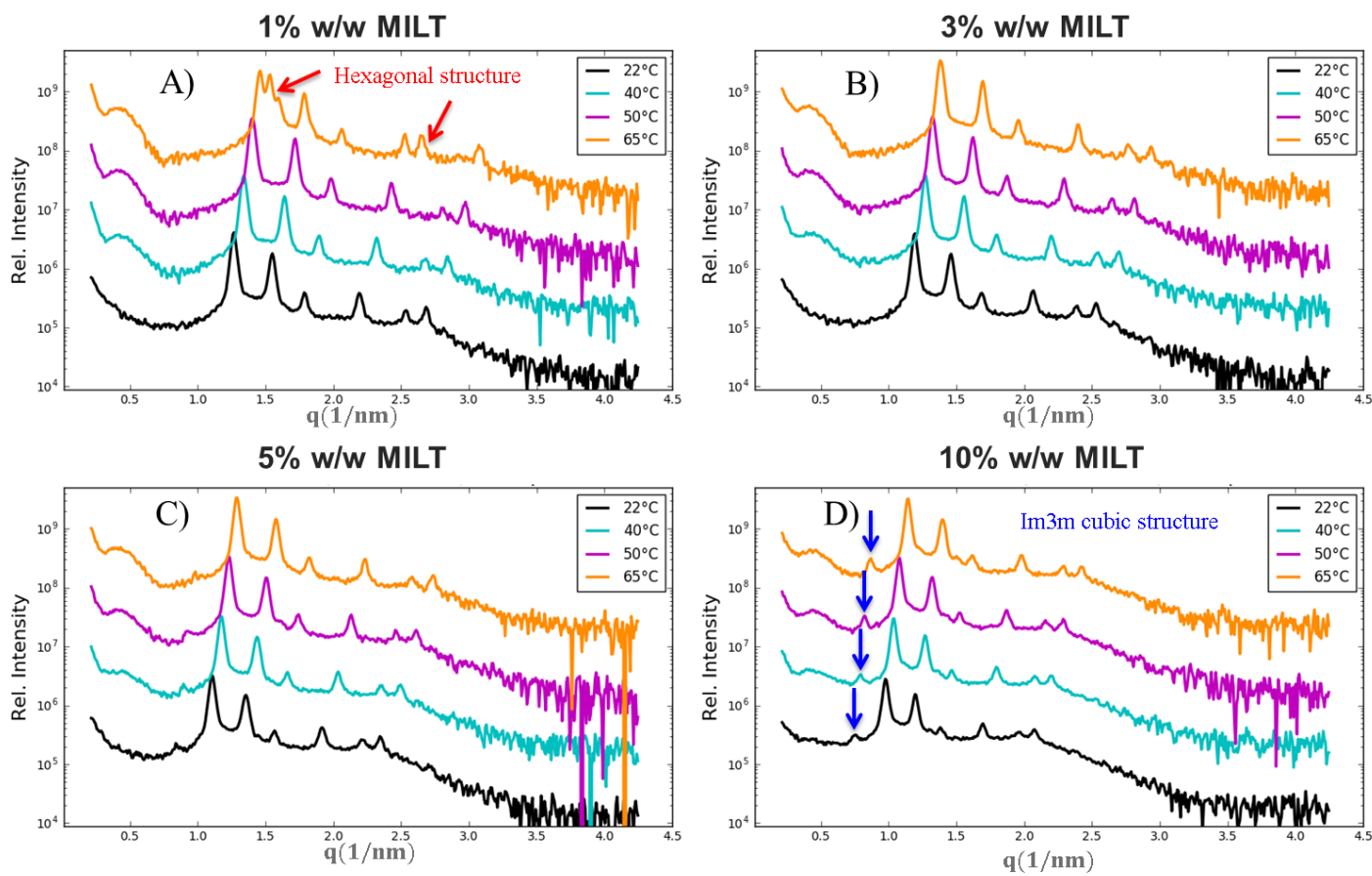


Figure 89. SAXS measurements for samples with loaded MILT after cubosomal preparation, in water medium. A) 1% w/w MILT, up to 50 °C the colloidal system is still cubic with all six peaks well defined, at 65°C there is coexistence of hexagonal (red arrows) and cubic phases. B) 3% w/w MILT and C) 5% w/w MILT present only cubic phase Pn3m throughout all temperatures. D) At 10% w/w MILT, as temperature rises, the first peaks of Im3m cubic phase (blue arrows) becomes more evident in the curve.

When in PBS medium, Figure 90, curious results were observed. For all loaded cubosomes, up to 50 °C, the cubosomes colloidal system holds the Pn3m cubic structure only expelling water from its structure due do the peak shifting to higher q values. Interestingly, at 65°C for 1% w/w loaded MILT (Fig.83-A) the nanoparticles undergo complete phase transition for hexagonal phase (red arrows), again, MILT loaded after the cubosomes were formed may induce this phase transition. For 3% w/w (Fig.83-B), there is coexistence of hexagonal and cubic phases given by the extra peaks in the curve (red arrows). For 5% (Fig.83-C) and 10% w/w (Fig.83-D) only Pn3m cubosomes exist in the dispersion, and differently from water, in PBS, there is no evidence of an Im3m peak at 10% w/w MILT.

Overall, MILT seems to be attached to the cubosomes structure in such a way, that at high concentrations, the nanoparticles do not undergo phase transition at higher temperatures (65 °C).

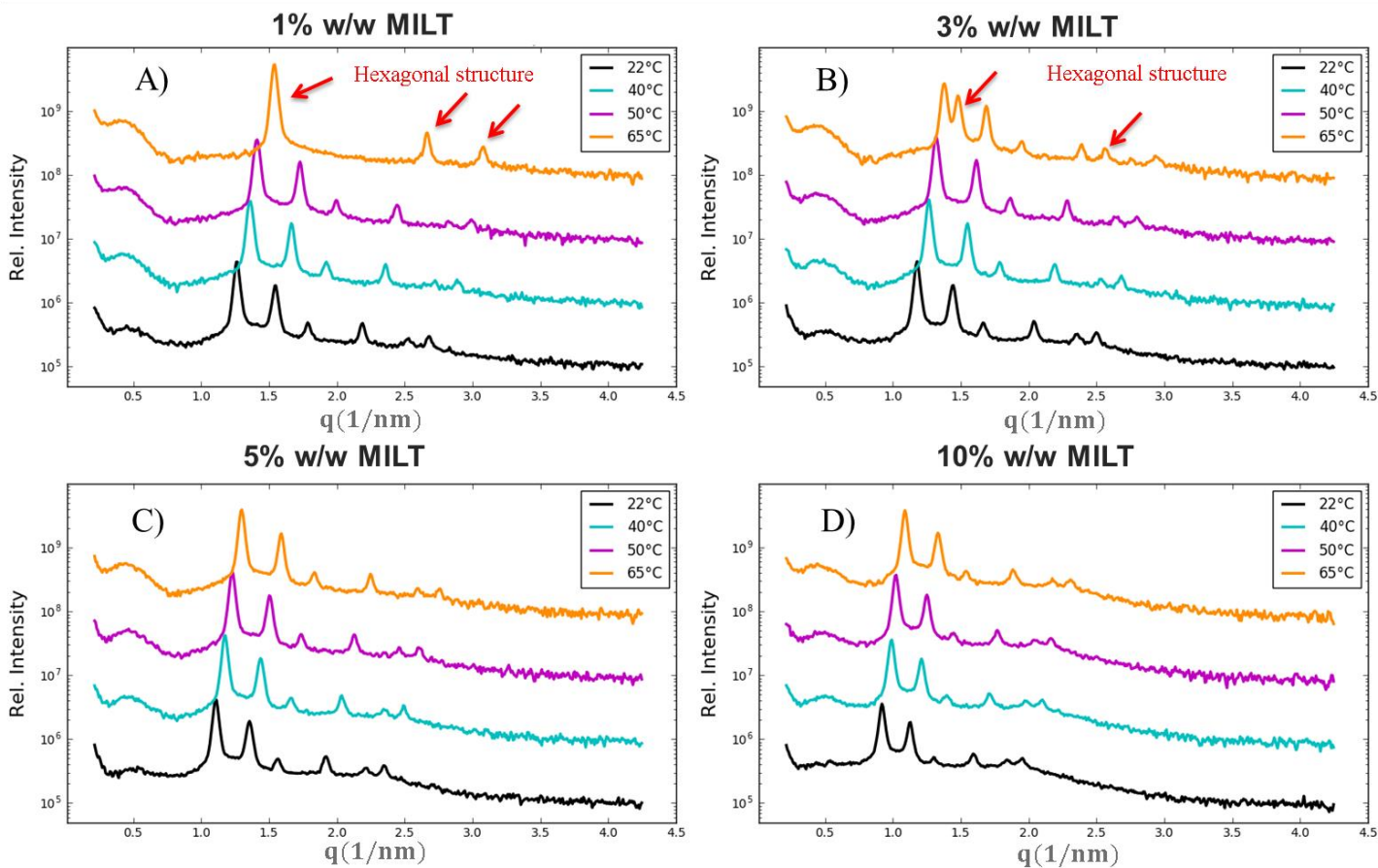


Figure 90. SAXS measurements for samples with loaded MILT after cubosomal preparation, in PBS medium. A) 1% w/w MILT, up to 50 °C the colloidal system is still cubic with all six peaks well defined, at 65°C there is complete phase transition for hexagonal phase (red arrows). B) At 3% w/w MILT there is coexistence of hexagonal (red arrows) and cubic phases at 65 °C. C) 5% w/w MILT and D) 10% w/w MILT only cubic Pn3m phase exists in the samples

6. Conclusions

In this project two lipids were used to successfully produce cubosomes. Monoolein (GMO) produced Im3m cubosomes by a top down method, SAXS revealed particles with lattice parameter 15.3(7) nm. The colloidal dispersion revealed particle sizes in the range of 300(8) nm and moderate polydispersion 0.160(20). TEM micrographs displayed squared shape cubosomes with average sizes 352(40) nm, compatible with DLS measurements. Cryo-EM measurements revealed particles with internal structure and lattice parameter similar to SAXS data.

When loading the model drug miltefosine (MILT), it was found by TEM that most particles had their sizes enlarged in a concentration dependent manner. Up to a concentration of 4% w/w MILT, the cubosomes would still hold their cubic Im3m structure, but at 5% w/w MILT, almost no particles with internal structure could be seen on cryo-EM. Due to problems with GMO availability, this protocol was abandoned during the project.

Myverol (MYV), a lipid mixture that contains approximately 60% of monoolein, was used to produce monoolein based cubosomes. For myverol based cubosomes, the proposed bottom up protocol produced successfully cubosomes with Im3m crystallographic structure and a lattice parameter ~12.3 nm, in both water and 2.25% glycerol media. TEM revealed particles with average sizes ~500 nm, both in aqueous and in glycerol media, cubosomes coexisted with other structures due to the presence of other molecules in the MYV mixture.

MILT also interacted with these cubosomes, by enlarging their lattice parameter as more MILT was loaded. In addition, at some MILT concentration, there was the formation of other structures in the samples, probably because of the other molecules present in the MYV mixture interacting with the drug. From TEM, nanoparticles presented sizes ranging from ~400 nm to ~1 μ m, revealing strong polydispersion. Interestingly, some nanoparticles revealed a leakage within their structures and curious shapes in TEM micrographs.

Phytantriol (PHY) cubosomes were reproduced from a well established protocol in literature. SAXS revealed nanoparticles belonging to the Pn3m crystallographic structure, differently from GMO/MYV cubosomes. The calculated lattice parameter was also smaller, ~6.74(07) nm and cubosomes were reproduced in water, PBS buffer and 2.25% glycerol media. The nanoparticles revealed sizes ~450 nm and moderate polydispersion (~0.2). In

order to decrease polydispersion of the cubosomes, the samples in water medium were submitted to extrusion, revealing that these nanoparticles had their sizes diminished (~200 nm) and polydispersion improved (~0.08). Lyophilization was also tested for conservation purposes and cubosomes were found to hold their internal structure after re-hydration. NTA revealed a total particle concentration of about $\sim 10^{12}$ particles/mL for all samples. TEM and cryo-EM presented particles with internal structure that withheld both squared and rounder shape and varied sizes, confirming the moderate polydispersion of DLS measurements. Samples were still submitted to higher temperatures, revealing that up to 50 °C the suspension was cubic, but at 65 °C the colloidal dispersion had a phase transition to isotropic phase L_2 .

MILT was loaded into cubosomes both via co-solubilization and addition after the nanoparticles were formed. Both processes revealed be to equivalent. MILT was hypothesized to be inserting itself into the lipidic moiety of the nanoparticles, causing an enlargement of the lattice parameter. Up to a concentration of 5% w/w, the cubosomes held their Pn3m conformation, and MILT did not seem to alter particle size or polydispersion. TEM presented particles with sizes larger than DLS. Interestingly, when submitted to higher temperatures, as more MILT was loaded into the cubosomes, nanoparticles would hold their Pn3m structure even at 65°C, differently from the blank samples. For higher quantities of loaded MILT (10%, 15% and 20% w/w) there was a phase transition to Im3m crystallographic symmetry for the cubosomal dispersion, revealed by SAXS.

Finally, cubosomes have proven to be remarkable nanoparticles, once they can hold their structures at high temperatures and be submitted to stressing processes, such as extrusion and lyophilization, without loss of biophysical properties.

7. Future Perspectives

In the future, cubosomes should be evaluated for encapsulation efficiency of MILT and release assays in order to make possible the proofing of the drug delivery system. In addition, a cytotoxicity test should be made to investigate if these nanoparticles are suitable for drug delivery. Finally, *in vitro* and *in vivo* assays should be made in order to evaluate the efficiency of MILT delivery against the effect of the drug itself.

8. Bibliography

- AKBAR, S. et al. Phytantriol based smart nano-carriers for drug delivery applications. **European Journal of Pharmaceutical Sciences**, v. 101, n. 1, p. 31–42, 2017.
- AKHLAGHI, S. P. et al. Impact of preparation method and variables on the internal structure, morphology, and presence of liposomes in phytantriol-Pluronic® F127 cubosomes. **Colloids and Surfaces B: Biointerfaces**, v. 145, p. 845–853, 2016.
- AKHTER, M. H. et al. Nanocarriers in advanced drug targeting: setting novel paradigm in cancer therapeutics. **Artificial Cells, Nanomedicine, and Biotechnology**, v. 46, n. 5, p. 873–884, 2018.
- ALCARAZ, N. et al. Clickable Cubosomes for Antibody-Free Drug Targeting and Imaging Applications. **Bioconjugate Chemistry**, v. 29, n. 1, p. 149–157, 2018.
- ALI, M. A. et al. Preparation and Characterization of SN-38-Encapsulated Phytantriol Cubosomes Containing α -Monoglyceride Additives. **Chemical and Pharmaceutical Bulletin**, v. 64, n. 6, p. 577–584, 2016.
- ALONSO, L.; ALONSO, A. Hemolytic potential of miltefosine is dependent on cell concentration: Implications for in vitro cell cytotoxicity assays and pharmacokinetic data. **Biochimica et Biophysica Acta (BBA) - Biomembranes**, v. 1858, n. 6, p. 1160–1164, 2016.
- ANDERSSON, S. et al. **Biomathematics: mathematics of biostructures and biodynamics**. [s.l.] Elsevier, 1999.
- ANGELOVA, A. et al. Small-Angle X-ray Scattering Investigations of Biomolecular Confinement, Loading, and Release from Liquid-Crystalline Nanochannel Assemblies. **The Journal of Physical Chemistry Letters**, v. 3, n. 3, p. 445–457, fev. 2012.
- ANSELMO, A. C.; MITRAGOTRI, S. Impact of particle elasticity on particle-based drug delivery systems. **Advanced Drug Delivery Reviews**, v. 108, p. 51–67, 2017.
- ASTOLFI, P. et al. Lyotropic Liquid-Crystalline Nanosystems as Drug Delivery Agents for 5-Fluorouracil: Structure and Cytotoxicity. **Langmuir**, v. 33, n. 43, p. 12369–12378, 2017.
- AZHARI, H. et al. Stabilising cubosomes with Tween 80 as a step towards targeting lipid nanocarriers to the blood–brain barrier. **European Journal of Pharmaceutics and Biopharmaceutics**, v. 104, p. 148–155, 2016.
- AZMI, I. D. M.; MOGHIMI, S. M.; YAGHMUR, A. Cubosomes and hexosomes as versatile platforms for drug delivery. **Therapeutic Delivery**, v. 6, n. 12, p. 1347–1364, 2015.
- BAO, G.; MITRAGOTRI, S.; TONG, S. Multifunctional Nanoparticles for Drug Delivery and Molecular Imaging. **Annual Review of Biomedical Engineering**, v. 15, p. 253–282, 2013.
- BARAUSKAS, J.; LANDH, T. Phase Behavior of the Phytantriol/Water System. **Langmuir**, v. 19, n. 23, p. 9562–9565, 2003.
- BARBOSA, L. R. S. et al. Small-Angle X-Ray Scattering Applied to Proteins in Solution. In: **Proteins in Solution and at Interfaces**. Hoboken, NJ, USA: John Wiley & Sons, Inc., 2013. p. 49–72.
- BARIONI, M. B. et al. Miltefosine and BODIPY-labeled alkylphosphocholine with leishmanicidal activity: Aggregation properties and interaction with model membranes. **Biophysical Chemistry**, v. 196, p. 92–99, 2015.
- BARRIGA, H. M. G.; HOLME, M. N.; STEVENS, M. M. Cubosomes; the next generation of smart lipid nanoparticles? **Angewandte Chemie**, v. 0, n. ja, 21 jun. 2018.
- BHATTACHARJEE, S. DLS and zeta potential – What they are and what they are not? **Journal of Controlled Release**, v. 235, p. 337–351, 2016.
- BLANCO, E.; SHEN, H.; FERRARI, M. Principles of nanoparticle design for overcoming biological barriers to drug delivery. **Nature Biotechnology**, v. 33, n. 9, p. 941–951, 2015.
- BOLLA, P. K. et al. A review on pH and temperature responsive gels and other less explored drug delivery systems. **Journal of Drug Delivery Science and Technology**, v. 46, p. 416–435, 2018.
- BRÖNNIMANN, C.; TRÜB, P. Hybrid Pixel Photon Counting X-Ray Detectors for Synchrotron Radiation BT - Synchrotron Light Sources and Free-Electron Lasers: Accelerator Physics, Instrumentation and Science

- Applications. In: JAESCHKE, E. J. et al. (Eds.). **Synchrotron Light Sources and Free-Electron Lasers: Accelerator Physics, Instrumentation and Science Applications**. Cham: Springer International Publishing, 2016. p. 995–1027.
- BURROWS, N. D.; PENN, R. L. Cryogenic Transmission Electron Microscopy: Aqueous Suspensions of Nanoscale Objects. **Microscopy and Microanalysis**, v. 19, n. 6, p. 1542–1553, 2013.
- BYE, N. et al. Nitroxide-Loaded Hexosomes Provide MRI Contrast in Vivo. **Langmuir**, v. 30, n. 29, p. 8898–8906, 29 jul. 2014.
- CABAN, S. et al. Nanosystems for drug delivery. **OA Drug Design and Delivery**, v. 2, n. 1, p. 1–7, 2014.
- CAFFREY, M. Crystallizing Membrane Proteins for Structure Determination: Use of Lipidic Mesophases. **Annual Review of Biophysics**, v. 38, n. 1, p. 29–51, 2009.
- CAI, K. et al. Bio-nano interface: The impact of biological environment on nanomaterials and their delivery properties. **Journal of Controlled Release**, v. 263, p. 211–222, 2017.
- CHENG, H. N. et al. Nanotechnology Overview: Opportunities and Challenges. In: **Nanotechnology: Delivering on the Promise Volume 1**. [s.l.] American Chemical Society, 2016. p. 1–12.
- CHIARI, B. G. et al. Physicochemical characterization of drug nanocarriers. **International Journal of Nanomedicine**, v. 12, p. 4991–5011, 2017.
- CHONG, J. Y. T. et al. Steric stabilisation of self-assembled cubic lyotropic liquid crystalline nanoparticles: high throughput evaluation of triblock polyethylene oxide-polypropylene oxide-polyethylene oxide copolymers. **Soft Matter**, v. 7, n. 10, p. 4768–4777, 2011.
- CHONG, J. Y. T. et al. High-throughput discovery of novel steric stabilizers for cubic lyotropic liquid crystal nanoparticle dispersions. **Langmuir**, v. 28, n. 25, p. 9223–9232, 2012.
- CLOGSTON, J. et al. Phase behavior of a monoacylglycerol: (Myverol 18-99K)/water system. **Chemistry and Physics of Lipids**, v. 107, n. 2, p. 191–220, 2000.
- CULLITY, B. D.; STOCK, S. R. **Elements of X-ray Diffraction**. New York, NY: Pearson Education, 2014.
- CZARNOCKI-CIECIURA, M.; NOWOTNY, M. Introduction to high-resolution cryo-electron microscopy. **Postepy biochemii**, v. 62, n. 3, p. 383–394, 2016.
- DA GAMA BITENCOURT, J. J. et al. Miltefosine-loaded lipid nanoparticles: Improving miltefosine stability and reducing its hemolytic potential toward erythrocytes and its cytotoxic effect on macrophages. **Biophysical Chemistry**, v. 217, p. 20–31, 2016.
- DANINO, D. Cryo-TEM of soft molecular assemblies. **Current Opinion in Colloid and Interface Science**, v. 17, n. 6, p. 316–329, 2012.
- DE SÁ, M. et al. Understanding Miltefosine–Membrane Interactions Using Molecular Dynamics Simulations. **Langmuir**, v. 31, n. 15, p. 4503–4512, 2015.
- DEMURTAS, D. et al. Direct visualization of dispersed lipid bicontinuous cubic phases by cryo-electron tomography. **Nature Communications**, v. 6, p. 8915, 17 nov. 2015.
- DEHPANDE, S.; SINGH, N. Influence of Cubosome Surface Architecture on Its Cellular Uptake Mechanism. **Langmuir**, v. 33, n. 14, p. 3509–3516, 2017.
- DONG, Y.-D. et al. Nonequilibrium Effects in Self-Assembled Mesophase Materials: Unexpected Supercooling Effects for Cubosomes and Hexosomes. **Langmuir**, v. 26, n. 11, p. 9000–9010, 2010.
- DONG, Y.-D. et al. Understanding the Interfacial Properties of Nanostructured Liquid Crystalline Materials for Surface-Specific Delivery Applications. **Langmuir**, v. 28, n. 37, p. 13485–13495, 2012.
- DUDKIEWICZ, A. et al. Characterization of nanomaterials in food by electron microscopy. **TrAC - Trends in Analytical Chemistry**, v. 30, n. 1, p. 28–43, 2011.
- DUMORTIER, G. et al. A Review of Poloxamer 407 Pharmaceutical and Pharmacological Characteristics. **Pharmaceutical Research**, v. 23, n. 12, p. 2709–2728, 2006.
- EISSA, M. M. et al. Miltefosine Lipid Nanocapsules for Single Dose Oral Treatment of Schistosomiasis Mansoni: A Preclinical Study. **PLOS ONE**, v. 10, n. 11, p. e0141788, 17 nov. 2015.
- ELISABETTA ESPOSITO, PAOLO MARIANI, MARKUS DRECHSLER, R. C. Structural Studies of Lipid-

- Based Nanosystems for Drug Delivery: X-ray Diffraction (XRD) and Cryogenic Transmission Electron Microscopy (Cryo-TEM). In: ALIOFKHAZRAEI, M. (Ed.). **Handbook of Nanoparticles**. 1. ed. Switzerland: Springer International Publishing, 2016. p. 1439.
- ERICSSON, E. M. et al. Glycerol monooleate–blood interactions. **Colloids and Surfaces B: Biointerfaces**, v. 68, n. 1, p. 20–26, 2009.
- ESPOSITO, E. et al. Lipid-based supramolecular systems for topical application: A preformulatory study. **AAPS PharmSci**, v. 5, n. 4, p. 62, 2015.
- FERREIRA, D. A. et al. Cryo-TEM investigation of phase behaviour and aggregate structure in dilute dispersions of monoolein and oleic acid. **International Journal of Pharmaceutics**, v. 310, n. 1, p. 203–212, 2006.
- FONG, W. K. et al. Generation of Geometrically Ordered Lipid-Based Liquid-Crystalline Nanoparticles Using Biologically Relevant Enzymatic Processing. **Langmuir**, v. 30, n. 19, p. 5373–5377, 20 maio 2014.
- FOSSUM, E. R.; HONDONGWA, D. B. A Review of the Pinned Photodiode for CCD and CMOS Image Sensors. **IEEE Journal of the Electron Devices Society**, v. 2, n. 3, p. 33–43, 2014.
- FRANKEN, L. E.; BOEKEMA, E. J.; STUART, M. C. A. Transmission Electron Microscopy as a Tool for the Characterization of Soft Materials: Application and Interpretation. **Advanced Science**, v. 4, n. 5, p. 1600476, 31 jan. 2017.
- FRASER, S. J. et al. Controlling nanostructure and lattice parameter of the inverse bicontinuous cubic phases in functionalised phytantriol dispersions. **Journal of Colloid and Interface Science**, v. 408, n. 1, p. 117–124, 2013.
- GALLEGO-URREA, J. A.; TUORINIEMI, J.; HASSELLÖV, M. Applications of particle-tracking analysis to the determination of size distributions and concentrations of nanoparticles in environmental, biological and food samples. **TrAC Trends in Analytical Chemistry**, v. 30, n. 3, p. 473–483, 2011.
- GAN, L. et al. Recent advances in topical ophthalmic drug delivery with lipid-based nanocarriers. **Drug Discovery Today**, v. 18, n. 5–6, p. 290–297, 2013.
- GUSTAFSSON, J. et al. Submicron Particles of Reversed Lipid Phases in Water Stabilized by a Nonionic Amphiphilic Polymer. **Langmuir**, v. 13, n. 26, p. 6964–6971, 1997.
- HARTNETT, T. E. et al. Physicochemical and cytotoxicity analysis of glycerol monoolein-based nanoparticles. **RSC Advances**, v. 5, n. 34, p. 26543–26549, 2015.
- HASSAN, P. A.; RANA, S.; VERMA, G. Making sense of brownian motion: colloid characterization by dynamic light scattering. **Langmuir: the ACS journal of surfaces and colloids**, v. 31, n. 1, p. 3–12, 2015.
- HE, B. B. **Two-Dimensional X-Ray Diffraction**. 1st. ed. Hoboken, New Jersey: John Wiley & Sons, Inc., 2009.
- HEDEGAARD, S. F. et al. Nanostructured aqueous dispersions of citrem interacting with lipids and PEGylated lipids. **RSC Advances**, v. 3, n. 46, p. 24576–24585, 2013.
- HELVIG INTAN D. M.; MOGHIMI, SEYED M.; YAGHMUR, ANAN, S. Recent Advances in Cryo-TEM Imaging of Soft Lipid Nanoparticles. **AIMS Biophysics**, v. 2, n. 2, p. 116–130, 2015.
- HINTON, T. M. et al. Bicontinuous cubic phase nanoparticle lipid chemistry affects toxicity in cultured cells. **Toxicology Research**, v. 3, n. 1, p. 11–22, 2014.
- HOU, J. et al. Nanoparticle tracking analysis versus dynamic light scattering: Case study on the effect of Ca²⁺ and alginate on the aggregation of cerium oxide nanoparticles. **Journal of Hazardous Materials**, v. 360, p. 319–328, 2018.
- IANCU, C. V et al. Electron cryotomography sample preparation using the Vitrobot. **Nature Protocols**, v. 1, p. 2813, 18 jan. 2006.
- JAIN, S. et al. Phytantriol Based “Stealth” Lyotropic Liquid Crystalline Nanoparticles for Improved Antitumor Efficacy and Reduced Toxicity of Docetaxel. **Pharmaceutical Research**, v. 32, n. 10, p. 3282–3292, 2015.
- JARZĘBSKI, M. et al. Particle tracking analysis in food and hydrocolloids investigations. **Food Hydrocolloids**, v. 68, p. 90–101, 2017.
- JENA, M. et al. Nanotechnology- future prospect in recent medicine: a review. **International Journal of Basic & Clinical Pharmacology**, v. 2, n. 4, p. 353–359, 2013.

- JURJ, A. et al. The new era of nanotechnology, an alternative to change cancer treatment. **Drug Design, Development and Therapy**, v. 11, p. 2871–2890, 2017.
- KARAMI, Z.; HAMIDI, M. Cubosomes: remarkable drug delivery potential. **Drug Discovery Today**, v. 21, n. 5, p. 789–801, 2016.
- KAURAV, M. et al. Nanoparticulate mediated transcutaneous immunization: Myth or reality. **Nanomedicine: Nanotechnology, Biology, and Medicine**, v. 12, n. 4, p. 1063–1081, 2016.
- KESTENS, V. et al. Validation of a particle tracking analysis method for the size determination of nano- and microparticles. **Journal of Nanoparticle Research**, v. 19, n. 8, p. 271, 2017.
- KHATTAK, S. F.; BHATIA, S. R.; ROBERTS, S. C. Pluronic F127 as a Cell Encapsulation Material: Utilization of Membrane-Stabilizing Agents. **Tissue Engineering**, v. 11, n. 5–6, p. 974–983, 2005.
- KHATUN, Z. et al. Elucidating diversity of exosomes: biophysical and molecular characterization methods. **Nanomedicine**, v. 11, n. 17, p. 2359–2377, 2016.
- KIM, D.-H. et al. Lyotropic liquid crystal systems in drug delivery: a review. **Journal of Pharmaceutical Investigation**, v. 45, n. 1, p. 1–11, 2015.
- KIM, H. et al. Microfluidics Synthesis of Gene Silencing Cubosomes. **ACS Nano**, 6 ago. 2018.
- KLEANDROVA, V. V. et al. QSAR-Based Studies of Nanomaterials in the Environment. In: **Materials Science and Engineering**. [s.l.] IGI Global, 2015. p. 1504–1532.
- KULKARNI, C. V. Lipid crystallization: from self-assembly to hierarchical and biological ordering. **Nanoscale**, v. 4, n. 19, p. 5779–5791, 2012.
- KUMAR, M. U.; BAPPADITYA, C.; MUHAMMAD, T. Advanced characterizations of nanoparticles for drug delivery: investigating their properties through the techniques used in their evaluations. **Nanotechnology Reviews**, v. 6, p. 355, 2017.
- LANCELOT, A.; SIERRA, T.; SERRANO, J. L. Nanostructured liquid-crystalline particles for drug delivery. **Expert Opinion on Drug Delivery**, p. 547–562, 2014.
- LARKIN, T. J. et al. Na⁺ and solute diffusion in aqueous channels of Myverol bicontinuous cubic phase: PGSE NMR and computer modelling. **Magnetic Resonance in Chemistry**, v. 55, n. 5, p. 464–471, 22 mar. 2016.
- LEE, B. K.; YUN, Y. H.; PARK, K. Smart nanoparticles for drug delivery: Boundaries and opportunities. **Chemical Engineering Science**, v. 125, p. 158–164, 2015.
- LESSER, M. 3 - Charge coupled device (CCD) image sensors. In: DURINI, D. B. T.-H. P. S. I. (Ed.). **High Performance Silicon Imaging: Fundamentals and Applications of CMOS and CCD sensors**. [s.l.] Woodhead Publishing, 2014. p. 78–97.
- LI, H. et al. CMOS Electrochemical Instrumentation for Biosensor Microsystems: A Review. **Sensors**, v. 17, n. 1, 2017.
- LI, T.; LIU, Z. **Outlook and Challenges of Nano Devices, Sensors, and MEMS**. [s.l.] Springer International Publishing, 2017.
- LIU, D. et al. The smart drug delivery system and its clinical potential. **Theranostics**, v. 6, n. 9, p. 1306–1323, 2016.
- LUO, Q. et al. A novel glyceryl monoolein-bearing cubosomes for gambogic acid: Preparation, cytotoxicity and intracellular uptake. **International Journal of Pharmaceutics**, v. 493, n. 1, p. 30–39, 2015.
- LUZZATI, V. et al. Structure of the Cubic Phases of Lipid–Water Systems. **Nature**, v. 220, n. 5166, p. 485, 2 nov. 1968.
- LUZZATI, V.; HUSSON, F. THE STRUCTURE OF THE LIQUID-CRYSTALLINE PHASES OF LIPID-WATER SYSTEMS. **The Journal of Cell Biology**, v. 12, n. 2, p. 207–219, 1962.
- MAGUIRE, C. M. et al. Benchmark of Nanoparticle Tracking Analysis on Measuring Nanoparticle Sizing and Concentration. **Journal of Micro and Nano-Manufacturing**, v. 5, n. 4, p. 41002–41010, 28 set. 2017.
- MARIANI, P.; LUZZATI, V.; DELACROIX, H. Cubic phases of lipid-containing systems: Structure analysis and biological implications. **Journal of Molecular Biology**, v. 204, n. 1, p. 165–189, 1988.
- MAT AZMI, I. D. et al. Modulatory Effect of Human Plasma on the Internal Nanostructure and Size

- Characteristics of Liquid-Crystalline Nanocarriers. **Langmuir**, v. 31, n. 18, p. 5042–5049, 12 maio 2015.
- MAZZONI, S. et al. Cytochrome-c Affects the Monoolein Polymorphism: Consequences for Stability and Loading Efficiency of Drug Delivery Systems. **Langmuir**, v. 32, n. 3, p. 873–881, 26 jan. 2016.
- MCKENZIE, B. E.; HOLDER, S. J.; SOMMERDIJK, N. A. J. M. Assessing internal structure of polymer assemblies from 2D to 3D CryoTEM: Bicontinuous micelles. **Current Opinion in Colloid and Interface Science**, v. 17, n. 6, p. 343–349, 2012.
- MENG, H. et al. Walking the line: The fate of nanomaterials at biological barriers. **Biomaterials**, v. 174, p. 41–53, 2018.
- MIELANCZYK, L. et al. Closer to the native state. Critical evaluation of cryo-techniques for Transmission Electron Microscopy: preparation of biological samples. **Folia histochemica et cytobiologica / Polish Academy of Sciences, Polish Histochemical and Cytochemical Society**, v. 52, n. 1, p. 1–17, 2014.
- MO, J.; MILLERET, G.; NAGARAJ, M. Liquid crystal nanoparticles for commercial drug delivery. **Liquid Crystals Reviews**, v. 5, n. 2, p. 69–85, 2017.
- MUDSHINGE, S. R. et al. Nanoparticles: Emerging carriers for drug delivery. **Saudi Pharmaceutical Journal**, v. 19, n. 3, p. 129–141, 2011.
- MULLER, F.; SALONEN, A.; GLATTER, O. Monoglyceride-based cubosomes stabilized by Laponite: Separating the effects of stabilizer, pH and temperature. **Colloids and Surfaces A: Physicochemical and Engineering Aspects**, v. 358, n. 1, p. 50–56, 2010.
- MUNOZ, C. et al. Effect of miltefosine on erythrocytes. **Toxicology in Vitro**, v. 27, n. 6, p. 1913–1919, 2013.
- MUNTIMADUGU, E.; KOMMINENI, N.; KHAN, W. Exploring the Potential of Nanotherapeutics in Targeting Tumor Microenvironment for Cancer Therapy. **Pharmacological Research**, v. 126, p. 109–122, 2017.
- MURA, S.; NICOLAS, J.; COUVREUR, P. Stimuli-responsive nanocarriers for drug delivery. **Nature Materials**, v. 12, n. 11, p. 991–1003, 2013.
- MURGIA, S. et al. Nanoparticles from Lipid-Based Liquid Crystals: Emulsifier Influence on Morphology and Cytotoxicity. **The Journal of Physical Chemistry B**, v. 114, n. 10, p. 3518–3525, 2010.
- NAGA M. LAKSHMI, PRASANNA R. YALAVARTHI, HARINI C. VADLAMUDI, JYOTSNA THANNIRU, GOWRI YAGA, H. K. Cubosomes as Targeted Drug Delivery Systems - A Biopharmaceutical Approach. **Current Drug Discovery Technologies**, v. 11, n. 3, p. 181–188, 2014.
- NAGAYAMA, K. Another 60 years in electron microscopy: development of phase-plate electron microscopy and biological applications. **Journal of Electron Microscopy**, v. 60, n. suppl_1, p. S43–S62, 1 ago. 2011.
- NALLA, A. Novel Herbal Drug Delivery System - an Overview. **World Journal of Pharmacy and Pharmaceutical Sciences**, v. 6, n. 8, p. 369–395, 2017.
- NASERI, N. et al. An update on nanoparticle-based contrast agents in medical imaging. **Artificial Cells, Nanomedicine, and Biotechnology**, v. 46, n. 6, p. 1111–1121, 2018.
- NASR, M.; GHORAB, M. K.; ABDELAZEM, A. In vitro and in vivo evaluation of cubosomes containing 5-fluorouracil for liver targeting. **Acta Pharmaceutica Sinica B**, v. 5, n. 1, p. 79–88, 2015.
- NATIONAL INSTITUTES OF HEALTH. **ImageJ**, 1987. Disponível em: <<https://imagej.nih.gov/ij/>>
- NAZARUK, E. et al. Design and Assembly of pH-Sensitive Lipidic Cubic Phase Matrices for Drug Release. **Langmuir**, v. 30, n. 5, p. 1383–1390, 2014.
- NAZARUK, E.; MAJKOWSKA-PILIP, A.; BILEWICZ, R. Lipidic Cubic-Phase Nanoparticles—Cubosomes for Efficient Drug Delivery to Cancer Cells. **ChemPlusChem**, v. 82, n. 4, p. 570–575, 2017.
- NGUYEN, T.-H. et al. Nanostructured liquid crystalline particles provide long duration sustained-release effect for a poorly water soluble drug after oral administration. **Journal of Controlled Release**, v. 153, n. 2, p. 180–186, 2011.
- NIKALJE, A. P. Nanotechnology and its Applications in Medicine. **Medicinal Chemistry**, v. 5, p. 081–089, 2015.
- NILSSON, C. et al. SPECT/CT imaging of radiolabeled cubosomes and hexosomes for potential theranostic applications. **Biomaterials**, v. 34, n. 33, p. 8491–8503, 2013.

- NILSSON, C. et al. PEGylation of Phytantriol-Based Lyotropic Liquid Crystalline Particles—The Effect of Lipid Composition, PEG Chain Length, and Temperature on the Internal Nanostructure. **Langmuir**, v. 30, n. 22, p. 6398–6407, 10 jun. 2014.
- PACHIONI, J. DE A. et al. Alkylphospholipids - A promising class of chemotherapeutic agents with a broad pharmacological spectrum. **Journal of Pharmacy and Pharmaceutical Sciences**, v. 16, n. 5, p. 742–759, 2013.
- PARK, K. Facing the Truth about Nanotechnology in Drug Delivery. **ACS Nano**, v. 7, n. 9, p. 7442–7447, 2013.
- PASSMORE, L. A.; RUSSO, C. J. Specimen preparation for high-resolution cryo-EM. **Methods in enzymology**, v. 579, p. 51–86, 16 jun. 2016.
- PATEL, H. R. et al. Poloxamers: A pharmaceutical excipients with therapeutic behaviors. **International Journal of PharmTech Research**, v. 1, n. 2, p. 299–303, 2009.
- PHAM, A. C. et al. Examining the gastrointestinal transit of lipid-based liquid crystalline systems using whole-animal imaging. **Drug Delivery and Translational Research**, v. 5, n. 6, p. 566–574, 2015.
- PILLON, M. C.; GUARNÉ, A. Complementary uses of small angle X-ray scattering and X-ray crystallography. **Biochimica et Biophysica Acta (BBA) - Proteins and Proteomics**, v. 1865, n. 11, p. 1623–1630, nov. 2017.
- PILZ, I.; GLATTER, O.; KRATKY, O. Small-angle x-ray scattering. In: **Enzyme Structure Part H**. Methods in Enzymology. [s.l.] Academic Press, 1979. v. 61p. 148–249.
- QIN, L. et al. Phytantriol based liquid crystal provide sustained release of anticancer drug as a novel embolic agent. **Drug Development and Industrial Pharmacy**, v. 42, n. 2, p. 307–316, 1 fev. 2016.
- QIU, H.; CAFFREY, M. The phase diagram of the monoolein/water system: Metastability and equilibrium aspects. **Biomaterials**, v. 21, n. 3, p. 223–234, 2000.
- RIBEIRO, L. N. DE M. et al. Use of nanoparticle concentration as a tool to understand the structural properties of colloids. **Scientific Reports**, v. 8, n. 1, p. 982, 2018.
- RÍOS-MARCO, P. et al. Alkylphospholipids: An update on molecular mechanisms and clinical relevance. **Biochimica et Biophysica Acta (BBA) - Biomembranes**, v. 1859, n. 9, Part B, p. 1657–1667, 2017.
- RIZVI, S. A. A.; SALEH, A. M. Applications of nanoparticle systems in drug delivery technology. **Saudi Pharmaceutical Journal**, v. 26, n. 1, p. 64–70, 2018.
- RIZWAN, S. B. et al. Characterisation of bicontinuous cubic liquid crystalline systems of phytantriol and water using cryo field emission scanning electron microscopy (cryo FESEM). **Micron**, v. 38, n. 5, p. 478–485, 2007.
- RIZWAN, S. B. et al. Preparation of phytantriol cubosomes by solvent precursor dilution for the delivery of protein vaccines. **European Journal of Pharmaceutics and Biopharmaceutics**, v. 79, n. 1, p. 15–22, 2011.
- RIZWAN, S. B.; BOYD, B. J. Cubosomes: Structure, Preparation and Use as an Antigen Delivery System. In: FOGED, C. et al. (Eds.). **Subunit Vaccine Delivery**. New York, NY: Springer New York, 2015. p. 125–140.
- SAGALOWICZ, L. et al. Crystallography of dispersed liquid crystalline phases studied by cryo-transmission electron microscopy. **Journal of Microscopy**, v. 221, n. 2, p. 110–121, 2006.
- SAGALOWICZ, L. et al. Study of Liquid Crystal Space Groups Using Controlled Tilting with Cryogenic Transmission Electron Microscopy. **Langmuir**, v. 23, n. 24, p. 12003–12009, 1 nov. 2007.
- SERIEYE, S. et al. Interface tuning and stabilization of monoglyceride mesophase dispersions: Food emulsifiers and mixtures efficiency. **Journal of Colloid and Interface Science**, v. 496, p. 26–34, 2017.
- SHERIF, S.; BENDAS, E. R.; BADAWY, S. The clinical efficacy of cosmeceutical application of liquid crystalline nanostructured dispersions of alpha lipoic acid as anti-wrinkle. **European Journal of Pharmaceutics and Biopharmaceutics**, v. 86, n. 2, p. 251–259, 2014.
- SHI, X. et al. Comparative studies on glycerol monooleate- and phytantriol-based cubosomes containing oridonin in vitro and in vivo. **Pharmaceutical Development and Technology**, v. 22, n. 3, p. 322–329, 3 abr. 2015.
- SINGH, T. et al. Application of Nanotechnology in Food Science: Perception and Overview. **Frontiers in Microbiology**, v. 8, p. 1501, 2017.
- SPICER, P. T. et al. Novel Process for Producing Cubic Liquid Crystalline Nanoparticles (Cubosomes). **Langmuir**, v. 17, n. 19, p. 5748–5756, 2001.

- SPICER, P. T. et al. Dry Powder Precursors of Cubic Liquid Crystalline Nanoparticles (cubosomes). **Journal of Nanoparticle Research**, v. 4, n. 4, p. 297–311, 2002.
- STEN ANDERSSON, M. JACOB LIDIN, K. L. Structure of the cubosome – a closed lipid bilayer aggregate. **Zeitschrift für Kristallographie - Crystalline Materials**, v. 210, n. 5, p. 315–318, 1995.
- STEWART, P. L. Cryo-electron microscopy and cryo-electron tomography of nanoparticles. **Wiley Interdisciplinary Reviews: Nanomedicine and Nanobiotechnology**, v. 9, n. 2, p. 1–16, 2017.
- SUN, T. et al. Engineered Nanoparticles for Drug Delivery in Cancer Therapy. **Angewandte Chemie International Edition**, v. 53, n. 46, p. 12320–12364, 7 out. 2014.
- TAHERI, M. L. et al. Current status and future directions for in situ transmission electron microscopy. **Ultramicroscopy**, v. 170, p. 86–95, 2016.
- TEBALDI, M. L. et al. Biomedical nanoparticle carriers with combined thermal and magnetic response: Current preclinical investigations. **Journal of Magnetism and Magnetic Materials**, v. 461, p. 116–127, 2018.
- TEYMOURI, M. et al. Investigation of Hexadecylphosphocholine (miltefosine) usage in Pegylated liposomal doxorubicin as a synergistic ingredient: In vitro and in vivo evaluation in mice bearing C26 colon carcinoma and B16F0 melanoma. **European Journal of Pharmaceutical Sciences**, v. 80, p. 66–73, 2015.
- TORCHILIN, V. P. Multifunctional, stimuli-sensitive nanoparticulate systems for drug delivery. **Nature Reviews Drug Discovery**, v. 13, n. 11, p. 813–827, 2014.
- TRAN, N. et al. Non-lamellar lyotropic liquid crystalline nanoparticles enhance the antibacterial effects of rifampicin against *Staphylococcus aureus*. **Journal of Colloid and Interface Science**, v. 519, p. 107–118, 2015.
- TRAN, N. et al. Dual-modality NIRF-MRI cubosomes and hexosomes: High throughput formulation and in vivo biodistribution. **Materials Science and Engineering: C**, v. 71, p. 584–593, 2017.
- TRAN, N. et al. Manipulating the Ordered Nanostructure of Self-Assembled Monoolein and Phytantriol Nanoparticles with Unsaturated Fatty Acids. **Langmuir**, v. 34, n. 8, p. 2764–2773, 27 fev. 2018.
- TYLER, A. I. I.; LAW, R. V.; SEDDON, J. M. X-Ray Diffraction of Lipid Model Membranes BT - Methods in Membrane Lipids. In: OWEN, D. M. (Ed.). **Methods in Membrane Lipids**. New York, NY: Springer New York, 2015. p. 199–225.
- VAN 'T HAG, L. et al. Lyotropic liquid crystal engineering moving beyond binary compositional space – ordered nanostructured amphiphile self-assembly materials by design. **Chemical Society Reviews**, v. 46, n. 10, p. 2705–2731, 2017.
- VARENNE, F. et al. Multimodal Dispersion of Nanoparticles: A Comprehensive Evaluation of Size Distribution with 9 Size Measurement Methods. **Pharmaceutical Research**, v. 33, n. 5, p. 1220–1234, 2016.
- WAKASKAR, R. R. Promising effects of nanomedicine in cancer drug delivery. **Journal of Drug Targeting**, v. 26, n. 4, p. 319–324, 2018.
- XIN PAN, KE HAN, XINSHENG PENG, ZHIWEN YANG, LINGZHEN QIN, CHUNE ZHU, XINTIAN HUANG, XUAN SHI, LINGHUI DIAN, MING LU, C. W. Nanostructured Cubosomes as Advanced Drug Delivery System. **Current Pharmaceutical Design**, v. 19, n. 35, p. 6290–6297, 2013.
- YAGHMUR, A. et al. Self-Assembly in Monoelaidin Aqueous Dispersions: Direct Vesicles to Cubosomes Transition. **PLoS ONE**, v. 3, n. 11, p. e3747, 18 nov. 2008.
- YANG, Z. et al. Optimization of the Preparation Process for an Oral Phytantriol-based Amphotericin B Cubosomes. **J. Nanomaterials**, v. 2011, p. 4:1–4:10, 2011.
- YOUNUS, M. et al. Bulk and dispersed aqueous behaviour of an endogenous lipid, selachyl alcohol: Effect of Tween 80 and Pluronic F127 on nanostructure. **Colloids and Surfaces B: Biointerfaces**, v. 169, p. 135–142, 2018.
- ZHANG, L. et al. Nanoparticles in medicine: Therapeutic applications and developments. **Clinical Pharmacology and Therapeutics**, v. 83, n. 5, p. 761–769, 2008.
- ZHOU, W.; SU, M.; CAI, X. Advances in nanoparticle sizing in suspensions: Dynamic light scattering and ultrasonic attenuation spectroscopy. **KONA Powder and Particle Journal**, v. 2017, n. 34, p. 168–182, 2017.